ENGINEERING FUNCTIONAL POROUS MATERIALS FOR GAS

ADSORPTION AND HETEROGENEOUS CATALYSIS

A Dissertation

by

LANFANG ZOU

Submitted to the Office of Graduate and Professional Studies of
Texas A&M University
in partial fulfillment of the requirements for the degree of

DOCTOR OF PHILOSOPHY

Chair of Committee,	Hong-Cai Zhou
Committee Members,	Kim R. Dunbar
	Janet Bluemel
	Haiyan Wang
Head of Department,	Simon North

May 2017

Major Subject: Chemistry

ABSTRACT

In the past two decades, functional porous materials have gained tremendous attention in scientific and technological research. Metal-organic frameworks (MOFs) and porous polymer networks (PPNs) emerged as novel categories of porous materials with ultrahigh porosity, enormous surface area, tunable pore size and shape, and adjustable functionalization. Hence, MOFs/PPNs have demonstrated great potential for gas adsorption and heterogeneous catalysis, which has been my research focus.

Firstly, utilizing labile MOFs as templates, a general post-synthetic method was invented to synthesize a series of Ti-MOFs. The crystallinity of these Ti-MOFs was well maintained throughout, as confirmed from powder X-ray diffractions and gas adsorption measurements. This work provides a first time reported systematic strategy to construct Ti-MOFs while highlighting the potential of Ti-MOFs in photocatalytic applications.

Two stable porphyrin based PPNs have been synthesized through a facile one-pot approach by the aromatic substitution reactions of pyrrole and aldehydes. Among them, PPN-24(Fe) performs high catalytic efficiency as a biomimetic catalyst for the oxidation reaction of 2, 2'-azino-bis(3-ethylbenzthiazoline-6-sulfonic acid) (ABTS) in the presence of H_2O_2.

In next section, we report the design of a flexible Zr-MOF system, namely PCN-700 series, for the realization of switchable catalysis in cycloaddition reactions of CO_2 with epoxides. The breathing amplitudes of the PCN-700 series are magnified through pre-functionalization of organic linkers and post-synthetic linker installation. Experiments

and molecular simulations confirm that the catalytic activities of the PCN-700 series can be switched on and off upon guest-induced reversible structural transformation.

MOFs have become a burgeoning field of research and a great potential candidate for hydrogen storage. As way of example, MOFs constructed by carboxylate, azolate or mixed linkers, are discussed in the context of hydrogen storage. Last but not least, the post-synthetic modifications on MOF materials to increase the hydrogen storage capacities will be carefully illustrated.

Intensive efforts have been made to investigate PPNs as one type of the most promising candidates for carbon capture. A detailed correlation study between the structural and chemical features of PPNs and their adsorption capacities will be discussed, mainly focusing on the physical interactions and chemical reactions.

DEDICATION

This work is dedicated to my beloved family for their love and support.

ACKNOWLEDGEMENTS

NOMENCLATURE

MOFs: metal-organic frameworks

PPNs: porous polymer networks

POPs: porous organic polymers

POFs: porous organic frameworks

CMPs: conjugated microporous polymers

PIMs: polymers of intrinsic microporosity

HCP: hypercrosslinked polymers

CTFs: covalent triazine-based frameworks

PAFs: porous aromatic frameworks

COFs: covalent organic frameworks

TB-MOPs: Tröger's base-derived microporous organic polymers

BILPs: benzimidazole-linked polymers

TBILPs: triazine-based benzimidazole-linked polymers

FCTFs: perfluorinated triazine linked frameworks

ALPs: azo-linked polymers

PCPs: porous cationic polymers

BIPLP: bis(imino)pyridine linked polymer

COP: covalent organic polymer

IUPAC: International Union of Pure and Applied Chemistry

HKUST: Hong Kong University of Science and Technology

MIL: Material from Institute Lavoisier

ZIFs: zeolitic imidazole frameworks

IRMOF: isoreticular metal-organic framework

UMCM: university of michigan crystalline material

PSMO: postsynthetic metathesis and oxidation

SBUs: secondary building units

BET surface area: Brunauer–Emmett–Teller surface area

CCS: carbon capture and storage

ICP-MS: inductively coupled plasma mass spectrometry

EDS: energy-dispersive X-ray spectroscopy

FE-SEM: field-emission scanning electron microscopy

TGA: thermogravimetric analyzer

SC-XRD: single-crystal X-ray diffraction

PXRD: powder X-ray diffraction

PSA: pressure swing adsorption

Abbreviations of Selected Chemicals

BDC: beneze-1,4-dicarboxylate

BET: Brunauer–Emmett–Teller

BTC: benzene-1,3,5-tricarboxylate

BPDC: 4,4'-biphenyldicarboxylate

DMF*: N,N*-dimethylformamide

DEF: *N,N*-diethylformamide

DMA: *N,N*-dimethylacetamide

BTB: 4,4′,4″-benzene-1,3,5-triyl-tribenzoate ligand

BTTri: 1,3,5-tris(1H-1,2,3-triazol-5-yl)benzene

BTT: 1,3,5-benzenetristetrazolate

AC: activated carbon

ABTS: 2, 2'-azino-bis(3-ethylbenzthiazoline-6-sulfonic acid)

MB: methylene blue

TPDC: *p*-terphenyl-4,4''-dicarboxylate

H_2Me_4-BPDC: 2,2',6,6'-tetramethylbiphenyl-4,4'-dicarboxylic acid

$H_2(CF_3)_2$-BPDC: (2,2'-bis(trifluoromethyl)-biphenyl-4,4'-dicarboxylatic acid)

H_2Me-BPDC: (2-methylbiphenyl-4,4'-dicarboxylic acid)

HATP: 2,3,6,7,10,11-hexaaminotriphenylene

TFPM: tetrakis(4-formylphenyl)methane

TBA: 1,2,4,5-benzenetetramine tetrahydrochloride

FA: fumarate

NDC: 2,6-napthalene dicarboxylate

TABLE OF CONTENTS

LIST OF FIGURES

xviii

LIST OF TABLES

1. INTRODUCTION*

In the past two decades, porous materials have gained tremendous attention in scientific and technological research due to their capability of adsorbing and interacting with atoms, ions and molecules.[1] The functionalities and prospective applications of the porous materials are largely dependent on their pore size distribution and pore surface properties. Under the motivation of achieving larger surface area and better framework properties, metal-organic frameworks (MOFs)[2] and porous polymer networks (PPNs)[3-4] emerged as novel categories of porous materials with ultrahigh porosity, enormous surface area and novel functionalization.

1.1 Metal-organic frameworks (MOFs)

MOFs are a novel category of inorganic-organic hybrid crystalline porous materials with infinite framework structure composed of inorganic secondary building units (SBUs, generally metal clusters) and organic linkers.[5] The variability of both inorganic composites and organic composites makes MOFs extremely diverse in structures, functions and applications. MOFs with pore walls of one-carbon-atom thin are quite common. In other words, almost all the atoms in forming MOFs can be used as a surface, therefore the surface areas of MOFs are very high. By careful selection of the

appropriate combination of organic ligand and metal units, MOFs can possess extraordinarily large pore size (the pore size can be as large as 98 Å) or exceptionally high Brunauer–Emmett–Teller surface areas (the BET surface area can be as high as 6240 m^2/g). Due to its crystalline nature, MOFs provide uniformly distributed pores that are suitable for the applications of gas storage[6], gas separation[7], sensors[8], drug delivery[9], catalysis[10-11] and many other applications.

1.2 Porous polymer networks (PPNs)

PPNs, another new category of hyper-crosslinked polymeric materials constructed from organic covalent bond exclusively, emerged as an alternative porous material with extremely high thermal and chemical stabilities.[12] PPNs can be crystalline (which also called as covalent organic frameworks, COFs) or amorphous, great structure tunable (pore size, surface functionality, etc.), light weight (composed of light elements, typically H, B, C, N, and O) and their BET surface area can be as high as 6461 m^2/g. Various chemical reactions have been applied to constructing organic porous materials, including Friedel–Crafts alkylations,[13] metal-catalyzed coupling reactions (Sonogashira coupling,[14] Yamamoto coupling,[12] etc.), Schiff-base chemistry,[15] and boronic acid condensation[16-17]. The combined favorable properties of extremely high stability, large surface area, tunable pore size and permanent porosity have enabled PPNs as ideal candidates for various applications, including gas adsorption, gas separation, sensors, and catalysis.

1.3 MOFs and PPNs for heterogeneous catalysis

Heterogeneous catalysis was one of the earliest proposed applications proposed for porous MOFs and PPNs, as well as one of the earliest demonstrated applications. Recently, rapid progress in catalysis was achieved for porous coordination solids, which can offer well-defined coordination nanospace and functional groups/sites appropriate for catalysis.

Using MOFs/PPNs as heterogeneous catalysts could have the following principal advantages: (1) enhanced catalyst reactivity and stability due to the spatial separation of catalytic sites in the framework, which can contribute to cooperative catalysis character of enzymes; (2) permeable channels and coordination nanospace, which endow recognition effects and allow the facile access of substrates to the catalytically active sites, bestowing the catalytic reactions with shape-, size-, chemo-, or enantio-selectivity; (3) framework flexibility and dynamics, which will bring new applications to catalysis by enforcing chemical, physical, or environmental stimuli responses; and (4) easy tunability and modification of the polar–nonpolar and hydrophobic–hydrophilic properties, which is essential for many catalysis reactions. (5), the ability to separate and reuse heterogeneous catalysts would be highly attractive in large-scale reactions, where separation and waste disposal can be costly. The last but important feature of MOFs for catalysis is that the assembly process of MOFs combines merits of various metal ions or clusters and designable organic ligands, which offers innumerous structural topologies and diversified porosities.

1.4 Metal-organic frameworks for hydrogen storage

The concerns of energy resource consumption from fossil fuel use, related global warming has gained momentum to develop sustainable energy carriers such as hydrogen gas (H_2). The energy density of hydrogen is much higher than petroleum such as gasoline and the combustion of hydrogen emits no carbon dioxide (CO_2). However, the application of H_2 as fuel in transportation would limited if there is not an effective storage technology due to its volatile nature. In the past few decades, MOFs have become a great potential candidate for hydrogen storage due to their exceptional high porosity, high crystallinity, uniform yet tunable pore size and pore shape, great diversity and various kinds of hydrogen occupation sites. In 2003, the initial H_2 storage data, a remarkable 4.5 wt % at 77 K and 1 atm, was demonstrated by MOF-5, which was synthesized by Zn ionic salt and beneze-1,4-dicarboxylate (BDC) ligand.[18] The maximum H_2 uptake in MOF-5 varied from 1.3 to 5.2 wt% at 77 K depending on fabrication and activation parameters. Since then, numerous reports of porous MOFs with different topologies and porosities have demonstrated relatively high H_2 storage. Coupled with measurements of porosity, some understanding of many factors that affect the hydrogen uptake by porous MOFs have been developed. Here, some technical elements are introduced in this section in tailoring MOFs as hydrogen storage resins, including syntax, synthesis, fabrication, evaluation and benchmark testing. As way of example, MOFs constructed by carboxylate, azolate or mixed linkers, are discussed in the context of hydrogen storage. Last but not least, the post-synthetic modifications on MOF materials to increase the hydrogen storage capacities will be carefully illustrated.

1.5 Porous organic polymers for carbon capture

One of the most pressing environmental concerns of our age is the escalating level of atmospheric CO_2, which necessitate the process of carbon capture. Since the beginning of the industrial age, the CO_2 concentration has increased from 280 to 390 ppm in 2011, an increase of approximately 40%. Carbon capture and storage (CCS) is a family of technologies, which can reduce CO_2 emissions. CCS includes three steps: a) separation of CO_2 from emission sources before entering the atmosphere (carbon capture); b) transportation to a storage site; and c) permanent subterranean or submarine storage. To sidestep the traditional "wet scrubbing" methods, which suffers from the high regeneration cost, fouling of the equipment and solvent boil-off, intensive efforts have been made to investigate the use of solid porous materials as an alternative approach, including MOFs and PPNs. Taking amine scrubbing as the model, aminated porous materials usually exhibit very large adsorption enthalpies for CO_2 and high CO_2/N_2 selectivity. However, constructed with the soft Lewis acids and hard Lewis bases, MOF materials usually suffer from limited physicochemical stability.

PPNs are a class of adsorbents that exhibit surface areas comparable to those of MOFs, but have much higher physicochemical stability arising from the entirely covalently bonding in the framework. By loading polyamine onto PPN-6, which has an exceptionally high surface area and an extremely robust all-carbon scaffold based on biphenyl rings, our group successfully demonstrated the polyamine tethered PPN-6 with dramatic increases in CO_2-uptake capacities at low pressures and exceptionally high CO_2/N_2 adsorption selectivity under ambient conditions. The key to obtaining porous polymers with high amine loading is

5

to judiciously select efficient reactions and starting materials with ultrahigh surface areas. PPN-6, constructed with Tetrakis(4-bromophenyl)methane using a modified Yamamoto homocoupling polymerization procedure, has an exceptionally high surface area and an extremely robust all-carbon scaffold based on biphenyl rings. After two postfunctionalized steps, amine-grafting PPN-6 was successfully obtained. Among these materials, PPN-6-CH_2DETA has the best performance. At 295 K and 0.15 bar, PPN-6-CH_2DETA takes up 3.0 mmol g^{-1} of CO_2 (11.8 wt%). This value is comparable to other top-performing materials, such as mmen-CuBTTri (9.5 wt% at 298 K) and MgMOF-74 (22.0 wt% at 293 K), but PPN-CH_2DETA stands out with respect to its physicochemical stability arising from the covalent bonding in the framework. Significantly, there was no apparent loss in capacity after 20 cycles.

Besides, a significant number of porous organic polymers (POPs) have been studied for carbon capture, some of which have demonstrated promising performances. The major advantages of POPs over other porous materials are their high porosity, structural diversity, and ultrahigh physicochemical stability, the combination of which enables an enormous scope of postsynthetic modifications to introduce specific CO_2-philic functionalities. In general, POPs can be handled under standard wet chemical reaction conditions without significant degradation of the framework or loss of porosity, and are ideal for applications in capturing CO_2 from harsh flue gas conditions.

2. FRAMEWORK TEMPLATING STRATEGY: A GENERAL STEPWISE POSTSYNTHETIC APPROACH TOWARDS TITANIUM METAL-ORGANIC FRAMEWORKS FOR PHOTOCATALYTIC CATALYSIS*

2.1 Background

Over the past few years, metal-organic frameworks (MOFs) have attracted tremendous attention owing to their crystalline nature, pore tunability, structure diversity, as well as numerous potential applications such as gas adsorption, separation, catalysis, and sensing.[19-22] In particular, most applications demand robust MOFs, making those constructed with high valent metals particularly desirable.[23-25] While great efforts have been devoted to the development of MOFs containing trivalent metals, such as Fe^{3+}, Cr^{3+}, and Al^{3+},[26-27] MOFs constructed with tetravalent metals are much less explored. Recently, the research on Zr-MOFs has flourished owing to the use of modulating reagent, which facilitates the formation of single crystals.[28-30] With the high charge to radius ratio (Z/r), Zr^{4+} forms strong coordination bonds with carboxylates, which endows the frameworks with extraordinary stability, enabling their applications under harsh conditions. However, titanium, even though in the same group as zirconium in the periodic table, has barely been adopted to construct MOFs despite its great abundance in the Earth's crust, low toxicity, and even higher Z/r ratio. Moreover, unlike zirconium clusters, which merely act

as inorganic nodes to sustain the frameworks, titanium-oxo clusters provide additional photocatalytic properties. Because Ti(IV) is coordinated by oxygen atoms, the titanium building blocks in Ti-MOFs can be viewed as TiO_2 nanoparticles. In addition, the integration of tunable functions on organic linkers of MOFs with those of the inorganic components will lead to Ti-MOF platforms promising for photocatalysis.

Férey, Serre, and coworks have initially demonstrated the preparation of titanium MOFs, MIL-91[31] and MIL-125[32]. In particular, MIL-125 and its NH_2-functionalized counterpart, MIL-125-NH_2[33], showed great potential in light-driven water splitting and CO_2 reduction applications.[34-35] Recently, another titanium MOF, NTU-9[36] was reported by Zhang group. However, no other Ti-MOFs have been reported despite the burgeoning of many other high-valent-metal MOFs. The daunting challenge of synthesizing Ti-MOFs reliably lies in the lack of general synthetic methods. Three major reasons could account for such situation: a) the high Z/r value on Ti^{4+} results in strong coordination bonds between titanium nodes and the ligands. Accordingly, the poor reversibility of the metal-ligand bond association/dissociation obstacles the formation of crystalline products;[37] b) most of the reactive titanium sources suffer from severe hydrolysis, which limits the variation of synthetic conditions; c) all the known titanium carboxylates exhibit low symmetry or unsuitable connectivity, which hampers the easy formation of periodic networks with the organic linkers.[38]

As the photocatalytic properties of Ti-MOFs can be greatly affected by the titanium oxo building units, the exploration of new synthetic approaches to diversify the category of Ti-MOF materials is of great importance. Framework templating (post-

synthetic metathesis) has emerged as an alternative synthetic strategy in the field of MOFs due to its exceptional capability of obtaining certain MOFs that cannot or hardly be achieved directly.[39-42] Moreover, the MOFs obtained from framework templating strategy have more predictable structures and topologies. However, the majority of the reported metal metathesis processes occur between two low valent metal species categorized as soft or borderline Lewis acids. For high valent (+3 or +4) ones, due to the inertness of the starting metal-ligand bonds, the exchange rates are extremely slow. Another serious drawback is that the parent framework would be damaged by these hard lewis acid species owing to a long reaction time ranging from a few days to several weeks. Recently, our group developed a post-synthetic metathesis and oxidation (PSMO) strategy to achieve a stable Cr(III)-MOF from the Mg(II) parent MOF, which undergoes an metal metathesis between same valent metal species (M(II) to M(II)) followed by an oxidation step (M(II) to M(III)).

2.2 Framework templating strategy towards Ti-MOFs

Along this line, we herein present a general synthetic method towards Ti(IV) MOFs, which is accomplished through M(II) to Ti(III) or M(III) to Ti(III) metathesis, and then a mild oxidation step to Ti(IV). Starting from judiciously selected template frameworks, PCN-333(Sc)[37], MIL-100(Sc)[43], MOF-74(Zn)[44], and MOF-74(Mg), ulitizing the PSMO strategy, we successfully synthesized a series of porous photoactive titanium MOFs, PCN-333(Sc)-Ti, MIL-100(Sc)-Ti, MOF-74(Zn)-Ti and MOF-74(Mg)-Ti (Figure

1). These Ti-MOFs not only maintain good crystallinity throughout, but also demonstrate

excellent photocatalytic degradation of methylene blue.
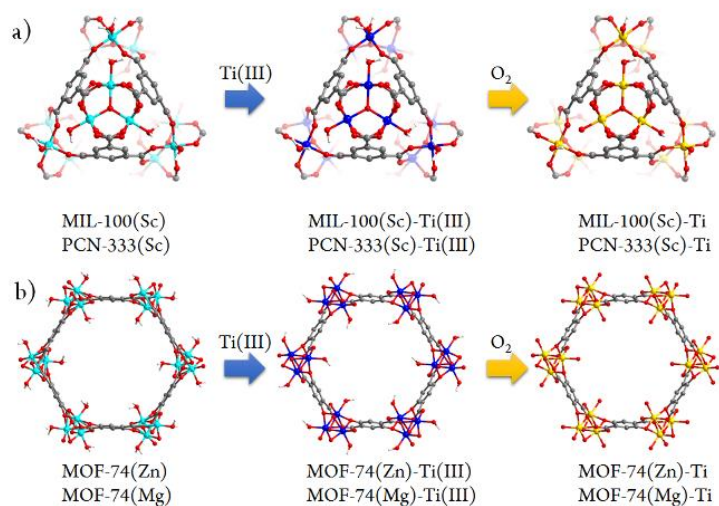
Figure 1. Schematic illustration of the stepwise procedure for the design of Ti-MOFs from the template MOFs: a) MIL-100(Sc) and PCN-333(Sc) metal metathesis with Ti(III), followed by metal node oxidation in the air; b) similar process for MOF-74(Zn) and MOF-74(Mg).

There are several prerequisites for the targeting metal species in the PSMO approach: a) the targeting high valent metal species have to exhibit a suitable reduced state that can be conveniently achieved; b) the reduced species in lower oxidation states can undergo metal metathesis with a considerable rate to guarantee the framework crystallinity; c) the reduced species can survive under exchanging environment. Fortunately, Ti(IV) meets all these prerequisites which enables PSMO as a feasible synthetic approach. The reduced state Ti(III), with lower charge and larger radius, undergoes a ligand dissociation rate around 10^5 sec^{-1} in the aqueous media, which is even faster than some M(II) transition metal species in the third period, such as Ni(II).[45] More

importantly, Ti(III)/Ti(IV) has higher redox potential than Cr(II)/Cr(III) in similar coordination environment of weak field ligands, making Ti(III) easier to handle than Cr(II) during the exchange process.

Meanwhile, the template MOFs were also selected with careful consideration. a) the metal species in these template MOFs cannot be reduced by Ti(III), avoiding producing the strong Lewis acidic Ti(IV) and even less stable low valent MOFs, to preserve the frameworks' crystallinity; b) all the template MOFs contain open metal sites, which are occupied by the weakly coordinated neutral solvent molecules. These open metal sites could effectively accelerate the metal metathesis rate. c) the metal species in the template MOFs are all six coordinated, which possess similar coordination environment with titanium.

We firstly chose two scandium MOFs, PCN-333(Sc) and MIL-100(Sc), as the template MOFs. As Sc(III) has almost the same radius with Ti(III), the skeleton of the framework won't be altered after metal metathesis. The typical exchange process is: First, the as-synthesized crystals were washed with anhydrous DMF, bubbled with nitrogen and transferred into the glove box, where $TiCl_3(THF)_3$ was added, resulting in an evident color change from white to purple in merely three minutes. In order to facilitate this metathesis process, the crystals were sealed in a vial and kept at 120°C for 24 hours. Meantime, the mother liquid was refreshed every 8 hours. After reaching the exchange equilibrium, the excess $TiCl_3$ molecules were removed by centrifuge, yielding the dark purple crystals. This crystalline sample was treated with oxygen/water-free methanol for three days and activated at 150ºC for 5 hours. The activated sample was oxidized in the air causing an

apparent color change from dark purple to white. Using this dry oxidation method, we would be able to keep the MOFs' crystallinity to the highest level.

The ratio of titanium in these two Ti-MOFs was analyzed using inductively coupled plasma mass spectrometry (ICP-MS) and energy-dispersive X-ray spectroscopy (EDS) analyses (Table 1). The metal exchange ratio of PCN-333(Sc)-Ti is 88.0%, which is much higher than the 48.8% of MIL-100(Sc)-Ti. Such difference can be ascribed to the more flexible lattice in PCN-333(Sc), as well as the faster diffusion rate for the elongated framework.[46-47] Although PCN-333(Sc) possesses the same inorganic building block with MIL-100(Sc), the longer linkers in PCN-333(Sc) endow the lattice with higher flexbility to facilitate the metal exchange completeness. Meanwhile, the larger ligand gives rise to the larger pores and windows in PCN-333(Sc), which further enhance the diffusion rate inside the MOF materials.

Table 1. EDS and ICP-MS analysis for Titanium MOFs.

Ti%[a]	333(Sc)-Ti	100(Sc)-Ti	74(Zn)-Ti	74(Mg)-Ti
EDS	85.9%	52.0%	100%	35.1%
ICP-MS	88.0%	48.8%	94.7%	37.9%

a) atomic percentage.

Despite of many successful examples in metal exchange, MOFs featured with one dimensional metal chains is conspicuously absent from the known examples of metal exchange. The successful metathesis of PCN-333(Sc) and MIL-100(Sc) provokes us to conduct metal metathesis in MOF-74. Considering that Zn^{2+} and Mg^{2+} ions, the weaker

lewis acidic species, bond more weakly with carboxylates compared with Sc^{3+}, MOF-74(Zn) and MOF-74(Mg) were selected as templates for metal metathesis. As expected, an exchange ratio of 94.7% was finally achieved for the metathesis of MOF-74(Zn) with $TiCl_3(THF)_3$. To the best of our knowledge, MOF-74(Zn)-Ti is the first reported example of MOFs which undergoes the complete metal exchange with one dimensional metal chain. Starting with MOF-74(Mg), a much lower exchange ratio, 37.9%, was observed, which can be attributed to the more robust framework arising from the stronger metal to solvent bonding compared to the Zn^{2+} isostructure.

2.3 The well-maintained crystallinity of Ti-MOFs

PXRD patterns of the MOFs before and after metal exchange well coincide with each other, indicating the obtained products have the same structure with templates and the crystallinity was well-maintained during the whole PSMO process (Figure 2). N_2 adsorption measurements were also conducted to evaluate the intactness of these Ti-MOFs (Figure 3). As can been observed from the N_2 adsorption isotherms, the porosity of the Ti-MOFs is kept intactness compared to their corresponding template MOFs. The small decrement could be ascribed to the inevitable loss of the ordered structure during metal exchange process as well as the increased crystal density due to the extra anions required to balance the charge of the Ti(IV) species.
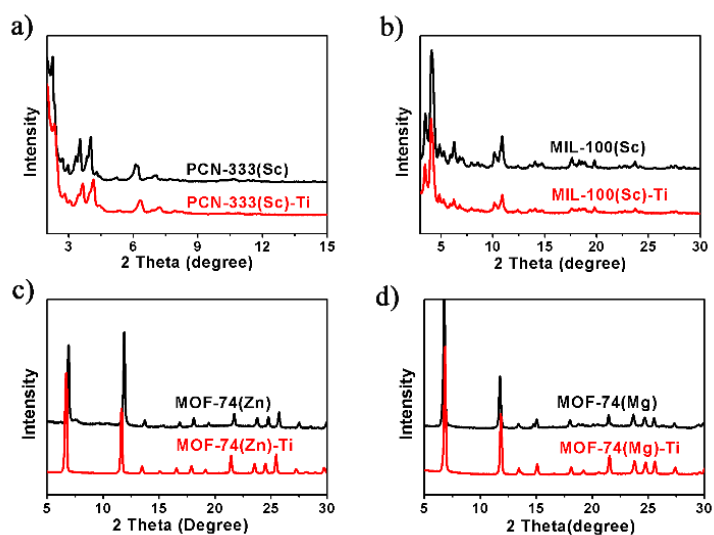
Figure 2. PXRD patterns for template MOFs and the corresponding titanium MOFs.
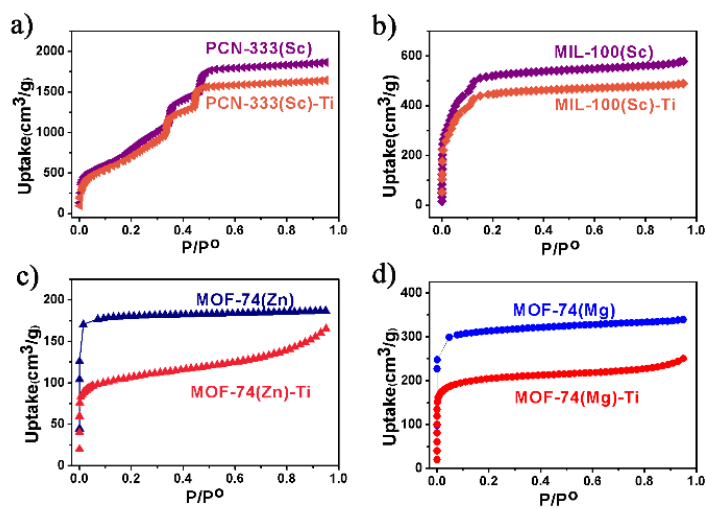
Figure 3. N$_2$ uptakes for template MOFs and the corresponding titanium MOFs at 77 K,

1 atm.

2.4 The optical properties of Ti-MOFs

With the diverse titanium-oxo clusters being exchanged into the frameworks, we investigated the optical properties of these titanium MOFs using diffuse reflectance UV-Vis absorption spectroscopy (Figure 4). Compared with the absorption edge at 380 nm of PCN-333(Sc)-Ti and MIL-100(Sc)-Ti, MOF-74(Zn)-Ti and MOF-74(Mg)-Ti show an extra absorption band centered at about 450 nm with the absorption edge extended to around 660 nm. Meanwhile, there were obvious color differences between these titanium MOFs: PCN-333(Sc)-Ti and MIL-100(Sc)-Ti are white, MOF-74(Mg)-Ti is orange, while MOF-74(Zn)-Ti is dark red. Such differences can be probably ascribed to two reasons. On one hand, PCN-333(Sc)-Ti and MIL-100(Sc)-Ti are composed of trinuclear cluster while MOF-74(Zn)-Ti and MOF-74(Mg)-Ti are composed of one dimensional titanium chain, which result in distinguished differences of HOMO-LUMO gaps. On the other hand, as a good electron donation moiety, DOBDC would provide effective ligand to metal charge transfer in Ti-MOF-74 strcutures, resulting in visible light absorption.
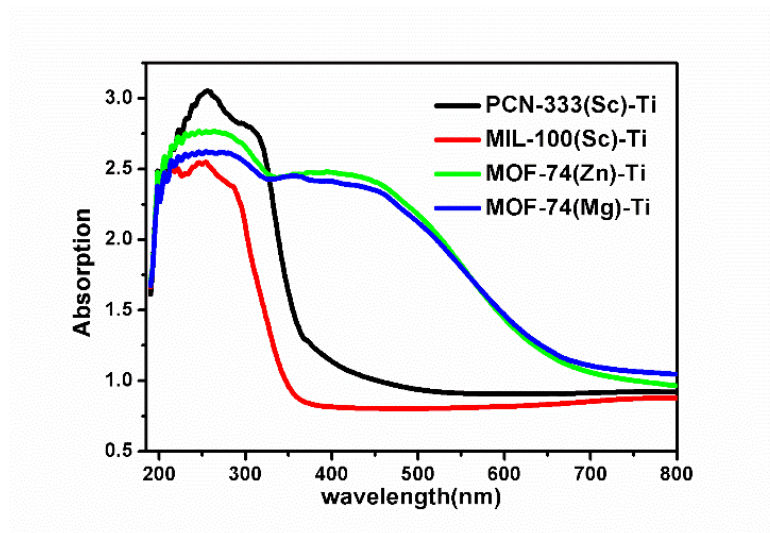
Figure 4. UV/Vis absorption spectra of PCN-333(Sc)-Ti (black), MIL-100(Sc)-Ti (red), MOF-74(Zn)-Ti (green) and MOF-74(Mg)-Ti (blue).

2.5 Photodegradation of methylene blue (MB) utilizing Ti-MOFs

To examine the photocatalytic potential of these titanium frameworks, the degradation of methylene blue (MB) was tested as a representative. 15 mg of MOFs was suspended in 15 mL of 500 μM aqueous solution of MB. The solution was stirred in the dark for 2 hours to achieve the adsorption equilibrium before illuminated with a 300 W Xe lamp. The concentration change of MB was monitored by measuring the optical absorption at 660 nm of the suspension at regular intervals (Figure 5a). The photo-degradation of MB in the presence of TiO_2 was relatively slow, with less than 4% of MB degraded after an illumination time of nine minutes. However, in the presence of PCN-333(Sc)-Ti and especially MOF-74(Zn)-Ti, the photodegradation of MB was much faster, with conversions up to 30% and 98% respectively after only nine minutes.

The excellent photocatalytic performance of MOF-74(Zn)-Ti can be attributed to its capability of absorbing broader range of the irrdiating light and longer excitation lifetime. To illustrate photodegaradation of MB within the system of MOF-74(Zn)-Ti, we herein present a proposed mechanism (Figure 5b): In this photochemical reaction, MOF-74(Zn)-Ti acts as the chromophore. Upon excitation, electrons transfer from DOBDC to the Ti-oxo metal center, reducing Ti^{4+} into Ti^{3+} ions, which separates the electron-hole couple. Meanwhile the oxidized DOBDC is stabilized by the formation of thermodynamic product, benzoquinone species, presumably by sequential electron transfer step.[48] The benzoquinone species are reduced by highly reductive MB which is followed by the oxidation of Ti^{3+} ions by O_2, fullfilling the catalytic cycle. The formation of Ti^{3+} and benzoquinone dicarboxylate intermediate efficiently prevented the electron–hole recombination, which inherently accelerate the photocatalytic activity of MOF-74(Zn)-Ti.
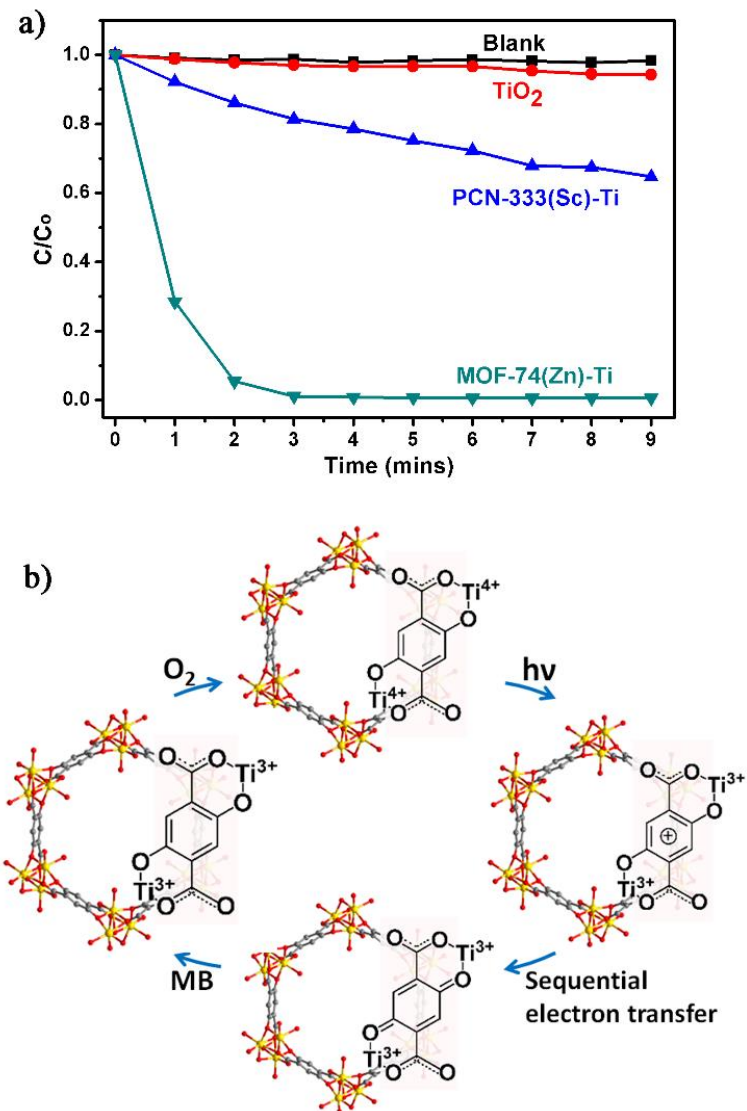
Figure 5. a)Photo-degradation of MB using PCN-333(Sc)-Ti, MIL-100(Sc)-Ti, MOF-74(Zn)-Ti, and MOF-74(Mg)-Ti in solution over time with Xenon light irradiation; b) Proposed mechanism of MB degradation of MOF-74(Zn)-Ti in the presence of air.

2.6 Summary

In summary, we have successfully demonstrated a systematic framework templating strategy towards various titanium MOFs, PCN-333(Sc)-Ti, MIL-100(Sc)-Ti,

18

MOF-74(Zn)-Ti and MOF-74(Mg)-Ti, which exhibit high porosity and excellent photocatalytic activity. The titanium ratio in PCN-333(Sc)-Ti and MOF-74(Zn)-Ti reaches up to 88.0% and 94.7%, respectively. The crystallinity is well maintained during the PSMO process as confirmed by nitrogen uptakes and PXRD patterns. This study manifests an effective method to explore promising Ti-MOF platforms for photocatalytic applications.

3. FACILE ONE-POT SYNTHESIS OF PORPHYRIN BASED PPNS AS BIOMIMETIC CATALYSTS[*]

3.1 Background

Catalytic activity of metalloprophyrin complexes have been extensively studied since the discovery of the heme-containing enzymes, cytochrome P450[49]. Inspired by the porphyrin core as the active site in cytochrome P450, many metalloporphyrin catalysts for hydroxylation, cyclopropanation, olefination, C-H insertion and N-H insertions have been explored.[50-51] Direct application of the metalloporphyrin complexes in aqueous solution is usually challenging due to the formation of catalytically inactive dimers in the oxidizing reaction media.[52] With this consideration, various methods have been developed to heterogenize metalloporphyrin catalyst, including covalent bond formation, ion-pair formation, encapsulation or immobilization on supports such as zeolites, clays or mesoporous silica.[53-55] However, these methods usually dilute the density of active sites,[56-57] yield unwelcome interactions between substrate and catalyst, or lead to leaching of the complexes from substrate.[58-59]

As an alternative solution, advanced porous materials have been demonstrated as promising candidates to heterogenize metalloporphyrin because of their tuneable

properties, high surface areas and controllable porosity. In the last two decades, MOFs have been extensively investigated in scientific and technological research. Recently, porphyrin derivatives have been introduced into MOFs by either linker modification or encapsulation.[60-61] MOFs possess many advantages, such as large surface area, tuneable structures, and feasible platform for post-synthetic modifications. However, most MOFs, constructed with soft Lewis acids (metal ions) and hard Lewis bases (carboxylates), suffer from limited stability, which highly restrained their potential in industry applications. Porous polymer networks (PPNs), hyper-cross linked organic polymers based on covalent-bonds connections, have provided an alternative way to construct functional porous materials with extremely high chemical and thermal stability. Some research has been focused on synthesizing PPN materials with metalloporphyrin active centers utilizing pre-synthesized metalloporphyrin monomers *via* either C-C cross coupling reactions using Pd-catalyst or condensation with tetra(4-aminophenyl)methane.[62-64] Nevertheless, their synthetic methodologies are usually not scalable due to the complicated synthesis procedure for the monomers or the requirement of expensive metal catalysts for polymerization. Preparation of porphyrinic porous organic polymers (POPs) with 2D planar structure via bottom-up strategy has been initially reported by Bhaumik *et al.*[65] However, incorporation of porphyrinic active site into 3D porous framework through the one-pot facile synthesis was absence thus far.

Herein, we report a facile one-pot synthetic strategy to produce large scale porphyrin containing PPNs, PPN-23 and PPN-24 (Figure 6), of which PPN-24 is the firstly reported 3D porphyrin based PPNs obtained by using this facile strategy. This unique

methodology is based on the extended condensation reaction between pyrrole and aromatic aldehydes including benzene-1, 3, 5-tricaialdehyde[66] (PPN-23) and tetrakis(4-formylphenyl)silane[67] (PPN-24). This condensation process yields black fluffy PPNs with high porosity, excellent thermal and chemical stability. Moreover, the synthetic procedure is very cost- and time- efficient and the final material can be easily functionalized with metal ions, such as iron(III), zinc(II), copper(II) and cobalt(II), through an effortless post-synthetic reaction.[68] The catalytic activity of PPN-24(Fe) has been well demonstrated by catalytic oxidation of 2, 2'-azino-bis(3-ethylbenzthiazoline-6-sulfonic acid) (ABTS) in the presence of H_2O_2. The catalytic activity of PPN-24(Fe) exhibits the feasibility of precisely designing stable porous polymer materials for mimicking heme-based protein applications.

3.2 Detailed synthetic methodology of PPN-23 and PPN-24

The synthesis were accomplished by treatment of pyrrole with benzene-1, 3, 5-tricaialdehyde (PPN-23) or tetrakis(4-formylphenyl)silane (PPN-24) in refluxed propionic acid media for 12 hours. Under acidic condition, aromatic aldehydes were activated through protonation, followed by electrophilic aromatic substitution of the activated carbons of pyrrole, and further condensation to yield macrocyclic porphyrin building blocks with free aldehyde groups. This condensation process continues until the finish of the polymerization. After the reaction, black fluffy powder was washed to afford the PPN-23 and PPN-24. FT-IR was employed to confirm the formation of porphyrin networks. Bands corresponding to 1720-1740 cm^{-1} (C=O stretching) are absent, suggesting all the

aldehyde starting materials have been consumed in the polymerization reaction. The strong bands observed at 3317 cm^{-1}, 969 cm^{-1} and 802 cm^{-1} can be attributed to the characteristic stretching, bending and rocking vibrations of N-H bonds in porphyrin center, confirms the formation of microporous porphyrin networks. Field-emission scanning electron microscopy (FE-SEM) images show that PPN-23 and PPN-24 are composed of agglomerated sphere-shaped particles with sizes ranging from 1.0 to 3.2 μm in diameter (Figure 7).
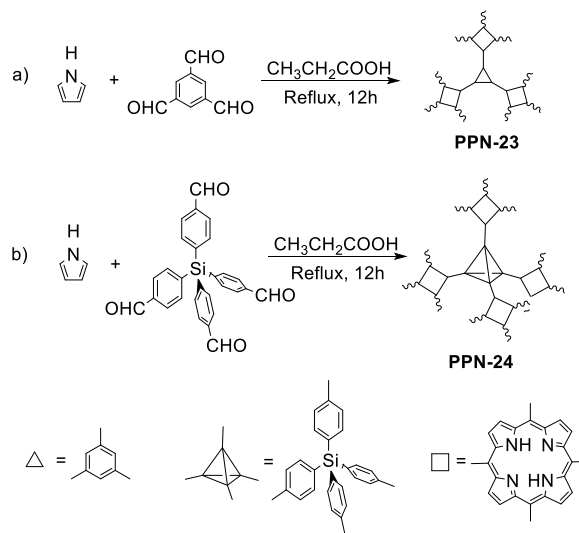
Figure 6. Synthetic strategy of a) PPN-23 and b) PPN-24: (Simplified using provided symbols).
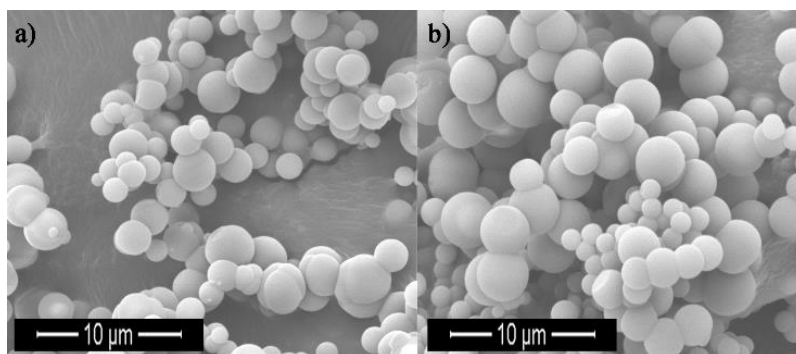
Figure 7. SEM images of a) PPN-23 and b) PPN-24.

3.3 Nitrogen adsorption measurements for PPN-23 and PPN-24

Porosities of these PPNs have been established from the N_2 sorption analysis at 77 K. As evident from Figure 8, both PPN-23 and PPN-24 exhibit type I isotherm, typical for microporous solids, where a steep gas uptake at low relative pressure and a mostly flat extrapolation in the intermediate sections of P/P^o are observed. N_2 uptakes of 102 cm^3 g^{-1} and 187 cm^3 g^{-1} have been obtained for PPN-23 and PPN-24, respectively. The Brunauer-Emmett-Teller (BET) surface areas for PPN-23 and PPN-24 are 271 m^2 g^{-1} and 478 m^2 g^{-1}, respectively (Langmuir surface areas 426 m^2 g^{-1} and 754 m^2 g^{-1}, respectively), suggesting the permanent porosity of PPN-23 and PPN-24.
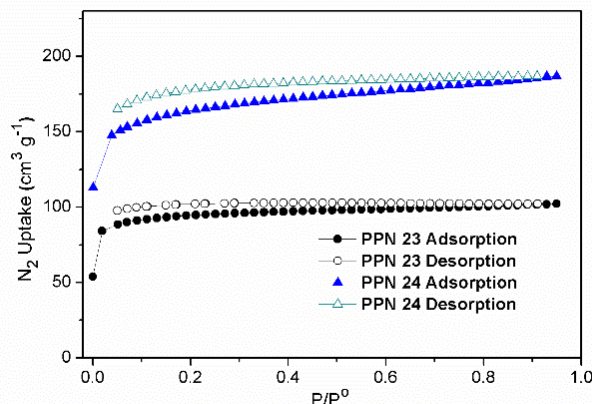
Figure 8. N_2 isotherms for PPN-23 and PPN-24 at 77 K, 1 atm.

3.4 Thermal and chemical stability test for PPN-24

PPN-24 was taken as an example for stability test. The high thermal stability of PPN-24 was confirmed by thermogravimetric analyzer (TGA) measurement. During the departure of the guest molecules below 70 °C, about 10% weight loss was observed. From the phase transition a decomposition temperature of around 320 °C is observed for the fresh sample. Moreover, the chemical stability was tested through treatment with water. After treatment with water for 36 hours, samples were measured by N_2 sorption at 77K after typical activation procedures. A reduction of the N_2 sorption capacity of less than 15% was observed, suggesting only a slight destroy of framework during these treatments. The excellent chemical stability can be ascribe to the strong covalent-bond connections, which endow the framework with high stability in aqueous solution. Both the thermal and chemical stability of PPN-24 boost their further applications, especially in biomimetic catalysis.

25

3.5 Biomimetic catalysis of ABTS in the presence of H_2O_2 using PPN-24(Fe)

To demonstrate these porphyrin based PPNs are ideal platform for heterogeneous biomimetic catalysis, we post-synthetically modified PPN-24 through the insertion of Fe(III) in porphyrin center. The as-synthesized PPN-24 was mixed with $FeCl_2$ (high reaction rate than $FeCl_3$) in DMF and heated at 100 ^{o}C for 12 hours to afford the catalytically active species PPN-24(Fe). Meanwhile Fe(II) was oxidized to Fe(III) by the oxygen in air. The color of PPN-24 also changed from black to dark red due to the presence of Fe(III) ion. The successful incorporation of iron was confirmed by electron dispersive spectroscopy (EDS), which proves the high density of active iron-porphyrin centers in PPN-24(Fe).

PPN-24(Fe) possesses all the prerequisites for heterogeneous artificial enzymes: a) a high density of active centers; b) excellent chemical and thermal stability; c) low cost and feasible synthetic procedure. As a probe reaction to evaluate the heme protein biomimetic capacity, the oxidation of 2-2'-azino-bis(3-ethylbenzthiazoline-6-sulfonic acid) (ABTS) to $ABTS^{+\bullet}$ by PPN-24(Fe) in the presence of H_2O_2 was examined (Figure 9a).[69-70] The oxidation product can be monitored with the absorbance of the soret band at 418 nm (Figure 9b) by ultraviolet–visible (UV-Vis) spectroscopy.[71] The reaction was performed with 30 mM ABTS, 10 mM H_2O_2, 5.0 mg/mL PCN-24(Fe) in critic buffer at room temperature. The increase of the absorbance at 418 nm well demonstrates the biomimetic activity of PCN-24(Fe) in aqueous environment. Meanwhile, we recorded the color change for the whole process, which changed from colorless to dark green in just 15 minutes (Figure 9c).
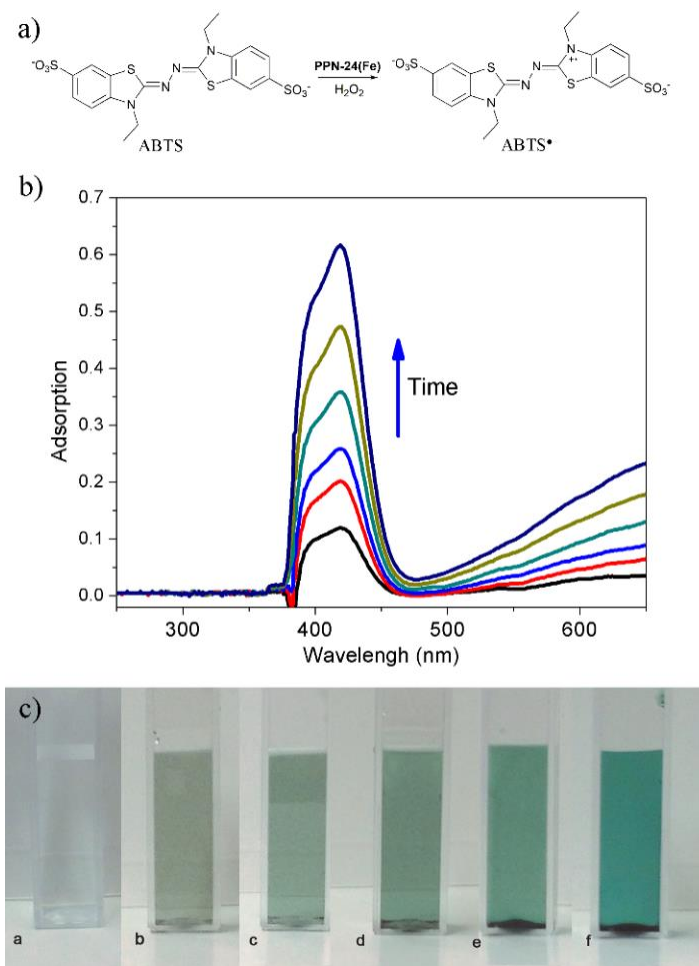
Figure 9. Oxidation reaction of ABTS catalyzed by PPN-24(Fe). a) The oxidation reaction scheme for ABTS in which ABTS is oxidized to ABTS$^{\bullet+}$ by PPN-24(Fe) in the presence of H_2O_2. b) UV-Vis absorbance changes over time for PPN-24(Fe) catalyzed ABTS oxidation, and c) The color changes of solution after (a) 1 min, (b) 3 min, (c) 5 min, (d) 7 min, (e) 10 min, (f) 15 min.

3.6 Summary

In this context, we have successfully demonstrated a facile one-spot synthetic strategy to construct 3D, porous, highly stable PPN-24(Fe), which exhibits great catalytic activity for the oxidation of ABTS. The integration of the high porosity and enhanced

27

thermal and chemical stability in PPN-24(Fe) are beneficial for future studies in the synthesis of biomimetic catalytically active PPN materials.

4. FLEXIBLE ZIRCONIUM METAL-ORGANIC FRAMEWORKS AS BIOINSPIRED SWITCHABLE CATALYSTS*

4.1 Introduction

The enzyme activity is often modulated through feedback loops and a variety of trigger-induced effects,[72] while most of the reactions promoted by artificial catalysts usually process according to the initial reaction conditions. Inspired by nature, chemists are now devoting their efforts to developing catalysts whose activity can be controlled by external stimuli.[73-74] Such systems are capable of alternating the environment of the active center, which in turn regulates the reaction rate and selectivity, functioning as allosteric catalysts.[75-76] However, the field is still in its infancy and the research on engineering stimuli-response molecules with high 'on'/'off' rate ratios, wide substrate scope and the ability to catalyze multiple classes of reaction has still remained a challenge. In this regard, flexible MOFs might be a suitable platform for the development of artificial switchable catalysts in consideration of their inherent cavities and dynamic behaviors.

MOFs are a promising class of highly ordered porous materials with diverse applications in the fields of gas storage/separation, sensing, and catalysis.[2, 8, 10, 77] An increasing number of MOFs with various structures, porosities and framework

---

compositions have been extensively explored in the past decades.[78] Among them, flexible MOFs are especially interesting because they combine crystalline order of the underlying coordination framework with cooperative structural transformability.[79-81] Additionally, they are able to respond to various chemical and physical stimuli such as light, pressure, temperature or guest molecules.[82-85] A prominent example is the so-called "breathing effect" in which the MOF framework experiences a reversible unit-cell dimensional change as a result of host-guest interactions.[86] This leads to unique sorption behaviors which have never been observed in other systems.[87-88] Moreover, the inherent cavities and dynamic behaviors of flexible MOFs are reminiscent of sophisticated biological systems such as regulatory enzymes. In nature, enzyme activity can be tuned by allosteric regulation in which a regulator induces a conformational change in the enzyme and thus a prominent variation in activity (Figure 10a). Likewise, flexible MOFs can allow the host structures to be altered by means of external stimuli, thus potentially blocking or unblocking the catalytic center inside, which resembles an allosteric enzyme in a sense (Figure 10b). Different from other porous materials such as zeolites and activated carbons, flexible MOFs respond to the stimuli with retention of high regularity, which allows for structure characterization by means of crystallography, therefore maximizing understanding of the correlation between the applied stimuli and the ensuing catalytic properties.[89-90]
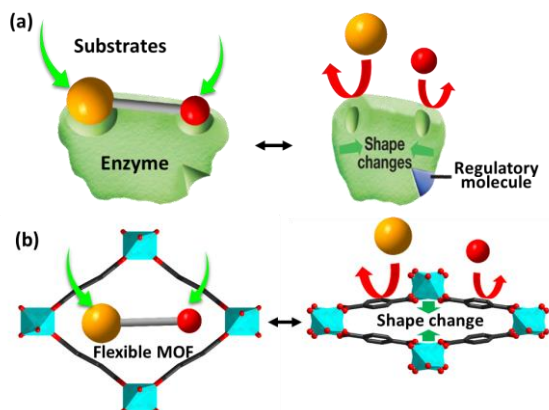
Figure 10. Schematic representation of allosteric enzymes (a) and flexible MOFs (b).

In order to design a switchable MOF catalyst, a highly stable framework with dynamic pore architectures is indispensable. The Zr_6 cluster, in this regard, could be a promising building unit for the construction of switchable MOF catalysts. Firstly, the dihedral angles between the Zr_6 cluster and carboxylate linker vary from 0 to 14.5° in different Zr-MOFs, suggesting extensive flexibility in the Zr–carboxylate junction.[28, 91] Secondly, the Zr_6 cluster can be easily modified with external carboxylate moieties by post-synthesis, providing a rather unique approach to control the breathing behaviors.[92-93] In addition, the terminal -OH^-/H_2O on Zr^{4+} are reported to be strong Lewis acidic sites, endowing the Zr-MOFs with additional catalytic properties.[94] And last but not least, the chemical inertness of Zr_6 clusters make the flexible Zr-MOFs robust platforms for a variety of catalytic applications.[95] Although Zr-MOFs is one of the research focuses in recent years, the reported Zr-MOFs usually show limited breathing amplitude that mainly derived from linker flexibility.[96-97]

Herein, we perform a comprehensive study on structural design, flexibility manipulation, porosity engineering, and catalytic-activity control within a flexible Zr-MOF system. PCN-700-Me$_2$, a flexible Zr-MOF, is initially synthesized through topology-guided design in combination with a kinetically controlled process[35]. The as-synthesized PCN-700 crystals exhibit a significant breathing behavior upon desolvation/solvation with the retention of single crystallinity, which allows us to study the structural transformation by using the single crystal crystallography. A successive single-crystal X-ray diffraction study suggests that the structural transformation occurs in a scissor-jack-like fashion, which involves not only the distortion of the Zr–carboxylate junction, but also the rotation of the carbon–carbon (C–C) bond between two adjacent phenyl rings. Therefore, the breathing amplitude of PCN-700 series can also be modulated through linker design to manipulate the C–C rotation. Moreover, the flexible behaviors are further magnified by subsequent installation of linear carboxylate linkers with different lengths between coordinatively-unsaturated Zr$_6$ clusters, which control the opening and closing of the porosity. Most interestingly, the dramatic contraction of the unit cell along the *c*-axis alters the cavity environment by blocking the Lewis active sites of the Zr$_6$ clusters, an 'off-switch' similar to the effect of regulators on allosteric enzymes. Furthermore, experiments and molecular simulations are conducted to confirm and explain the conformation induced activity change. With the readily tunable flexibility and porosity, as well as switchable catalytic activity in PCN-700 series, a wide range of promising applications can be envisioned.

32

4.2 Results and discussion

4.2.1 Design and synthesis of the parent MOF

Zirconium has been demonstrated to form hexanuclear clusters with diversified connectivity ranging from 6-connected to 12-connected.[98] Among them, the combination of Zr_6 clusters with linear linkers usually gives rise to a rigid **fcu** net, a kind of thermodynamically stable products in which the Zr_6 cluster is 12-connected (Figure 11a).[28] Indeed, the reactions between Zr^{4+} ions and linear linkers such as BDC, BPDC and TPDC (BDC = 1,4-benzenedicarboxylate, BPDC = 4,4'-biphenyldicarboxylate, and TPDC = *p*-terphenyl-4,4''-dicarboxylate) consistently yield the 12-connected **fcu** net (UiO-66, UiO-67 and UiO-68, respectively) under solvothermal conditions. Fundamentally, this phenomenon can be understood through enthalpy changes: the Zr–carboxylate bond formation is a process associated with a negative enthalpy change, dictating that high-connected networks are thermodynamically more favorable than the low-connected ones.[99-100] In order to obtain flexible Zr-MOFs, a topology-guided design is adopted in combination with kinetically controlled synthesis. After careful examination of the **fcu** net, it is clear that the **fcu** net can be turned into a flexible **bcu** net by removing four linkers in the equatorial plane of the octahedral Zr_6 cluster (Figure 11b).[101] The resulting **bcu** net can be expected to shrink along the *c*-axis while expanding within the *ab*-plane by changing the dihedral angles between the Zr_6 cluster and the carboxylate linker (Figure 11c).
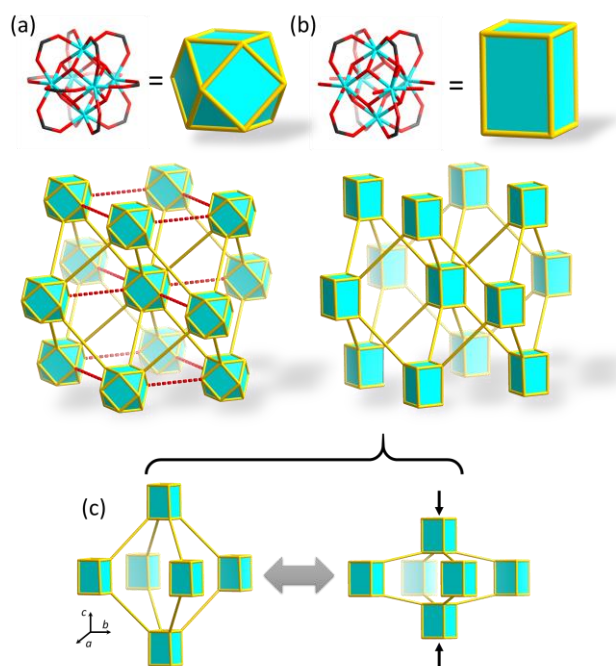
Figure 11. Topology-guided design of PCN-700. (a) fcu net formed with 12-connected nodes; (b) bcu net formed with 8-connected nodes; and (c) a flexible single bipyramid in bcu net shrinking along *c*-axis while expanding within *ab*-plane.

We and other groups have demonstrated that the vertex geometry of MOFs can be controlled by the substitutes on the linkers.[93, 102] For example, bulky functional groups can be introduced on the 2- and 2′-positions of BPDC linker to create steric hindrance, therefore twisted the two carboxylate groups off the coplanar position (Figure 12a and b). Thus, it is necessary for the formation of the **fcu** net to overcome the rotational energy barrier of the two adjacent phenyl rings and form in-plane carboxylates. This will increase the energy battier of **fcu** net formation, as two carboxylate groups on the linker are required to be coplanar in order to give rise to an **fcu** net. As a result, a **bcu** net can be readily obtained at relatively low temperature as a kinetically favorable product,

34

designated as PCN-700-Me$_2$ (Fig. 12d and f). It should be noted that if the reaction temperature is raised to 150 ^{o}C or higher, the **fcu** net will be generated as a thermodynamically preferred product (Fig. 12c and e).

Single-crystal X-ray diffraction (SC-XRD) study reveals that PCN-700-Me$_2$ crystalizes in the tetragonal crystal system with a *P*4$_2$/*mmc* space group (Fig. 12f). Each Zr$_6$ cluster is coordinated to eight (CH$_3$)$_2$-BPDC linkers [(CH$_3$)$_2$-BPDC = 2,2'-dimethylbiphenyl-4,4'-dicarboxylate] and eight terminal -OH$^-$/H$_2$O. The overall structure can be simplified as a **bcu** net which is able to shrink along *c*-axis while expand in the *ab*-plane (Fig. 11d). Usually, the breathing behaviors of MOFs can be triggered by guest molecules. To quantify the structural flexibility, the crystals of PCN-700-Me$_2$ were examined before and after solvent removal by SC-XRD. The result shows that PCN-700-Me$_2$ sustains significant reduction in the *c*-axis parameter (from 14.92 Å to 11.24 Å) and unit cell volume (from 8844 Å^3 to 6933 Å^3) upon solvent removal, which prompts us to gather SC-XRD data for the intermediates during the structural transformation, in the hope of disclosing the breathing mechanism.
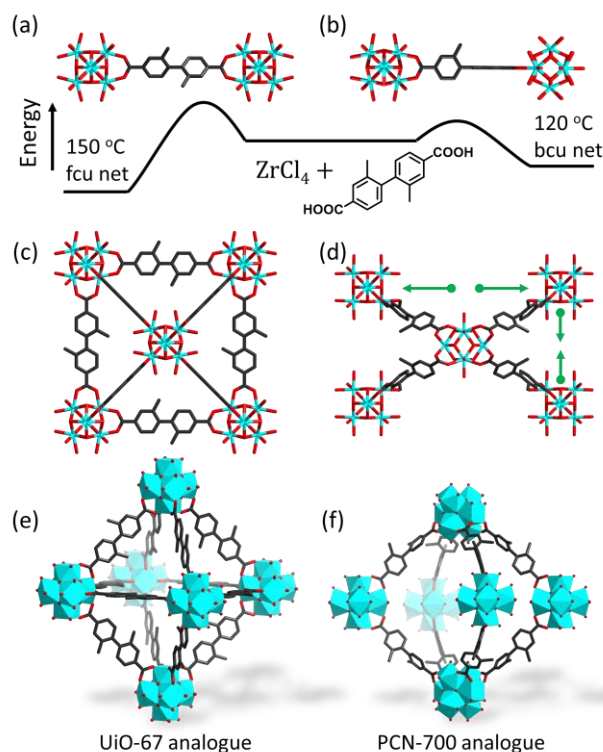
Figure 12. Kinetic control in the synthesis of PCN-700. (a) Linker conformation in fcu structure, a thermodynamic product favored at high temperature (150 °C); (b) linker conformation in bcu structure, a kinetic product favored at relatively lower temperature (120 °C); (c) fcu structure viewed in the *c*-axis direction; (d) bcu structure viewed in the *c*-axis direction. Green arrow indicates the contraction mode; (e) overview of fcu structure; and (f) overview of bcu structure.

4.2.2 SC-XRD investigation of structural evolution

The most distinctive advantage of MOFs is their long-range ordered crystalline nature, which can provide a unique insight into the structure-property correlation by means of crystallography.[103-104] However, most flexible MOF crystals tend to crack upon desolvation, necessitating the characterization of the structural changes by sophisticated *in situ* PXRD techniques.[105-106] The robust PCN-700, on the other hand, retains high crystalline quality after solvent removal/incorporation, which provides an ideal platform

36

to gather accurate SC-XRD data for the intermediates during the structural changes in order to shed light on the breathing mechanism.

With this in mind, we carried out successive SC-XRD analyses on PCN-700-Me$_2$ during desolvation, generating "snapshots" for the breathing process. Crystallographic data clearly shows that PCN-700-Me$_2$ exhibits a scissor-jack-like behavior, shrinking along the c-direction by tweaking the metal–linker conjugation angle (Figure 13a). A significant decrease in c-axis parameter (from 14.92 Å to 11.24 Å) and a slight increase in a/b-axis parameter (from 24.35 Å to 24.84 Å) are also observed upon guest removal. The flexible Zr–carboxylate connection, acting as a hinge, is primarily responsible for the breathing behavior. As shown in Figure 13f, PCN-700-Me$_2$ undergoes a large conformational change which is associated with the bending of Zr–O–C angle (from 133° to 130°) and, more intuitively, the varying dihedral angle between the equatorial plane of O–Zr–Zr–O and the plane of carboxylate (from 10° to 32°). The bending of Zr–carboxylate bond affords a closer packing along c-direction, which gives rise to a shrinkage of the c-axis. A closer investigation indicates that the breathing motion of PCN-700-Me$_2$ is a collective result. Along with the bending of Zr–carboxylate bond, we also observe a rotation of C–C bond between two phenyl rings, which alleviates the steric hindrance within the structure by arranging the two methyl groups on adjacent linkers as far apart as possible. As a collateral effect of the rotation of the C–C bond, the Zr$_6$ cluster tilts about 14° (Figure 13d), eliminating the mirror planes originally passing through Zr$_6$ clusters. Although the reduced symmetry changes the unit cell assignment, all of the derivative structures in this work are still assigned with same unit cell as in pristine PCN-700-Me$_2$

to clearly illustrate the structural transformation. An overlap of structural conformations during desolvation (Figure 13g) underlines the fact that the bending of Zr–carboxylate junction and the conformational change of the organic linker together account for the breathing behavior of PCN-700-Me$_2$.
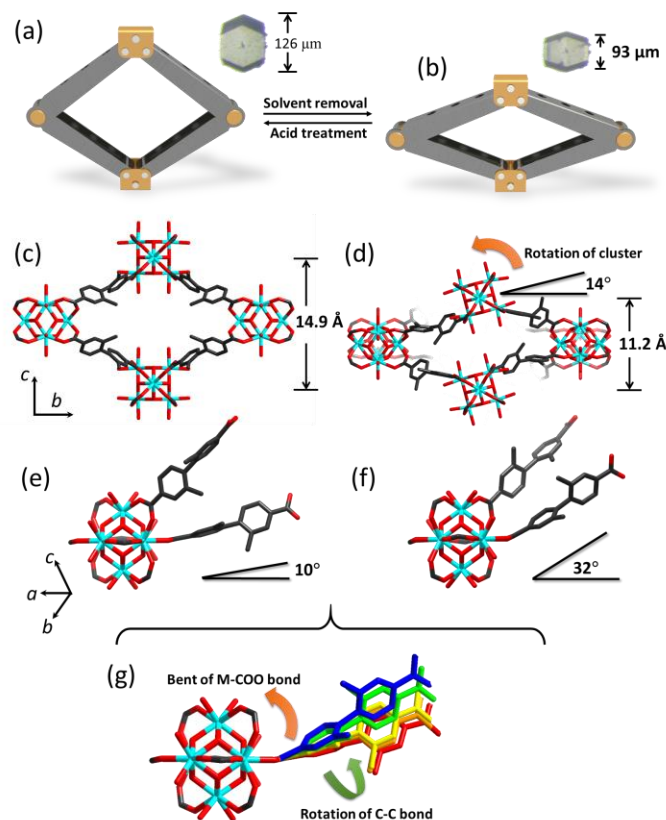
Figure 13. SC-XRD study of the breathing behavior. (a) and (b) Graphic representations of PCN-700-Me$_2$ structures before and after desolvation. Inserted photos are the microscope view of the respective single crystal, manifesting the exceptionally large *c*-axial breathing. (c) and (d) Crystal structures of PCN-700-Me$_2$ before and after desolvation. Orange arrow indicates the rotation of cluster. (e) and (f) A close view of linker conformation before and after desolvation. And (g) an overlap of structural conformations during desolvation.

It should be noted that the axial breathing amplitude of PCN-700-Me$_2$ is much larger than the volumetric breathing amplitude, which is rare among the reported flexible MOFs. For example, the largest axial breathing amplitude is 100% in MIL-88D, while its volumetric breathing amplitude is 230%.[107] In contrast, the **bcu** network expands across the *ab*-plane and simultaneously shrinks along the *c*-axis, or vice versa, which magnifies the axial rather than volumetric breathing amplitudes. PCN-700-Me$_2$ is a unique case with exceptionally large axial breathing, so much that the nearly uniaxial breathing behavior can be directly observed on a real crystal under a microscope (Figure 13a and b). One particular pristine PCN-700-Me$_2$ crystal was measured with a length of 126 µm along *c*-axis (*c*-direction is determined by Apex 2), it shrank to 93 µm upon activation (35% contraction, determined by Zeiss AxioImager.M2 Microscope). These values match very well with the cell parameters determined by SC-XRD (32% contraction, determined by Apex 2). Such high elastic behavior in macroscopic single crystals is rarely observed to the best of our knowledge.[108]

4.2.3 Modulate MOF flexibility through linker design
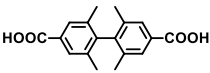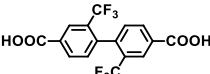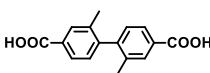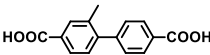
The SC-XRD investigation of the breathing mechanism manifests the structure-property correlations, which further enable us to judiciously modulate the flexibility of the PCN-700 system. Since PCN-700-Me$_2$ undergoes unit-cell dimensional contraction along *c*-axis, which involves a rotation of the C–C bond between phenyl rings, we speculate that the framework flexibility can be tuned by changing the substituents on the phenyl rings of the linker. Linkers with bulky substituents will form a relatively rigid framework because

the substituents repel each other along *c*-axis which hinders the structural contraction. Meanwhile, the C–C bond rotation will also be restrained due to the steric hindrance of the substituents, which further rigidifies the framework. To tune the breathing amplitude, linkers with substituents of different bulkiness were synthesized, and designated as H_2Me_4-BPDC (2,2',6,6'-tetramethylbiphenyl-4,4'-dicarboxylic acid), $H_2(CF_3)_2$-BPDC (2,2'-bis(trifluoromethyl)-biphenyl-4,4'-dicarboxylatic acid), and H_2Me-BPDC (2-methylbiphenyl-4,4'-dicarboxylic acid) (Table 2). As expected, H_2Me_4-BPDC and $H_2(CF_3)_2$-BPDC give rise to MOFs with dramatically increased structural rigidity because of the elevated steric hindrance. Among them, PCN-700-Me_4 exhibits the highest degree of rigidity while only small changes along *c*-axis (15.36 Å to 14.08 Å) and unit cell volume (9008 $Å^3$ to 8170 $Å^3$) were observed upon desolvation.

Intuitively, linkers with less bulky substituents tend to form more flexible MOF structures, as demonstrated in MIL-53 and MIL-88 systems.[109-110] However, this is not always the case because steric effect could possibly lead to different framework topologies.[111] As in the case of PCN-700 system, the substituents on the phenyl rings are required to be large enough to provide two off-plane carboxylate groups in order to form the **bcu** structure. As far as steric hindrance is concerned, H_2Me-BPDC is expected to generate an even more flexible MOF than PCN-700-Me_2. While H_2Me_2-BPDC produces PCN-700 analogue when reacting with $ZrCl_4$, however, only the UiO-67 isostructure was obtained by using H_2Me-BPDC under identical synthetic conditions. Clearly, the steric hindrance between the methyl group and hydrogen can be readily overcome under the solvothermal conditions, therefore the thermodynamic product, **fcu** net, is formed. In order

to obtain a **bcu** net, at least one methyl group needs to be preinstalled on each phenyl ring of the linker. By far, PCN-700-Me$_2$ is the most flexible one we obtained with the PCN-700 structure.

Table 2. Linkers utilized to tune the breathing amplitude.

Linker	Topology	In DMF			Without solvent			Δc/	ΔV/
		c / Å	a / Å	V / Å^3	c / Å	a / Å	V / Å^3	%	%
HOOC— —COOH **H$_2$Me$_4$-BPDC**	**bcu**	15.36	24.22	9008	14.08	24.08	8170	9.09	10.3
HOOC— CF$_3$ —COOH F$_3$C **H$_2$(CF$_3$)$_2$-BPDC**	**bcu**	15.00	24.40	8930	12.09	24.67	7352	24.1	21.5
HOOC— —COOH **H$_2$Me$_2$-BPDC**	**bcu**	14.92	24.35	8844	11.24	24.84	6933	32.7	27.6
HOOC— —COOH **H$_2$Me-BPDC**	**fcu**	-	-	-	-	-	-		

4.2.4 Magnify breathing amplitude through linker installation

With the most flexible PCN-700-Me$_2$ in hand, we intend to explore its breathing amplitude. Since PCN-700-Me$_2$ crystals shrink upon the removal of guest, we propose that they could swell if the guest-host interaction is strong enough. Indeed, some solvents are reported to induce a large swelling of flexible MOFs. For instance, the structure of MIL-

88C can be completely opened up by diethylformamide, generating a huge increase in cell volume of about 170%. However, PCN-700-Me$_2$ shows a very limited dependence on the solvents; only slight changes in unit cell parameters (from 15.40 Å to 14.17 Å) were observed in various solvents such as water, methanol, hexane, dichloromethane, acetone, isopropanol, dimethylformamide (DMF), acetonitrile, and diethylformamide. For most of the flexible MOFs, the desolvated sample with a shrunken structure usually can be restored by soaking in solvents. But the desolvated PCN-700-Me$_2$ maintains its structure in common solvents at room temperature and is reversed by treating with trifluoroacetic acid/DMF solution. In this sense, PCN-700-Me$_2$ solid can be considered as 'rigid' under common solvents. This is tentatively attributed to the existence of hydrogen interaction between terminal OH$^-$/H$_2$O groups from adjacent clusters and the rigid nature of M^{IV}–carboxylate conjunctions. Compared with M^{II}-and M^{III}-based MOFs, the M^{IV}-based MOFs usually shows a higher degree of rigidity possibly due to the stronger M^{IV}–carboxylate interaction,[112] so that the weak van der Waals interactions between solvent molecules and framework is not strong enough to open up the structure. In order to open up PCN-700-Me$_2$, we need guest molecules that interact strongly with the framework. Given that the 8-connected Zr$_6$ cluster can bind to carboxylate moieties through coordination bonds,[113-115] we speculate that the structure of PCN-700-Me$_2$ can be opened up by carboxylates as guests. In our previous work, we have demonstrated that linear carboxylate linkers with proper lengths can be installed between neighboring Zr$_6$ clusters by replacement of terminal OH$^-$/H$_2$O ligands (Figure 14).[93] Herein, we use linker installation method to explore the possible breathing amplitude of PCN-700-Me$_2$.

42
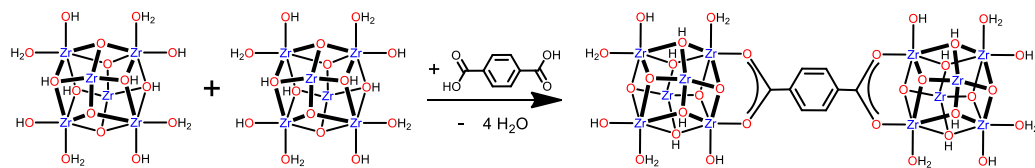
Figure 14. Schematic representation of linker installation process.

To carry out linker installation, PCN-700-Me$_2$ crystals are exposed to a DMF solution of linear linker at 75 °C for 24 h. Four linear linkers with different lengths, namely FA (fumarate), BDC (1,4-benzenedicarboxylate), NDC (2,6-napthalene dicarboxylate) and BPDC (4,4'-biphenyldicarboxylate), have been successfully installed in PCN-700 respectively. By virtue of high stability, single crystal to single crystal transformation can be realized which enabled us to uncover structures of resulting MOFs *via* SC-XRD. The existence and position of subsequently installed linkers are unambiguously observed in the crystallographically resolved structures. As shown in Figure 14b, the subsequently installed linkers bridge adjacent clusters together along the *c*-axis. Each cluster is 10-connected with eight original Me$_2$-BPDC and two new linkers. The resulting MOFs after linker installation can be formulated as Zr$_6$O$_4$(OH)$_6$(H$_2$O)$_2$(Me$_2$-BPDC)$_8$L$_2$ where L stands for the different installed linkers. From the topological point of view, the overall structure is transformed to a rigid **bct** net from a flexible **bcu** net. As illustrated in Figure 15a, the subsequently installed linkers support the MOF structure as the jack screws support the scissor jack. As a result, four rigid MOFs with gradually changed cell parameters are derived from the flexible parent MOF. The channel size along *a*-axis is directly correlated

to the linker length. The length of FA (4.95 Å) is shorter than the distance between adjacent Zr_6 clusters in pristine PCN-700-Me$_2$ (6.98 Å) so that the installation of FA squeezes the structure. The installation of BDC linker did not change the unit cell parameter by a large amount, whereas the NDC and BPDC open up the structures. These results are reinforced by PXRD patterns and N_2 isotherms (Figure 15d). Because of the uniaxial breathing mode of PCN-700-Me$_2$, the 1D channel that perpendicular to the *ab*-plane has hardly changed regardless of the large breathing amplitude (Figure 15c and e).

Similar to a scissor jack that can be lifted and lowered by driving screws, the crystal height along *c*-direction, parallel to the *c*-axis parameter, can also be precisely controlled by changing the lengths of installed linkers. For comparison, one batch of crystals with identical size are picked and installed with different linkers respectively. We show that the cell parameters along *c*-axis is tunable in a range of 11.8 Å to 19.1 Å, and the crystal height (*c*-direction) varies from 101 µm to 156 µm. As shown in Figure 15, the change of crystal size matched very well with the change of cell parameters.

It is worth pointing out that the linker installation can induce a much larger unit cell dimension change (62% contraction along *c*-axis) than the removal of solvent (32% contraction along *c*-axis), indicating that a larger breathing amplitude can be achieved by stronger guest–host interactions such as coordination bonds.
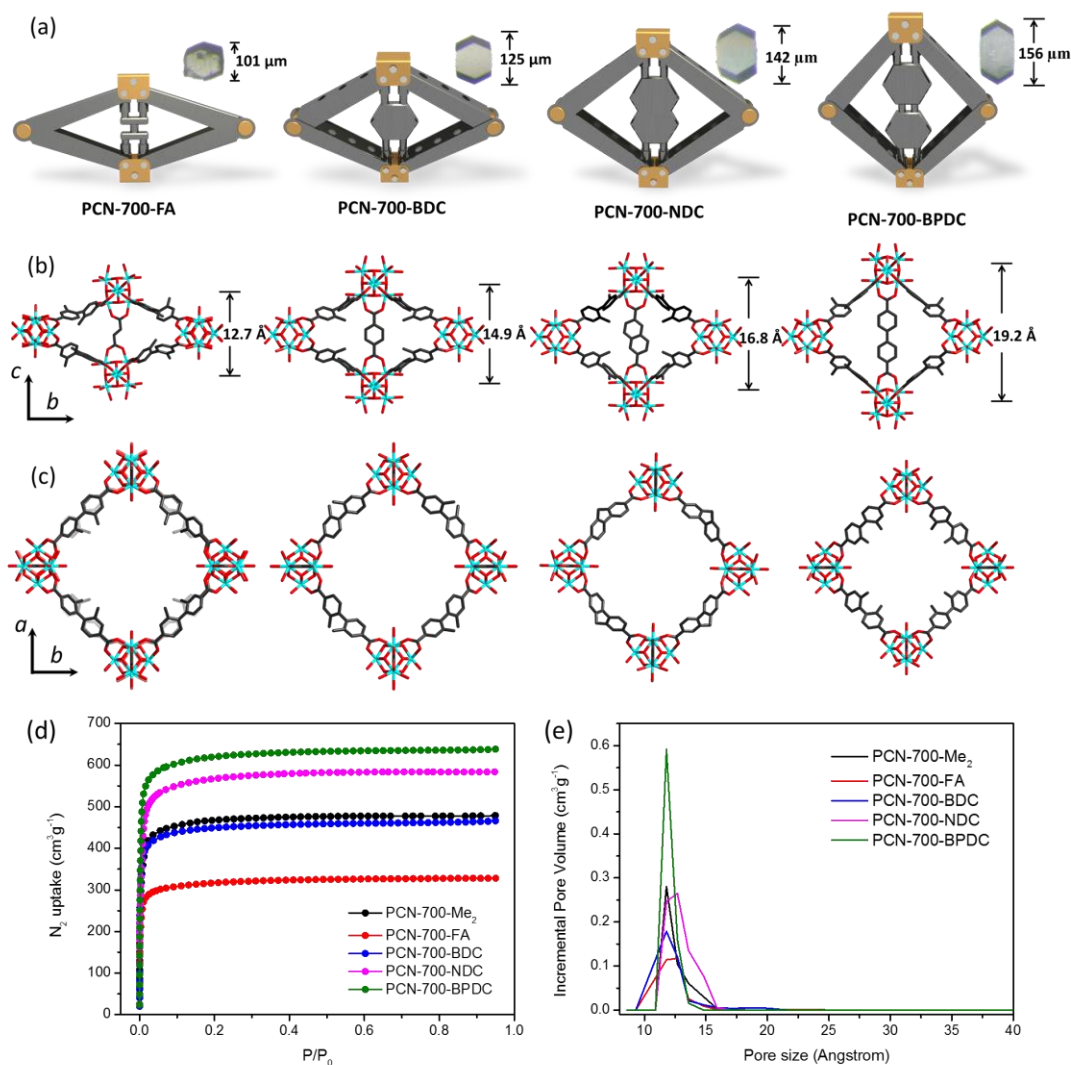
Figure 15. Porosity engineering by linker installation. (a) Representations of PCN-700-Me₂ structures with different linkers installed. Inserted photos are the microscope view of the corresponding single crystal. (b) Single crystal structures PCN-700-Me₂ with different linkers along *a*-axis showing dramatic change of *c* lattice parameter. (c) Single crystal structures PCN-700-Me₂ with different linkers along *c*-axis showing the slight change in 1D channels. (d) and (e) N₂ isotherms and pore size distribution of PCN-700-Me₂ and derivates.

4.2.5 Reversible control of catalytic activity

Flexible MOFs, with inherent cavities and dynamic behaviors, are expected to possess interesting properties as host matrices for catalysts. For example, the stimuli-induced structural transformation may change the cavity environment and in turn influence the catalytic activity of the encapsulated catalyst, which is a potential mimic of allosteric regulation. In other words, the surrounding environment of the catalytic sites in a MOF performs a similar function to the enzyme pocket in enzymatic catalysis. Nevertheless, flexible MOFs for switchable catalysis have not been widely explored. This could be ascribed to the fact that the close-conformation of flexible MOFs can be opened up by solvent molecules under common catalytic conditions. In contrast to most flexible MOFs, the desolvated PCN-700-Me$_2$ sample shows little dependence on the nature of solvent. In fact, it hardly expands in any common solvents at room temperature. These observations suggest that PCN-700-Me$_2$ solid can be considered as 'rigid' under common catalytic reaction conditions. The closed conformation and opened conformation is expected to show dramatically different catalytic activity in the same solvent.

The atom-economical cycloaddition reactions of CO_2 with epoxides yield cyclic carbonates, which have wide applications in pharmaceutical and chemical industry. As a proof of concept, this reaction is selected to evaluate the Lewis-acid catalytic activity of PCN-700-Me$_2$. The performances of as-synthesized PCN-700-Me$_2$ (denoted as PCN-700-o, o stands for open conformation) and desolvated PCN-700-Me$_2$ (denoted as PCN-700-c, c stands for closed conformation) samples were examined with different epoxides at 50 ^{o}C under 1 atm CO_2 pressure and solvent-free condition (Table 3). In order to eliminate

the possibility of size selectivity, substrates with small sizes were selected to ensure negligible pore diffusion that might affect the reaction rates under the given set of reaction conditions. Propylene oxide conversion steadily increased from 36% to 90% as the reaction time elapsed from 2 to 10 h and then levelled off. So the reaction time is set to be 10 h for all the catalysts. Considering the mild reaction condition, solvent free protocol and high TON/TOF, PCN-700-o stands out from the reported MOFs for catalyzing the cycloaddition reaction of CO_2. Importantly, the activity of PCN-700-o can be turned off by the removal of solvent. As shown in Table 3, the desolvated sample, PCN-700-c, shows prominently decreased performance. Yet, the catalytic activity of PCN-700-c can be restored by acid treatment which expands the shrunken structure to the original state. In this way, the reversible control of catalytic activity through a breathing effect is realized. The catalytic activity of PCN-700-Me$_2$ was turned on and off for four times, demonstrating a successful reversible control of the catalytic activity towards CO_2 fixation reaction (Figure 16).

Table 3. Catalytic synthesis of cyclic carbonates from CO_2 and epoxides.[a]

1a-1d
R = Me (a), Ph (b), Et (c), CH_2Cl (d)

2a-2d
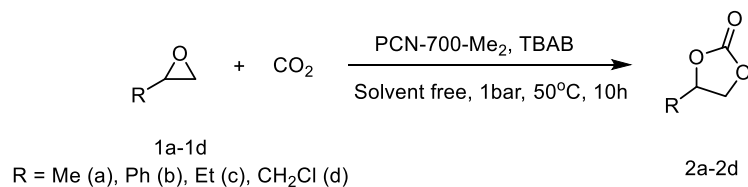
Entry	R	Catalyst	Conversion(%)[c]	TON[d]	TOF(h^{-1})[e]
1	Me	-	15.1	-	-
2	Me	$ZrCl_4$[b]	67.9	131.8	13.2
3	Me	PCN-700-o	93.2	244.0	24.4
4	Me	PCN-700-c	29.1	76.2	7.6
5	Ph	PCN-700-o	83.3	218.0	21.8
6	Ph	PCN-700-c	37.0	96.9	9.7
7	Et	PCN-700-o	91.7	240.0	24.0
8	Et	PCN-700-c	27.5	72.0	7.2
9	CH_2Cl	PCN-700-o	92.3	241.6	24.2
10	CH_2Cl	PCN-700-c	30.2	79.0	7.9

[a] Typical reaction conditions: 5.0 mmol epoxides, 0.3 mmol TBAB, 6.0 mg PCN-700 (0.0191 mmol Zr), under CO_2 balloon, reaction temperature 50 °C, reaction time 10 h. [b] 6.0 mg $ZrCl_4$. [c] Conversion calculated from the ^1H NMR spectra. [d] Turnover number (product (mmol)/metal (mmol)). [e] Turnover frequency (product (mmol)/metal (mmol)/time (h)).
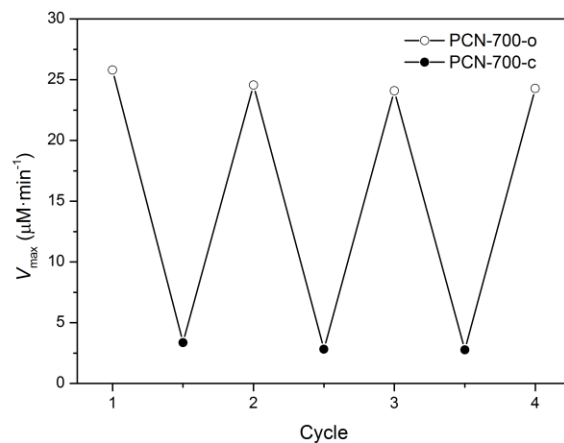
Figure 16. Reversibility test of PCN-700-Me$_2$ catalyzed cycloaddition reaction of CO$_2$ with propylene oxide at 50 °C for 10 h.
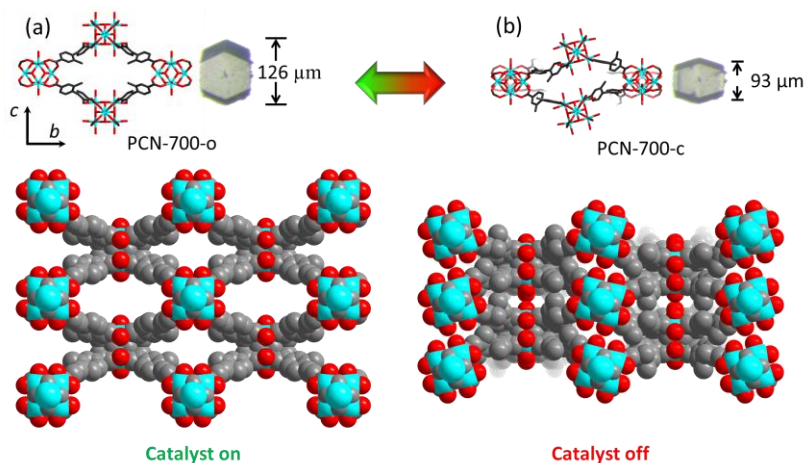
Figure 17. Structure of PCN-700-o (a) and PCN-700-c (b) showing the accessibility of active -OH$^-$/H$_2$O center (as shown in red).

In order to elucidate the mechanism of the switchable catalytic activity, control experiments were further conducted. The difference in catalytic activity of PCN-700-o and PCN-700-c could be possibly attributed to (i) different diffusion rates of substrate and (ii) different Lewis acid sites. To eliminate the influence of substrate diffusion, V_{max},

49

represents the maximum rate achieved by catalysts at saturating substrate concentrations, was measured. V_{max} of PCN-700-o and PCN-700-c was calculated to be 25.8 and 3.35 $\mu M \cdot min^{-1}$ respectively, showing a clear difference in maximum reaction velocity. Usually, V_{max} depends on the efficiency and concentration of active sites, which is believed to be the $-OH^-/H_2O$ groups on the Zr_6 clusters.[94] To prove this, control experiments were carried out under the same condition using UiO-67 as a Lewis acid which has no accessible $-OH^-/H_2O$ groups on the clusters. The V_{max}(UiO-67) was tested to be 2.19 $\mu M \cdot min^{-1}$ which is about 11 times smaller than V_{max}(PCN-700-o), indicating the prominent influence of $-OH^-/H_2O$ groups. In PCN-700 structure, there are two pairs of symmetrically independent $-OH^-/H_2O$ groups on one Zr_6 cluster along c-direction and b-direction, respectively. The $-OH^-/H_2O$ groups along c-direction and b-direction in PCN-700-o are both accessible by substrates (Figure 17a) whereas $-OH^-/H_2O$ groups in PCN-700-c are only accessible from b-direction because of the close packing of ligand and clusters along c-direction, leaving no room for substrates (Figure 17b).

The halved active site in PCN-700-c is expected to reduce the V_{max} by half. However, the experimental data suggested that the V_{max} (PCN-700-c) is actually reduced by 87% compared to that of V_{max} (PCN-700-o). We propose that the $-OH^-/H_2O$ groups along c-direction are more active than those along b-direction, thus burying the $-OH^-/H_2O$ groups along c-direction caused a dramatic decrease of catalytic activity for PCN-700-c. Indeed, we observed that the $-OH^-/H_2O$ groups along c-direction selectively deprotonate to react with basic metal hydroxides, whereas the $-OH^-/H_2O$ groups along b-direction tend to act as bases to react with molybdic acid. To test our hypothesis, we used density

50

functional theory to calculate the relative acidities of Zr_6 models of PCN-700-o and PCN-700-c. The calculated ΔpK_a value for the PCN-700-o-Zr_6 model (the pK_a of $-OH^-/H_2O$ along the *b*-direction minus that along the *c*-direction) is 0.56. Similarly, this ΔpK_a value for the PCN-700-c-Zr_6 model is 2.82. The stronger acidity of $-OH^-/H_2O$ along the *c*-direction than that along the *b*-direction is consistent with the experimental observations above-mentioned. The different acidity in the two directions can be tentatively attributed to the unequal electron distribution resulting from the asymmetric organic linkers. Consistent with this explanation, the asymmetric character is more notable in PCN-700-c than that in PCN-700-o, which explains the larger ΔpK_a value of PCN-700-c-Zr_6 than that of PCN-700-o-Zr_6. In addition, the calculated ΔpK_a value along the *b*-direction for the closed and open Zr_6 models (pKa of $-OH/H_2O$ in *b*-direction of PCN-700-c-Zr_6 minus that of PCN-700-o-Zr_6) is 1.55. Thus, the remarkable decrease of acidity along the *b*-direction, as well as the only availability of the *b*-direction for catalysis in PCN-700-c, results in a much lower catalytic activity of PCN-700-c than that of PCN-700-o. In short, upon removal of solvent, PCN-700-Me$_2$ experiences a dramatic shrinkage along *c*-axis which changes the cavity environment and catalytic activity. From what we observed, we consider this unique function as a simple mimic of complicated allosteric enzymes, allowing manually control of catalytic properties.

4.3 Conclusions

We present here a comprehensive study on a flexible Zr-MOF system as a switchable catalyst. The parent structure (PCN-700-Me$_2$) is constructed through topology-

guided design in combination with kinetically controlled synthesis. Single crystal X-ray diffraction was employed to study the mechanism of the structural transformation, which reveals that PCN-700-Me$_2$ squeezes its unit cell along *c*-axis in a scissor-jack-like fashion. Organic linkers with different functional groups are utilized to rationally adjust the framework flexibility. A linker installation strategy is further exploited to magnify the breathing amplitude. Furthermore, the activity of PCN-700-Me$_2$ as a Lewis acid catalyst can be turned on and off by structural breathing, making it a bioinspired switchable catalyst. In light of its tunable flexibility and porosity, as well as switchable catalytic activity, PCN-700 system can be expected to serve as a versatile platform for a variety of promising applications. We believe that the concept of switchable catalysis within flexible MOF systems will not only lead to a new generation of catalysts, but also open up a field of study intersecting with both crystalline porous materials and artificial enzymes.

5. HYDROGEN STORAGE IN METAL-ORGANIC FRAMEWORKS*

5.1 Introduction

The concerns of energy resource consumption from fossil fuel use, related global warming has gained momentum to develop sustainable energy carriers such as hydrogen gas (H_2). The energy density of hydrogen is much higher than petroleum such as gasoline and the combustion of hydrogen emits no carbon dioxide (CO_2). However, the application of H_2 as fuel in transportation would limited if there is not an effective storage technology due to its volatile nature. The currently used liquid fuels, such as gasoline and diesel, can be easily stored in simple tanks at ambient condition. A gaseous fuel, such as hydrogen poses a real challenge because up to 13 kg of hydrogen would be consumed per trip of 450 km driven, suggesting safe hydrogen storage and transport technologies are critical in the 21st century. In general, hydrogen can be stored in through compression or entrapped. The former by liquefaction or isothermal compression and the latter by storage in solid porous materials.[116-117] Based on the interaction strength between the hydrogen molecules and the framework, the storage methods usually can be divided into two categories: chemisorption and physisorption.

According to the International Union of Pure and Applied Chemistry (IUPAC), chemisorption is defined as "the adsorption that results from strong interactions, such as

chemical bond formation between the hydrogen and the material". The physisorption is the "adsorption in which the non-chemical bonding forces involved is van der Waals forces, which do not involve a significant change in the electronic orbital patterns of the species involved". In physisorbed materials, hydrogen molecules are normally adsorbed on the pores' surface of the materials. Since the interaction energy is very low and no activation energy is needed, the physisorption processes are usually reversible. The H_2 adsorption inside the porous materials such as metal-organic frameworks, porous carbons,[118-119] organic polymers[120-121] and zeolites[122-123] belongs to this category. Much research has been focused on the synthesis of highly porous materials with enhanced interactions with hydrogen.

In the past few decades, metal-organic frameworks (MOFs),[2, 84, 121, 124-126] constructed with coordination bonds between organic linkers and inorganic metal clusters, have become a burgeoning field of research and a great potential candidate for hydrogen storage due to their exceptional high porosity, high crystallinity, uniform yet tunable pore size and pore shape, great diversity and various kinds of hydrogen occupation sites. The U.S. Department of Energy (DOE) 2017 target for a hydrogen storage system, is set at "5.5 weight-percent gravimetric capacity, 40 g L^{-1} of volumetric capacity at an operating temperature of -40 to 60 °C under a maximum delivery pressure of 100 bar".[6] It is very important to be aware that the targets are for an entire system, so the performance of the storage material must be even better in order to account for the storage container as well as temperature regulating apparatus. In 2003, the initial H_2 storage data, a remarkable 4.5 wt % at 77 K and 1 atm, were demonstrated by MOF-5, which was synthesized by Zn

ionic salt and beneze-1,4-dicarboxylate (BDC) ligand.[18] The maximum H_2 uptake in MOF-5 varied from 1.3 to 5.2 wt% at 77 K depending on fabrication and activation parameters. Since then, numerous reports of porous MOFs with different topologies and porosities have demonstrated relatively high H_2 storage. Coupled with measurements of porosity, some understanding of many factors that affect the hydrogen uptake by porous MOFs have been developed.

A number of monographs have been devoted to meta-organic frameworks (MOFs) fabrication, activation and use as hydrogen storage materials.[127-131] Here, some technical elements are introduced in tailoring MOFs as hydrogen storage resins, including syntax, synthesis, fabrication, evaluation and benchmark testing. As way of example, MOFs constructed by carboxylate, azolate or mixed linkers, are discussed in the context of hydrogen storage. Last but not least, the post-synthetic modifications on MOF materials to increase the hydrogen storage capacities will be carefully illustrated. [6, 132-134]

5.2 Syntax used for hydrogen storage

As it is already mentioned in the introduction, there is a great need to standardize definitions and terminologies before we explore the hydrogen storage in MOFs.

5.2.1 Adsorption or absorption

Adsorption (Figure 18a) refers the adhesion of atoms, ions, or molecules to a surface while absorption (Figure 18b) is a physical or chemical process in which atoms, ions or molecules permeation through the bulk volume of the materials and incorporated

into the internal structure of the adsorbent. From the figure, it can be seen that the adsorption requires a large surface area to be effective.
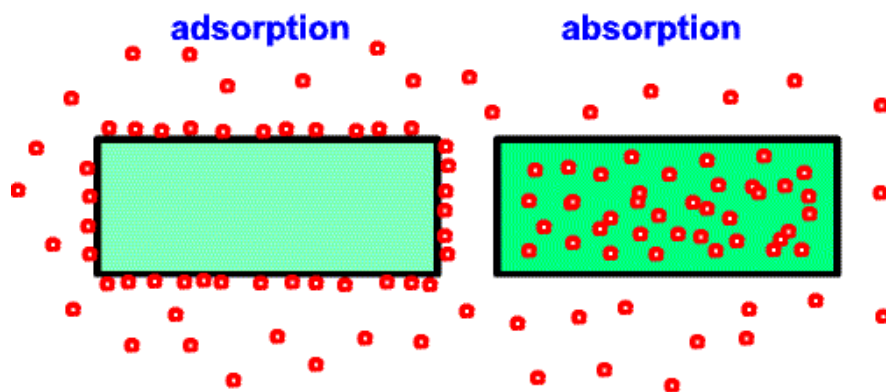
Figure 18. A simplified schematic of adsorption versus absorption.

5.2.2 Chemisorption and physisorption

Chemisorption is a process which involves a chemical reaction between the surface and the adsorbate while new chemical bonds are generated at the adsorbent surface. Usually, chemisorption only occurs in a monolayer on the surface. Physisorption, also called physical adsorption, is a process in which the force involved are the weak intermolecular van der Waals forces. The physisorption is normally multilayer adsorption, which highly depends on the temperature and pressure. There is no hard boundary between the physisorption and the chemisorption and the H-H bond is treated as a distinction. If the H-H bond is destroyed in the sorbed state, then it is considered chemisorption; otherwise, it is a physisorption phenomenon. In general, the binding energy threshold is about 0.5 eV per adsorbed species to differentiate the process of physisorption and chemisorption.

56

5.2.3 Langmuir surface area and BET surface area

Porous materials can be classified by their pore sizes into three categories, macroporous (> 500 Å), mesoporous (20-500 Å) and microporous (< 20 Å). The microporous materials can be further classified as: ultramicroporous (< 7 Å) or supermicroporous (8-20 Å). Most MOFs reported so far are microporous materials, while the development of the mesoporous MOFs bursts out recently.

The Langmuir adsorption model (Figure 19a), in which only a monolayer of gas molecules is allowed to adsorb onto the surface, explains adsorption by assuming the adsorbate behaves like ideal gas under isothermal conditions. In the Langmuir model, the following assumptions are proposed specifically for the simplest situation: the adsorption of a single adsorbate onto a series of equivalent sites on the surface.

1. The surface containing the adsorbing sites is homogeneous, which is a perfectly flat plane with no corrugations;

2. The gas molecule adsorbs into an immobile state;

3. All adsorbing sites are equivalent;

4. Each site can hold at most one molecule (mono-layer coverage only); and

5. There are no interactions between adsorbates on adjacent sites.
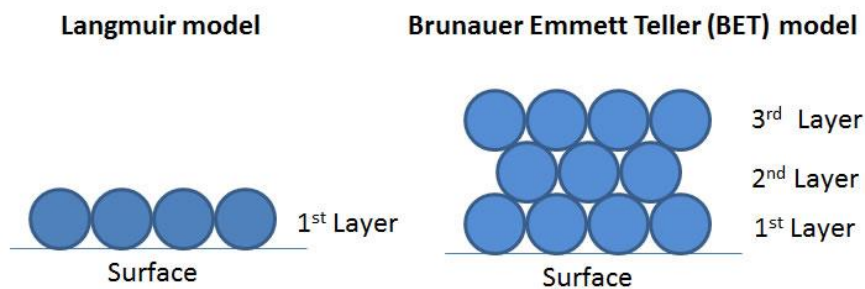
Figure 19. A one-dimensional representation of the process involving adsorption of hydrogen molecule onto a surface, (a) Langmuir model monolayer adsorption, or (b) Brunauer–Emmett–Teller (BET) multilayer adsorption.

The Brunauer, Emmett and Teller (BET) theory was developed by Stephen Brunauer, Paul Emmett, and Edward Teller and they published a paper about the "physical adsorption of gas molecules on a solid surface" in 1938. This BET theory is an extension of the Langmuir theory. The BET model is in which multiple layers of gas may be adsorbed to the surface (Figure 19b). For a given nitrogen isotherm, the BET model will always predict a smaller surface area than the Langmuir model. The BET theory extended the Langmuir theory to incorporate multi-layer adsorption, where the:

1. Gas molecules physically adsorb in infinite layers;

2. The layers are non-interacting; and

3. The Langmuir model is valid for each independent layer.

In the analysis of surface coverage, nitrogen gas is commonly used due to its high purity, gas inertness, low cost (compared to helium) and the strong interactions with most solids. Liquid nitrogen temperature (77K) is usually employed when measuring the nitrogen uptake due to the weak interactions between gaseous and solid phases to achieve

detectable amounts of adsorption. The data collected are displayed in the form of an isotherm, which plots the amount of nitrogen adsorbed as a function of the relative pressure. There are five types of adsorption isotherms possible.[135]

Type I isotherm: Type I isotherm is a pseudo-Langmuir isotherm (Figure 20). Microporous materials with pore diameters less than 20 Å usually have this type of isotherm. This isotherm depicts monolayer adsorption, which can be readily explained by the Langmuir isotherms.

Type II isotherm: A type II isotherm (Figure 20) has a different profile from that obtained from a single layer Langmuir model. At low pressure (concentration), material micropores are filled with gas molecules, such as nitrogen gas. The plateau region represents the formation of the monolayer. At higher pressure, multilayer adsorption occurs and continues until condensation due to capillary forces occurs.

Type III isotherm: A type III isotherm (Figure 20) shows the formation of a multilayer. Since there is no asymptote observed in the curve, no monolayer is formed, but BET is not applicable.

Type IV isotherm: A type IV isotherm (Figure 20) occurs when capillary condensation occurs. At the lower pressures, it shows the formation of a monolayer followed by a formation of multilayers at higher pressure regions. Mesoporous materials with pore diameters between 20 - 500 Å have this type of isotherm.

Type V isotherm: Type V isotherms (Figure 20) are very similar to type IV isotherms and but are not applicable to BET model.

In both Type IV and V isotherms, phenomenon of capillary condensation of gas can be seen.
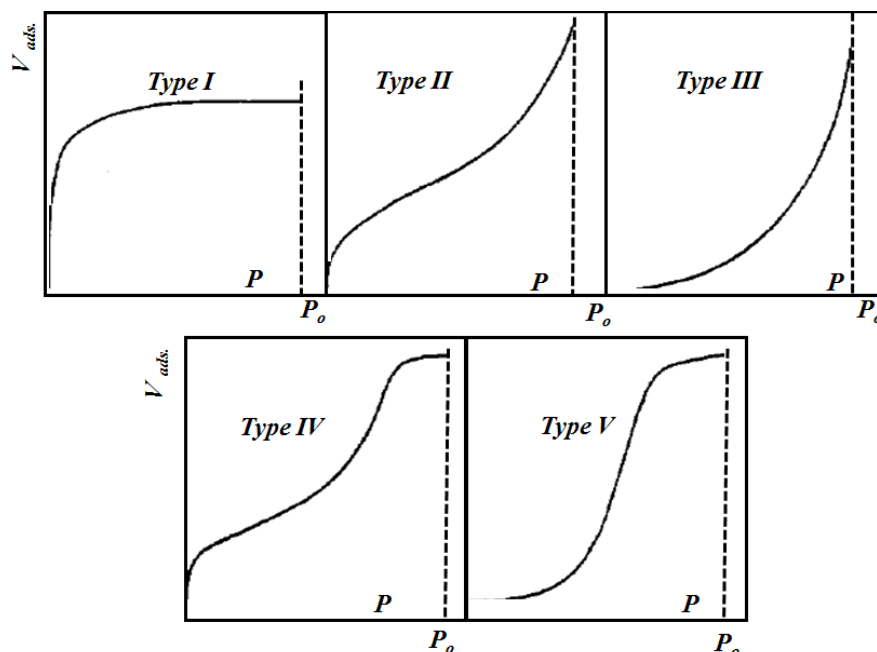
Figure 20. The type I-V isotherm plots the gas volume adsorbed as pressure increases (where P_o stands for saturation pressure). Reprinted from ref.[135].

When using the BET model to calculate the surface area, special care needs to be taken since the calculation results highly depend on the selected pressure region.[136] The Grand Canomical Monte Carlo (GCMC) simulation has been developed to calculate the BET surface area using the nitrogen isotherm and the results have already been confirmed by comparing with the experimental results.[137] In addition, the difference between the Langmuir surface area and the BET surface area becomes smaller if the MOFs have a

larger crystal density. In other words, when the void volume increases, the difference between the Langmuir and BET surface area becomes significant.

5.2.4 Excess and total adsorption amount of hydrogen

The hydrogen uptake is usually represented as the excess or total adsorption amount. The excess adsorption is the difference between the gas phase hydrogen which would be presented in the equal volume of the adsorbed phase with and without the adsorbent.[138] As we all know, the hydrogen gas density increases as pressure increases. Hence, the excess adsorption would reach saturation at high pressure and then decrease. So we can conclude that at lower pressures, the excess and total adsorption amounts are very close. The total adsorption of hydrogen can be calculated from the excess adsorption isotherm and the total skeletal volume of the adsorbents.[139]

The total amount of adsorbed gas can be expressed as follows.[140]

$$N(total) = N(excess) + d(gas) * V(pore) \tag{1}$$

where *N(total)* is the total adsorption (mg g^{-1}), *N(excess)* is the excess adsorption (mg g^{-1}) which is the quantity measured, *d(gas)* is the compressed gas at a given temperature and pressure in g cm^{-3} and V_{pore} is the volume of pores.

Generally, hydrogen adsorption capacities in MOFs can also be represented in wt%, which can be expressed as:

$$wt\% = \frac{mass\ (hydrogen)}{mass\ (sample) + mass\ (hydrogen)} \tag{2}$$

61

5.2.5 Isosteric heat of the hydrogen adsorption

For all the materials, the hydrogen uptake capabilities decrease with the increase of temperature. The strength of this decrease as well as the hydrogen uptake capability at low pressure are mainly governed by the heat of adsorption. Typically, the isosteric heat of hydrogen adsorption can be calculated from the adsorption isotherms measured at two independent temperatures, for example nitrogen at 77 K and argon at 87 K, respectively.[141-142] The isosteric heat of hydrogen adsorption is one of the key thermodynamic variables for the design of a practical hydrogen adsorption samples. However, the small temperature range leads to a very high uncertainty when the heat of adsorption is calculated. Only a few publications presented the isosteric heat of adsorption with higher accuracy from several isotherms measured at various temperatures.

5.3 Engineering novel MOFs for hydrogen storage

Metal-organic frameworks (MOFs) have been fabricated using hydrothermal or solvothermal conditions. The hydrothermal synthetic conditions use water as the solvent while the solvothermal conditions use high boiling point organic solvent, such as *N,N*-dimethylformamide (DMF), *N,N*-diethylformamide (DEF), *N,N*-dimethylacetamide (DMA). Normally, both inorganic metal salts and organic linkers are dissolved in solvents and placed in sealed vials to produce MOFs at high temperature, generally ranging from 60 - 180 °C. Modulating agents, which can balance the association / dissociation of the coordination bonds, are another very important factor in the MOF synthesis, especially for the formation of the crystalline MOFs starting from high valent metal ions. Sometimes,

mixed solvents are utilized to control the reaction polarity, the solubility of the starting materials as well as the rate of the product recrystallization, so that highly crystalline products can be formed. For example, solvents with low boiling point could be added in order to facilitate the product formation during the synthesis. Every MOF is unique and the synthetic conditions usually vary a different MOF materials.

The assembly process of MOFs combines merits of various inorganic metal ions or clusters and designable organic linkers, which offers large structural topologies and diversified porosity properties. For the coordinating atoms in the organic linkers, they can be oxygen, nitrogen and sometimes mixed coordinated atoms in one linker. For the geometry, the organic linkers can be linear, trigonal, and tetragonal and so on. For the connectivity, the organic linkers can be two connected, three connected, four connected, and sometimes, even six or eight connected. The varieties of the organic linkers provide lots of chances to synthesize novel MOF materials. Starting from the organic linkers, we can classify the MOF materials into three categories: MOFs based on carboxylate linkers, MOFs based on azolate linkers and MOFs based on mixed linkers. These three categories of MOFs are discussed in the following sections.

5.3.1 MOFs based on carboxylate linkers

Organic carboxylate linkers are the most commonly reported ligands used to synthesize MOFs with exceptional high surface area. Various metal ions, such as Zn, Cu, Mn, Co, Cr, Ni, Al and lanthanide metals, have been utilized in the synthesis of MOFs.

The structures, functionalization and the hydrogen storage capabilities of several MOFs will be demonstrated in this chapter.

In 2003, the first hydrogen sorption properties using MOF material (Figure 21), MOF-5, was reported by Yaghi's group.[18] MOF-5 are constructed with inorganic four connected Zn clusters and organic linkers, benzene-1,4-dicarboxylate (BDC), with a cubic three-dimensional extended porous structure.[139] Due to the isolated linkers, which are accessible from all sides to the gas molecules, such a structure is ideal for hydrogen storage. An extraordinarily high apparent surface area (about 2000 $m^2\,g^{-1}$ equivalent to the area of a regular football field) was observed due to the scaffolding-like nature of MOF-5. At 77 K and 0.7 bar, 4.5 weight-percent (wt%) hydrogen absorption was observed using MOF-5 as absorbent. And later revised maximum hydrogen capacity of 4.5 – 5.2 wt% at 77 K and 50 bar for MOF-5 [131], that has been confirmed independently.[143-144]
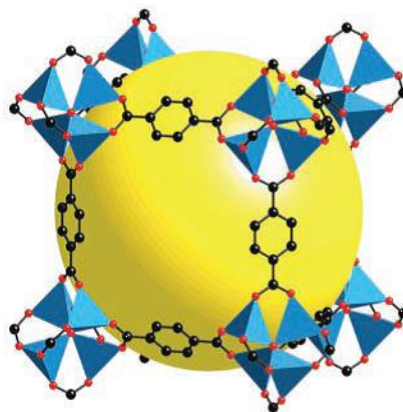
Figure 21. Single-crystal X-ray structure of MOF-5 illustrated for a single cube fragment of their respective cubic three-dimensional extended structure. On each of the corners is a cluster of an oxygen-centered zinc tetrahedron that is bridged by six carboxylates of an organic linker. The large yellow spheres represent the largest sphere that would fit in the cavities without touching the van der Waals atoms of the frameworks. Reprinted from ref.[139].

64

The hydrogen uptake varied as a function of pore size and degree of ionic or electrostatic forces through formulation of Zn-MOF-5 variants. Here, the metal center and inorganic linkers were fixed but the organic ligand varied, the maximum hydrogen uptake increased with surface area. Among them, MOF-177 (Figure 22), which is synthesized with Zn_4 inorganic cluster and 4,4′,4″-benzene-1,3,5-triyl-tribenzoate (BTB) ligand (Figure 22b), has the highest apparent surface area of 4746 m^2 g^{-1}. Indeed, its hydrogen uptake is the highest (7.5 wt% at 77 K and 70 bar).[143]
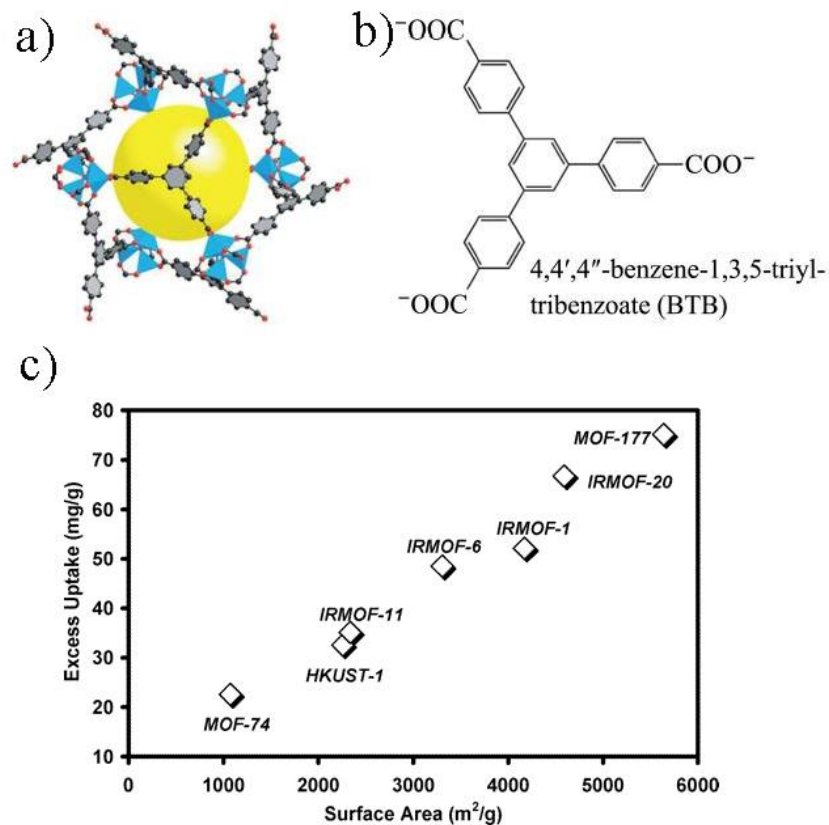
Figure 22. a) Single crystal structure of MOF-177; b) The synthetic ligand for MOF-177, BTB; c) Saturation H_2 uptake plotted against Langmuir surface area. Reprinted from ref. [143].

The Sabo group demonstrated the effect of Pd in MOF-5 on hydrogen adsorption.[145] After being incorporated with Pd in MOF-5, the surface area was anticipated to be decreased. However, the hydrogen capacity was found to be 1.86 wt% at 77 K and 1 bar, while the hydrogen adsorption is only 1.15 wt% at 77 K and 1 bar before the Pd impregnation. The enhanced storage capacity can be ascribed to dissociation of hydrogen molecules causing a primary spillover at the Pd catalyst and meantime MOF-5 acting as a secondary spillover receptor. This would increase the isosteric heat of hydrogen adsorption, which improves the hydrogen adsorption capacity.

Hong Kong University of Science and Technology MOF-1 (HKUST-1) is the firstly-reported Cu MOF[146] (Figure 23), which is composed of copper paddlewheel clusters and trigonal benzene-1,3,5-tricarboxylate (BTC) linker. HKUST-1 is a face-centered cubic crystal with a BET surface area of about 1500 m^2 g^{-1}. The advantage of HKUST-1 compared with MOF-5 is that it has open metal sites, which are occupied with the weakly coordinated solvent molecules. These solvent molecules can be removed, leading to an increase in the local interaction energy of hydrogen molecules. This observation can be confirmed with the isosteric heat (q_{st}, 3.8-5.2 kJ mol^{-1}) of hydrogen adsorption in HKUST-1, which is about 1.0-2.0 kJ mol^{-1} larger compared with that of MOF-5. Accordingly, the hydrogen uptake of HKUST-1 almost double that of MOF-5 at low pressures.[147-148] However, at high pressures, MOF-5 has a much higher hydrogen adsorption capacity compared with HKUST-1, which indicates that the hydrogen adsorbed capacity at low pressures strongly depends on the binding affinity of H_2 to the frameworks,

66

while the amount adsorbed at higher pressures is mainly determined by the surface area of the framework.[149]
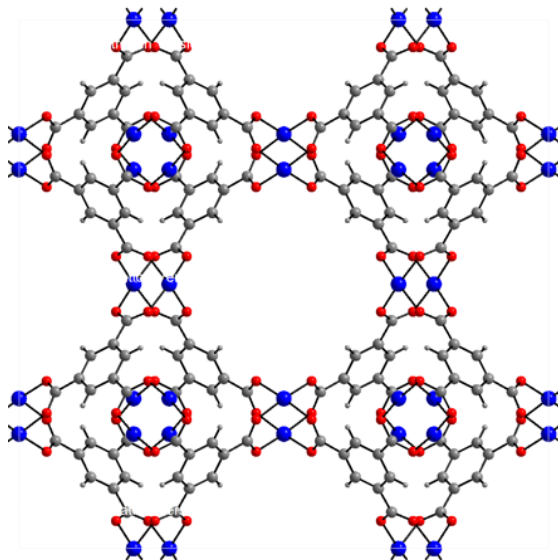
Figure 23. Single crystal X-ray structure of HKUST-1 (copper is denoted as a color in blue, oxygen in red and carbon in grey).

Several Cr- and Al-based MOFs have also been evaluated for the hydrogen adsorption. Material from Institute Lavoisier MOF-53 (MIL-53) is composed of trivalent metal ions (Cr/Al/Sc/Fe) and BDC ligands (Figure 24).[86, 150] MIL-53 is highly porous and shows both high chemical and high thermal stability. It exhibits one-dimensional channel filled with free disordered solvent molecules. When the free molecules are removed, the pore size of MIL-53(Cr) decreased from 13.04 Å to 7.85 Å, indicating very high breathing effect. It was found that the transition between the hydrated form and the anhydrous solid is fully reversible. The MIL-53(Cr) showed a maximal hydrogen capacity of 3.1 wt% at 77 K and 16 bar, whereas MIL-53(Al) exhibited the capacity of 3.8 wt%.
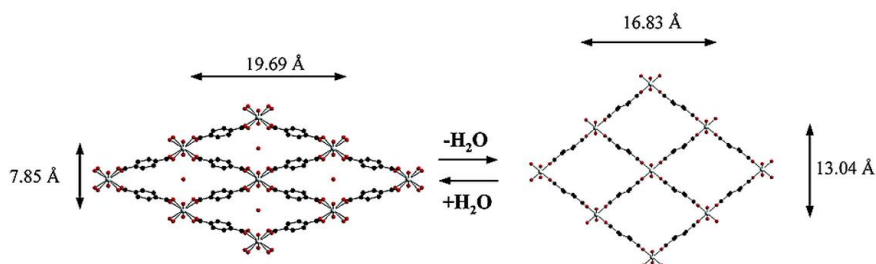
Figure 24. Representation of the structure of MIL-53 showing the breathing effect due to the removal of water molecules: hydrated (left) and anhydrous form (right). The anhydrous form of MIL-53 was tested for the hydrogen adsorption experiment. Reprinted from ref.[86].

Furthermore, the hydrogen adsorption using Cr-based MIL-100 and MIL-101 as adsorbents was carefully examined by the Férey group (Figure 25).[26, 151-153] MIL-100 was composed of trimeric chromium (III) octahedral clusters and the BTC ligand. MIL-100 has two types of cages in its structure: the smaller cage is delimited by twelve pentagonal faces and the larger by sixteen faces, which include twelve pentagonal and four hexagonal faces. The accessible diameters of the two cages are 25 Å and 29 Å, respectively. The MIL-100 had a Langmuir surface area of 2700 m^2 g^{-1} and a maximum hydrogen uptake of 3.28 wt% at 77 K and 26.5 bar. MIL-101 was built up from the same trimeric chromium (III) octahedral clusters and BDC linkers. MIL-101 also has two types of cages with accessible diameters of 29 Å and 34 Å, respectively. However, additional treatment is required for MIL-101 to remove most of the BDC ligands in the pores. The Langmuir surface area of MIL-101 is 5500 m^2 g^{-1} and the hydrogen adsorption capacity can reach to 6.1 wt% at 77 K and 80 bar. This higher hydrogen adsorption capacity of MIL-101 could be ascribed to its high adsorption heat (9.3 to 10.0 kJ mol^{-1} at low coverage), which arose

from the strong adsorption affinity between the unsaturated metal sites and hydrogen molecules.
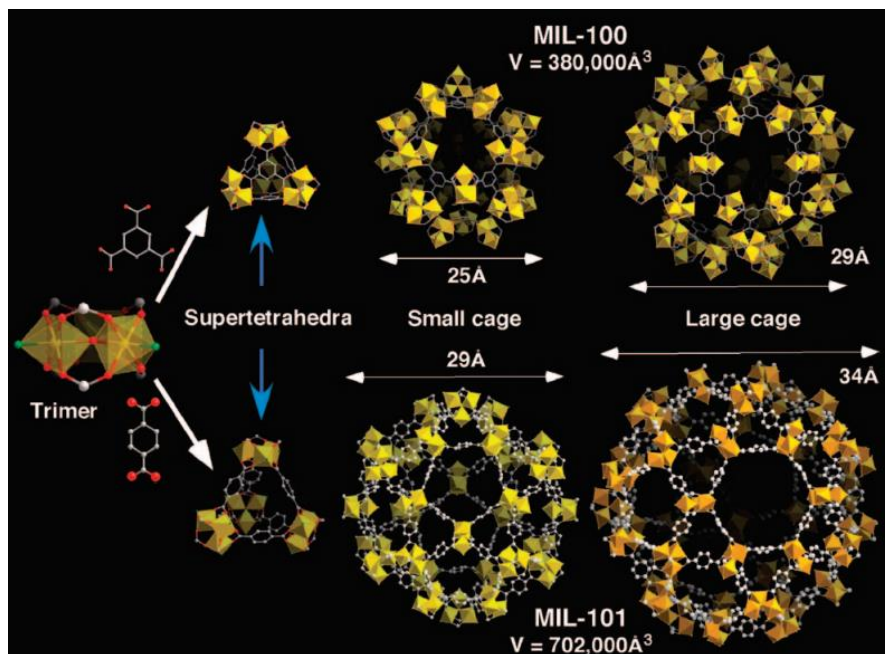
Figure 25. "Schematic view of the porous solids MIL-100 and MIL-101. Left: Trimers of chromium octahedra which assemble with either BTC (MIL-100) or BDC (MIL-101) to form the hybrid supertetrahedra; Center: Hybrid supertetrahedra; Right: Cages of MIL-100 and MIL-101."[26] Reprinted from ref.[153].

In addition, Zhou group developed a general synthetic method, which is derived from the rationalization of the MOF growth from both a kinetic and a thermodynamic perspective, to synthesize 34 large single crystals of iron-containing MOFs (Figure 26).[37] Among them, PCN-250 was constructed with 6-connected (Fe$_2$M) building blocks and a rectangular tetratopic linker. Interestingly, anther framework isomer of PCN-250, PCN-250′ was synthesized under a different synthetic condition. Along one axis, the ligands

constructing the same cube in PCN-250 adopt mirror configurations and are alternatively arranged while in PCN-250′, ligands adopt the same configuration in the one cube and mirror configuration in the adjacent cubes along any axis. PCN-250 shows a record high H_2 uptake of 3.07 wt% and 28 g L^{-1} at 1.2 bar and 77 K. Also, PCN-250 exhibits one of the highest total H_2 volumetric uptake of 60 g L^{-1} at 40 bar and 77 K. The high uptakes of H_2 can be attributed to suitable size of the cages in PCN-250 and the well-dispersed and highly charged open metal sites. Moreover, PCN-250 can be maintained stable in water for more than six months.
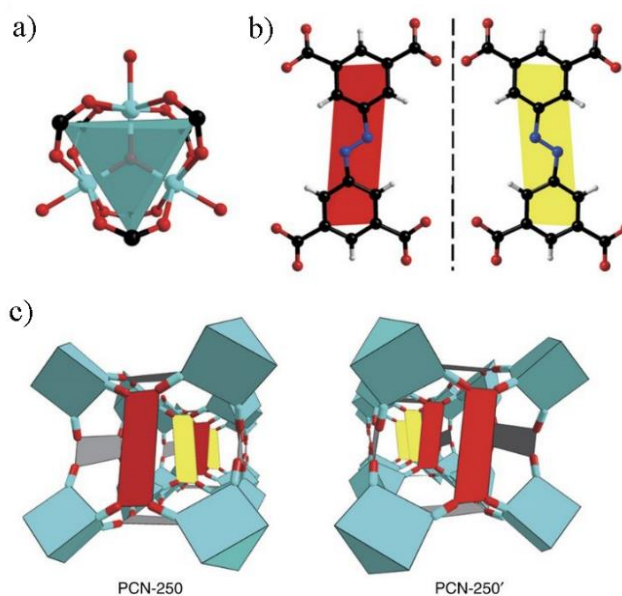
Figure 26. Structures of PCN-250 and PCN-250′.

5.3.2 MOFs based on azolate linkers

All the aforementioned MOFs are using oxygen as the coordinated atom, the coordinated atom can also be nitrogen. Lots of heterocyclic ligands have been successfully used in the synthesis of the porous MOF materials, including imidazole, triazole, pyrazole, and tetrazole.

Among them, zeolitic imidazole frameworks (ZIFs) are a special category of MOFs constructed with organic imidazolate linkers and the tetrahedrally coordinated zinc/cobalt clusters. Various ZIFs have been well documented and they usually have exceptional high chemical, thermal and water stability, which enable great promise for real industrial hydrogen adsorption.[154-155] For example, ZIF-8 (Figure 27), constructed with six-ring ZnN_4 clusters and MeIM (2-methylimidazolate), is a prototypical ZIF compound with a sodalite zeolite-type structure. The excess hydrogen adsorption capacity of ZIF-8 is 3.1 wt % at 77 K and 30 bar.[154, 156-158] To our surprise, both of the two strongest adsorption sites are associated with organic linkers, instead of metal clusters, which is in strong contrast with carboxylates based MOFs. This discovery is very important and it will lead to the right direction to optimize this class of ZIF materials for hydrogen adsorption.

Recently, the Long group reported a copper framework, Cu-BTTri starting from the trizaolate linker, 1,3,5-tris(1H-1,2,3-triazol-5-yl)benzene (BTTri, Figure 28).[159] Cu-BTTri has a sodalite structure, which consists of BTTri linked (Cu_4Cl) square clusters in which each copper center has a terminal solvent molecules directed toward the interior of the large pore. After activation, the framework has exposed copper metal sites, which can

71

enhance the interactions between the hydrogen molecules and the framework. The BET

surface area of CuBTTri is 1770 $m^2 g^{-1}$ and the H_2 uptake capacity is 1.2 wt% at 1.2 bar

and 77 K. Moreover, Cu-BTTri exhibits a really high thermal stability of up to 270 °C

and exceptional stability in air, boiling water, and even acidic media.

ZIF-8 (SOD)

Zn +
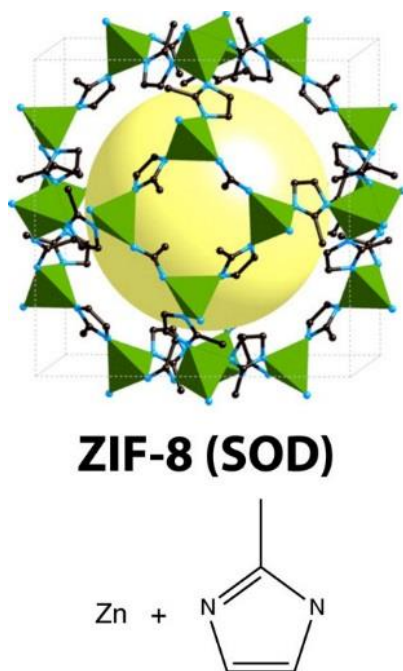
Figure 27. Imidazolate linker, structure, and network topology of ZIF-8. Yellow sphere
represents the free volume in the frameworks. Reprinted from ref.[158].

Long *et al*. synthesized another new Mn-based MOF by using the tritopic

tetrazolate ligand, BTT (1,3,5-benzenetristetrazolate) (Figure 29).[129] This framework

showed a high nitrogen surface area of up to 2100 $m^2 g^{-1}$. The framework contained

coordinately unsaturated Mn sites, which have a strong hydrogen binding. So the isosteric

heat of hydrogen adsorption at zero surface coverage is 10.1 kJ mol^{-1}. As a result, the high

hydrogen adsorption heat gives rise to the high total hydrogen uptake (6.9 wt% at 77 K and 90 bar). Surprisingly, since the hydrogen adsorption did not reach to the saturation yet at 90 bar, the hydrogen adsorption is anticipated to further increase with pressure.
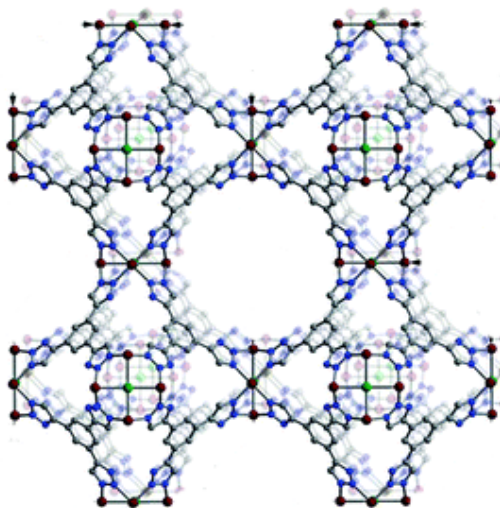
Figure 28. A portion of the structure of the sodalite-type framework of Cu-BTTri. Purple is Cu, green is Cl, gray is C, and blue is N, respectively; framework atoms are omitted for clarity. Reprinted from ref.[159].

5.3.3 MOFs based on mixed linkers

Mixed ligand coordination systems have also been taken advantage of to explore their hydrogen storage potential. Although it becomes increasingly difficult to design materials that contain two different metal-binding functionalities, frameworks with impressive hydrogen storage properties have been demonstrated using this strategy. A novel approach for the bottom-up assembly of hierarchical building blocks: simple molecular building blocks (MBBs) and the resultant super molecular building blocks (SBBs) to build highly coordinated nets. Indeed, Cu(TZI)$_3$ was synthesized from the

solvothermal reaction between 5-tetrazolylisophthalic acid (H_3TZI) and Cu salt in a DMF/ethanol solution (Figure 30).[160] H_3TZI possesses two carboxylate groups and a tetrazolate ring. In this structure, the carboxylate groups serve to construct the famous paddlewheel building unit, while the tetrazolate groups to form a triangular cluster. In this triangular cluster, each copper ion exhibits two empty coordination sites, which presumably have a higher affinity with hydrogen molecules and hence enhance the isosteric heat of adsorption. As expected, the isosteric heat of adsorption is 9.5 kJ mol^{-1} while the H_2 uptake is 2.4 wt% at 1 bar and 77 K. Similar approach may reduce the serendipity associated with this method and could potentially lead to particularly complex, but well-engineered and effective hydrogen storage materials.
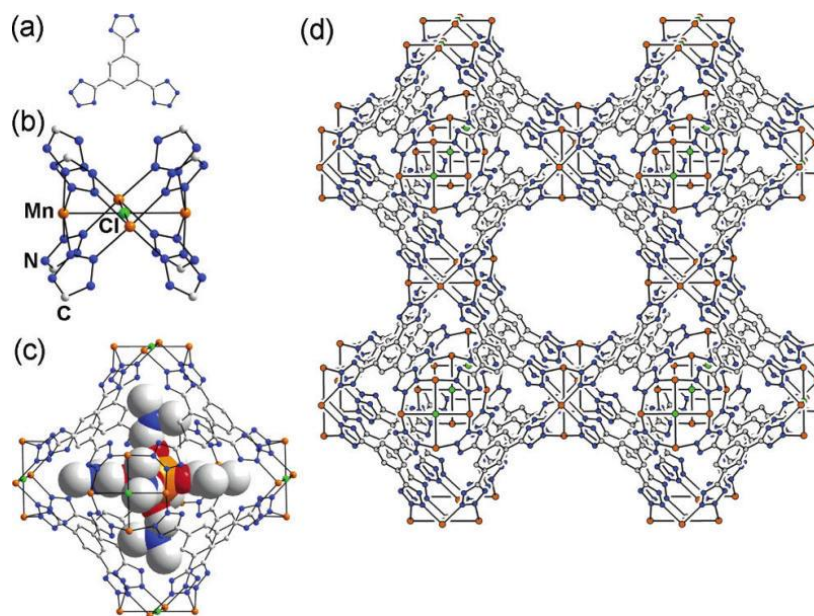
Figure 29. Portions of the crystal structure: (a) chemical structure of the ligand H_3BTT, (b) a square-planar Mn_4Cl cluster connected by eight tetrazolate linkers, (c) a sodalite cage-like unit, and (d) a cube of eight such units sharing square Mn_4Cl faces. Reprinted from ref.[129].
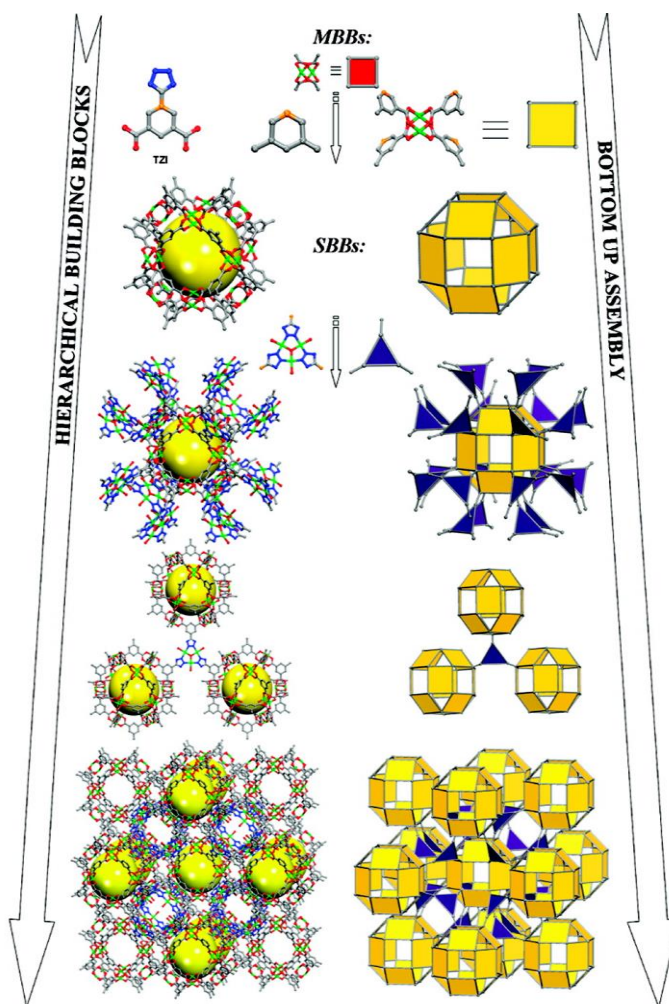
Figure 30. (Left) Select fragments from the crystal structure. C = gray, N = blue, O = red, Cu = green; the 5-position of the 1,3-BDC ligand is highlighted in orange; the yellow spheres indicate the cavity of truncated cuboctahedra; some spheres, all solvent molecules, and all hydrogen atoms have been omitted for clarity. (Right) Schematic showing the corresponding strategy from MBBs to SBBs to MOFs. Reprinted from ref.[160].

5.4 Postsynthetic modification of MOFs to improve the hydrogen storage

Postsynthetic modification of MOFs is a widely used powerful strategy to change

the functional properties of MOF materials, such as the surface area, pore size and pore

volume, and to synthesize novel MOFs, which cannot or hardly be achieved using the

direct synthetic method. Moreover, specific functional groups can be incorporated into the frameworks to change their chemical properties or provide strong interaction sites for hydrogen without losing their crystallinity.

5.4.1 Post modification of the inorganic clusters

Modification of the inorganic clusters is less common compared with the postsynthetic modification of the organic linkers. The Zhou group also developed the postsynthetic metathesis and oxidation (PSMO) strategy to synthesize novel MOF materials.[161-163] Starting with the labile Mg-MOFs, they firstly used Fe(II) and Cr(II) to exchange with the Mg cations in the MOFs so that the exchange process is accelerated and the overall structure can be preserved. Then, the intermediate Fe(II)- and Cr(II)-MOFs can be oxidized in the air to form the ultra-water-stable Fe(III)- and Cr(III) MOFs while maintaining the single crystallinity. Significantly, the single crystalline MOFs that contain high valence metals, especially Cr(III), were very rare until this work.

The Férey group reported amine-grafting at open metal sites in MIL-101(Cr).[164] By replacing coordinated water molecules with ethylene diamine, diethylenetriamine, or 3-aminopropyltrialkoxysilane, the effective BET surface area is anticipated to be reduced. But the powder X-ray diffraction (PXRD) patterns are well indexed with each other, which confirms that the crystallinity before and after postsynthetic modification is well maintained. Then metal complexes, such as $[PdCl_4]^{2-}$, $[PtCl_6]^{2-}$ or $[AuCl_4]^{-}$, were incorporated into the MOF materials. They were reduced to afford nanoparticles around

2 - 4 nm in size, which could increase the hydrogen storage ability as confirmed by several reports.[165-166]

In another report, Hupp and his co-workers reported that the H_2 storage capacity of MOFs can be increased by the postsynthetic modification of the open metal sites with a pyridine ligand.[167] A careful investigation reveals that the MOFs' internal surface area, pore volume, and ability to absorb molecular hydrogen can be modulated by postsynthetic modification. However, it should be noted that the hydrogen uptake capacity decreases significantly as compared to the frameworks with open metal sites.

Suh and his co-workers demonstrated that the gas adsorption properties can be changes by postsynthetic replace coordinated water molecules with bidendate organic linkers (Figure 31).[168] Firstly, they synthesized a porous MOF, SNU-30, by the solvothermal reaction, which has open metal sites coordinated by water molecules. Then linker 3,6-di(4-pyridyl)-1,2,4,5-tetrazine (bpta, Figure 31a), was postsynthetically inserted between two paddle-wheel shaped zinc clusters to afford the single crystalline SNU-31SC, which divided the channels into smaller pores, enabling efficient gas movement. Moreover, the inserted bpta linkers can be removed by immersing the SUN-31SC in *N,N*-diethylformamide (DEF) and at the same time, the crystallinity was well maintained upon modification. The BET surface area of SNU-30 measured from the N_2 isotherm was 704 $m^2\ g^{-1}$. At 1 bar and 77 K, the H_2 uptake of SNU-30 reached to 1.42 wt% and the isosteric hydrogen adsorption heat for SNU-30 ranges from 8.12 to 7.27 kJ mol^{-1}. In addition, an excess of hydrogen uptake of SNU-30 reaches to 2.75 wt % while the total uptake reaches

to 3.27 wt % at 61 bar and 77 K. Interestingly, the postsynthetically modified framework did not adsorb H_2, N_2, O_2, CH_4 but selectively adsorbed CO_2.
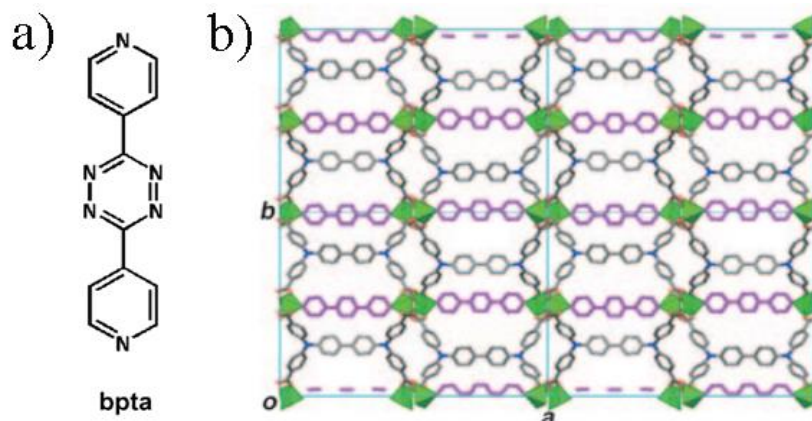
Figure 31. a) The chemical structure of ligand, bpta; b) The X-ray crystal structure of SNU-31 SC. Views seen on the *ab* plane. Color scheme: Zn=green, C=gray, O=red, N=blue, bpta linker=pink.

5.4.2 Post modification of the organic linkers

The hydrogen uptake capacity of MOFs can also be modulated by post-modification of organic linkers, which have been successfully demonstrated by the Cohen group (Figure 32) by incorporating of phenyl groups into the frameworks.[169] The MOFs connected with NH_2 functionalized ligand, NH_2-MOFs, which include isoreticular metal-organic framework 3 (IRMOF-3), 1,4-diazabicyclo[2.2.2]octane scaffold MOF 1 (DMOF-1), and university of michigan crystalline material-1 (UMCM-1). UMCM-1-NH_2 can react with anhydrides or isocyanates to form amide groups. The pore volume, pore size and the surface area of the MOFs will be changed by this postsynthetic modification. At the same time, this modification will alter the isosteric heat of the hydrogen adsorption and the

hydrogen uptake capacities. The hydrogen storage capacities of IRMOF-3-AMPh (where AMPh is the benzoic anhydride substituent), IRMOF-3-URPh (where URPh is the isocyanate substituent), and UMCM-1-AMPh increased up to 1.73 wt %, 1.54 wt %, and 1.54 wt %, respectively, at 77 K and 1 atm. In comparison, IRMOF-3 and UMCM-1-NH$_2$ only demonstrated the hydrogen uptake as 1.51 wt % and 1.35 wt %, respectively. Moreover, the isosteric heats of hydrogen adsorption in MOFs having aromatic ring substituents were higher compared with those with alkyl chain substituents. These results suggest that the optimal interaction geometry between the MOF and H$_2$ is that the H$_2$ molecules are located at the centers of the phenyl rings in the ligand.

IRMOF-3-AMPh   **IRMOF-3-URPh**   **UMCM-1-AMPh**
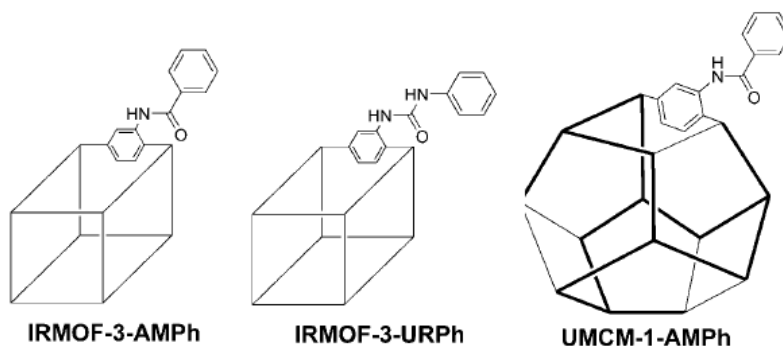
Figure 32. Schematic representation of the three modified MOFs of IRMOF-3-AMPh, IRMOF-3-URPh, and UMCM-1-AMPh.

Recently, the effect of lithium (Li) on hydrogen adsorption properties of MOFs has already been thoroughly explored by several theoretical research groups, such as the grand canonical ensemble Monte Carlo (GCMC) simulations.[170-173] The GCMC simulations have been validated by the fact that the simulated results by GCMC match

79

very well with the experimental data for the hydrogen storage in MOFs without Li. Then the GCMC technique was utilized to simulate five Li-doped MOFs (Figure 33). Simulation results suggest that the Li atoms are preferred to bind to the center of the aromatic rings with Li atoms on adjacent aromatic rings on the opposite sides, as we can see from Figure 33. More importantly, the high electron affinity of the aromatic rings can create positive Li sites, leading to a very strong binding affinity between H_2 and MOFs. From their results, the hydrogen uptake of Li-MOF-C30, in which the molar ratio of C/Li is 5, would reach to 3.89 wt % at 20 bar and 300 K and 4.56 wt % at 50 bar and 300 K, which exhibits the highest storage capacity for hydrogen at room temperature to-date. In contrast, the hydrogen uptakes for the MOF-C30 before doping Li were only 0.25 wt % at 300 K and 20 bar and 0.56 wt % at 300 K and 50 bar, respectively. From the results, we can conclude that doping Li on MOFs is a very critical strategy to enhance hydrogen uptake at room temperature.[174]
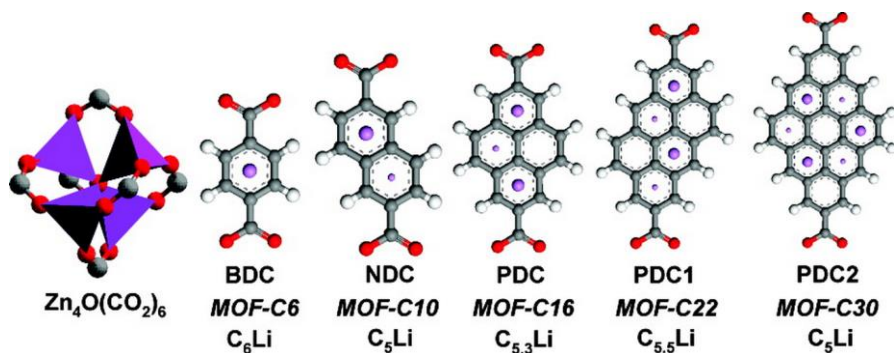
Figure 33. "Li-doped MOFs. In each case the zinc cluster couples to six aromatic linkers through the O-C-O common to each linker. These MOFs are named according to the number of aromatic carbon atoms. The large violet atoms in the linkers represent Li atoms above the linkers while small violet Li atoms lie below the linkers. The CxLi ratio considers only aromatic carbon atoms."[20] Reprinted from ref.[170].

80

Hydrogen uptake increased with increasing surface area (Figure 34), where the hydrogen BET surface area was determined using hydrogen adsorption isotherms for Li-doped MOF at 300K compared to the un-doped MOF at 77K, using rigid rotor model for hydrogen diameter of 0.351 nm. For both MOF systems without Li and Li-doped, there is a linear correspondence of H_2 uptake with the H_2 BET surface area. It was also found that the slope increased with increasing ratio of Li to C. The data confirmed that the Li concentration is the driving force for increasing H_2 uptake capacity at ambient temperature.
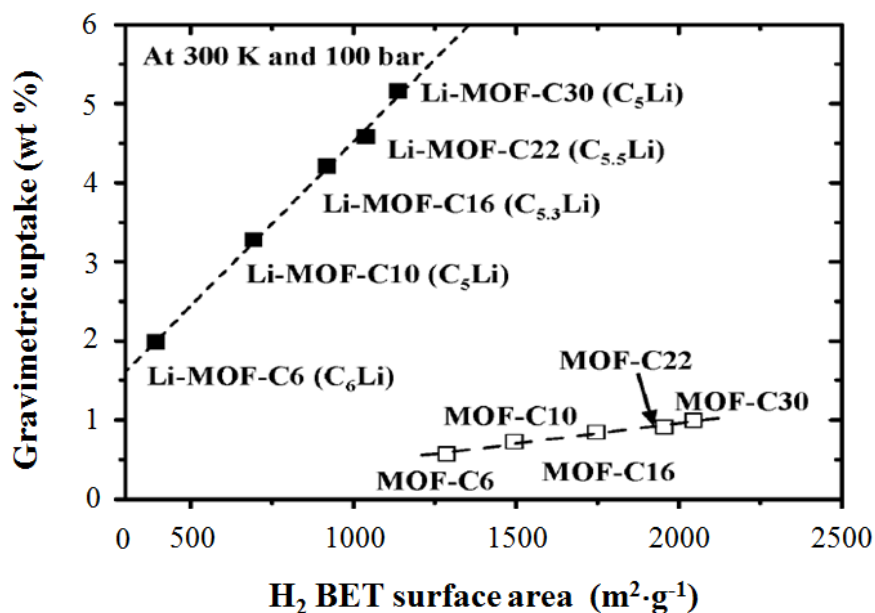
Figure 34. "Gravimetric H_2 uptake at 300 K and 100 bar plotted against the H_2 BET surface area for MOF without Li and Li-MOF systems. This demonstrates that both surface area and the ratio of Li to C are important for the higher performance in hydrogen uptake".[20] Reprinted from ref.[170].

The promoting effect of Li on H_2 adsorption on MOFs was confirmed by Mulfort and Hupp groups (Figure 35).[175-176] They doped Li on a special Zn MOFs and the hydrogen uptakes before and after the Li doping was found to be 0.93 wt % and 1.63 wt % at 77 K and 1 bar, respectively. After being doped with Li, the Zn-MOF nearly doubled the hydrogen capacity. Notably, the striking increase in H_2 uptake cannot be solely attributed to strong interactions between H_2 and Li. Instead, it is most likely augmented by the increased ligand polarizability and framework displacement effects.
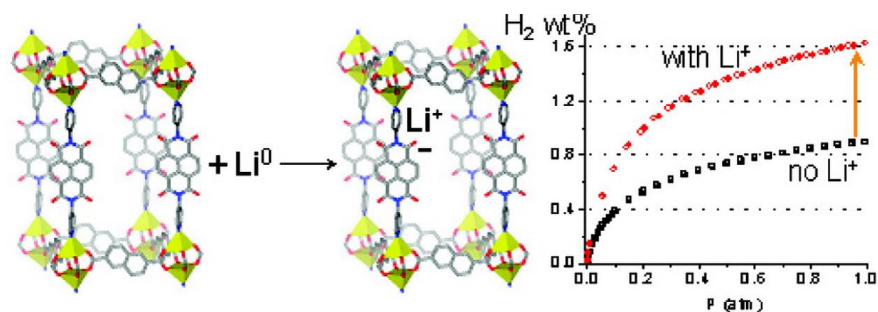
Figure 35. Left: The chemically reduction of Zn MOF in the solid state by lithium metal; Right: the comparison of the hydrogen uptake before and after the lithium reduction. Reprinted from ref.[176].

5.4.3 Post modification of MOFs by doping catalysts

Li and Yang groups have successfully demonstrated that the hydrogen uptake capacities in MOFs would greatly increase by doping Pt/AC (activated carbon) catalyst into MOF materials (Figure 36).[177] For spillover experiments, the active carbon was the primary receptor for hydrogen spillover and MOFs are the secondary spillover receptor. The hydrogen molecules are adsorbed rapidly on the Pt catalyst and then dissociated into hydrogen atoms. Then the hydrogen atoms would diffuse into the active carbon and then

to the MOF surface. The H_2 uptake on pure IRMOF-8 was ~0.5 wt % at 298 K and 100 bar. In a Pt/AC and IRMOF-8 physical mixture (at 1:9 weight ratio), the hydrogen adsorption amount was increased to 1.8 wt % under the same conditions.[178] In addition, if Pt/AC and IR-MOF-8 are well-connected by more carbon bridges, the hydrogen uptake can reach to 4 wt % at 298 K and 100 bar, which is the highest experimental hydrogen uptake capacity reported for MOFs at ambient temperature. And there is no apparent saturation even at 100 bar, suggesting that a further increase in hydrogen uptake capacity can be reached at higher pressures. The isosteric heat of the hydrogen adsorption ranged between 20 and 23 kJ mol^{-1}, which can be ascribed to that the hydrogen atoms have a much stronger binding ability to both the inorganic metal clusters and the organic linkers compared with molecular hydrogen. Similar results were also obtained by using the combination of Pt/AC catalyst with other MOFs, including MOF-5, MOF-177, covalent organic-framework 1 (COF-1), HKUST-1 and MIL-101.[179]
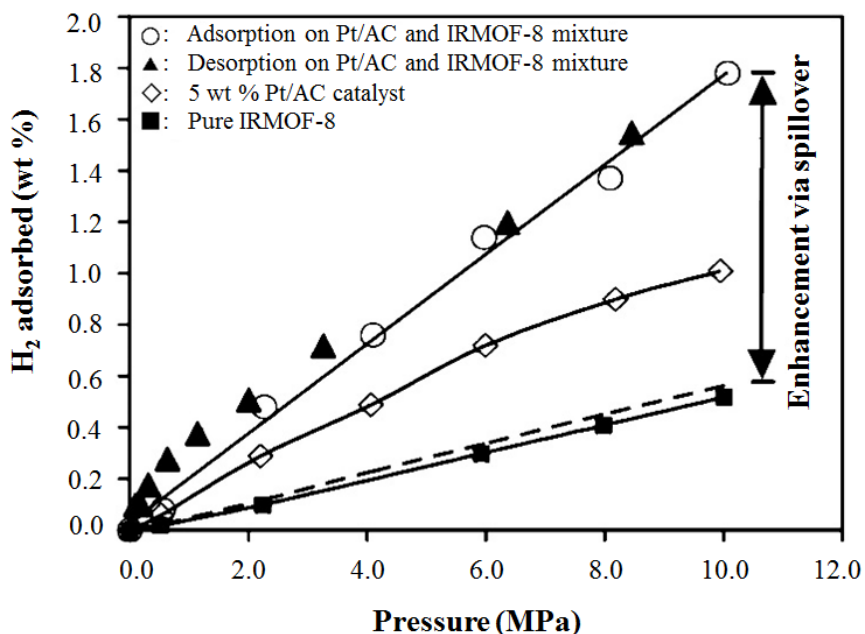
Figure 36. "High-pressure hydrogen isotherms at 298 K for pure IRMOF-8 (■), 5 wt % Pt/AC catalyst (◊), a mixture of Pt/AC and IRMOF-8: adsorption (○), desorption (▲)."[1]Reprinted from ref.[177].

5.5 Summary

MOFs with defined crystalline structures, extremely high surface areas and very high pore volumes can be regarded as good candidate materials for hydrogen storage. MOFs usually exhibit excellent performance for hydrogen adsorption at very low temperatures, such as 77 K and 87 K. However, it is still a great challenge to store hydrogen at ambient temperature, which can be ascribed to the relatively weak interactions between molecular hydrogen and MOFs. To achieve high H_2 storage capacity in a MOF at ambient temperature, the MOF should possess not only a very high surface area but also a high isosteric heat of H_2 adsorption.

6. POROUS ORGANIC POLYMERS FOR POST-COMBUSTION CARBON CAPTURE

6.1 Introduction

The CO_2 concentration in the atmosphere has increased dramatically in the past few decades and is held as one of the major causes for global warming.[180] Since the beginning of the industrial age, the CO_2 concentration has increased from 280 to 390 ppm in 2011, an increase of approximately 40%.[181] These emissions stem predominately from the burning of fossil fuels (coal, petroleum, and natural gas) and are projected to continue to increase in the foreseeable future.[182] The increase of the CO_2 concentration affects the incoming and outgoing energy in the atmosphere, resulting in a significant increase of the average atmospheric temperature. It is beyond all doubt that strategies to mitigate the increase of the CO_2 concentration in the atmosphere are urgently required.[183]

Carbon capture and storage (CCS)[184] is a family of technologies, which can reduce CO_2 emissions.[185-186] CCS includes three steps: a) separation of CO_2 from emission sources before entering the atmosphere (carbon capture); b) transportation to a storage site; and c) permanent subterranean or submarine storage. In the latter two steps, captured CO_2 is pressurized to ~100 bar or more and transported to a storage site, where it is injected and trapped underground for hundreds to thousands of years. So far, a growing number of fully integrated CCS projects have reached pilot prior to commercialization. However, the large energy penalty and considerable cost of the carbon capture process are slowing down the deployment of commercial CCS projects.

6.1.1 Carbon capture scenarios

Exploring cost-effective and scalable technologies for carbon capture from emission sources is regarded as one of the most efficient strategies to reduce anthropogenic CO_2 emissions.[187] Generally, based on the fundamental chemical process involved in the combustion of fossil fuels, three basic CO_2 capture scenarios can be adopted: a) post-combustion capture, b) pre-combustion capture, and c) oxy-fuel combustion.[188-189] In addition, the carbon capture used for CH_4 purification and direct air capture will also be discussed.

Post-combustion capture: The goal of the post-combustion process is to separate CO_2 from N_2 after combustion of fossil fuels before it enters the atmosphere. The combustion of fossil fuels in air generates flue gas consisting of 15% CO_2, majority N_2, and other minor components such as H_2O, CO, NO_x, and SO_x (Table 4).[159] After the removal of SO_x, flue gas enters the carbon capture process at near atmospheric pressures and elevated temperatures (40 - 80 °C).[190-191] This carbon capture scenario is the most feasible on a short time scale since many of the proposed technologies can be retrofitted to the existing fossil fuel consuming power plants.

Pre-combustion capture: In pre-combustion capture, a primary fuel reacts with oxygen or air, producing synthesis gas (syngas), mainly composed of CO and H_2. Then CO passes through a shift converter and reacts with steam to produce CO_2 (25% - 35%) and additional H_2 (30% - 50%) at high pressure (5 - 40 bar) in the catalytic reactor (Table 4). Therefore, the target in pre-combustion is to separate CO_2 from H_2.[192] The capture usually operates at elevated pressures (~30 bar) and temperatures (~40 °C) with an adsorbent bed. A

pressure drop is later applied to recycle those adsorbents.[189,193] The energy requirement of this pressure swing adsorption (PSA) cycle is low. However, the temperature and efficiency associated with H_2-rich turbine fuel are problematic.

Oxy-fuel combustion: In a conventional oxy-fuel combustion setup, nearly pure oxygen is fed into the plant and diluted with CO_2 from the flue steam to a partial pressure of 0.21 bar. In this way, not only can the temperature of the fuel combustion be easily controlled, but also the NO_x impurity can be reduced when coal is burned in an O_2-enriched atmosphere.[194] The gaseous product contains mainly CO_2 (55 - 65%) and H_2O (25 – 35%). After condensation and water removal, nearly pure CO_2 can be directly subjected to sequestration.[195] While pre-combustion and post-combustion capture cannot be easily implanted for industry, 95% of carbon capture processes has been achieved by oxy-fuel combustion.[196] One significant advantage of this process is that flue gas is almost entirely composed of CO_2, which greatly benefits the following separation process. Most of the existing power plants can be readily retrofitted with an oxy-fuel combustion system. However, the stringent requirement for nearly pure oxygen significantly enhances the cost, making the implementation of oxy-fuel combustion challenging.

CH_4 purification: Carbon capture can also be utilized for natural gas purification (mainly CH_4).[197-198] When natural gas is extracted from wells, it often contains 20 – 40 wt% of CO_2, which is generally vented to the atmosphere. The significant challenge in this separation is the special technologies and materials are required to withstand high pressures during extraction of natural gas.

Table 4. Benchmark parameters showing typical compositions of gases (vol%) in post-combustion, pre-combustion and methane reformation processes as well as several physical parameters relevant to carbon capture.[189]

	Post-combustion	Pre-combustion[a]	Kinetic Diameter (Å)	Quadrupole moment[b]
CO_2	15-16%	25-35%	3.30	43.0
N_2	70-75%	0.3-2.3%	3.64	15.2
H_2		30-50%	2.89	6.62
H_2O	5-7%	15-40%	2.65	
O_2	3-4%		3.45	3.9
CO	20 ppm	0.5-0.7%	3.75	25.0
SO_x	800 ppm			
NO_x	500 ppm			
H_2S		0.1-0.2%	3.60	

[a]before water-gas shift reaction; [b]10^{-27}esu^{-1} cm^{-1}.

Direct carbon capture: The target here is to separate CO_2 directly from the atmosphere, where CO_2 is highly dilute with a partial pressure of 400 ppm. Until now, relatively few adsorbents have demonstrated effective abilities to remove CO_2 through direct sequestration.[199] However, carbon capture in enclosed environments, such as submarines and aircraft, have been reported using materials including supported poly(ethylene imine) or poly(ethylene glycol).

6.1.2 Currently used materials

All large scale commercial CO_2 capture systems rely on the basic premise of the original patent, wherein some bases dispersed in an aqueous solution binds to acidic gases present in the flue gas stream. Hundreds of plants operate on these systems with more coming on-line in the future.[200] The process involves the absorption of CO_2 into an aqueous solution of amine with low volatility at ambient temperature and the regeneration of amine by stripping with water vapor at 100 °C to 120 °C. Aqueous amine solutions, however, have several major drawbacks, which have generally made it uneconomical for implementation in existing power plants.[201] Engineering and system design concerns of the typical corrosiveness of amine solutions and vapors means that costly designs must be implemented for longevity, and frequent housekeeping is necessary to keep the system running safely.[202] The volatility and stability of some amines also pose problems in material lifetime, requiring additives and recharging of amines that are lost or oxidized.[203-204] In addition, the parasitic energy costs associated with stripping CO_2 from the sorbents can divert 20-30% of generated energy towards the capture process, resulting in the largest economic barrier.[205-206] Therefore, commercial amine systems have been developing other approaches to tackle the problems inherent involved with aqueous amine capture.[207-209]

As an alternative, porous solid materials have been demonstrated as potential media for carbon capture,[210-212] including zeolites,[154, 213-214] porous carbons,[215-216] and silica[217-218]. Carbon capture by traditional sorbents, such as zeolites and porous carbons, is much more energy-efficient as compared to aqueous amine solutions. First, the absence of new chemical bonds formation between the sorbates and sorbents leads to significantly

less energy demands for regeneration. In addition, the heat capacities of sorbents are only a fraction of that of the amine solution, further reducing the energetic costs involved with heating aqueous solutions.[219] However, the porous carbons are limited by low CO_2/N_2 selectivities, while zeolites suffer from impaired performance in the presence of water.[220,221] Therefore, there is an urgent need to develop advanced sorbents with excellent CO_2/N_2 selectivity, high CO_2 capacity, and enduring performance under flue gas conditions.

More recently, metal-organic frameworks (MOFs) have garnered a significant amount of attention as porous materials for carbon capture.[7, 189, 222-223] MOFs comprise metal-containing nodes and organic linkers that are assembled through coordination bonds. They have geometrically and crystallographically well-defined structures and in many cases, these structures are robust enough to allow the removal of included guest species, resulting in permanent porosity. The crystallinity of MOFs also allows precise structural characterization by diffraction methods, thus facilitating their rational design and the formulation of structure–function relationships. Such remarkable and easy tunability is quite different from those of traditional porous materials, such as zeolites and activated carbon. However, constructed with soft Lewis acids and hard Lewis bases, MOF materials usually suffer from limited physicochemical stability.

Porous organic polymers (POPs) are composed predominantly of carbon, boron, oxygen, and nitrogen that are connected through strong covalent bonds.[16, 22, 224-225] A significant number of POPs have been studied for carbon capture, some of which have demonstrated promising performances.[193] The major advantages of POPs over other

porous materials are their high porosity, structural diversity, and ultrahigh physicochemical stability, the combination of which enables an enormous scope of postsynthetic modifications to introduce specific CO_2-philic functionalities. In general, POPs can be handled under standard wet chemical reaction conditions without significant degradation of the framework or loss of porosity, and are ideal for applications in capturing CO_2 from harsh flue gas conditions.

6.1.3 Porous organic polymers

POPs are a new category of hyper-crosslinked polymeric materials constructed from organic covalent bonds exclusively.[226-228] POPs can be successfully synthesized by incorporating multitopic monomers, which provide cross-links between propagating polymer chains, into well-known step growth and chain growth polymerizations. POP materials have been used in many potential and important applications, such as gas adsorption,[229-230] gas separation,[231-232] optoelectronics,[233-234] catalysis,[78, 235] proton conductivity,[236] chemical sensor,[237] drug delivery,[238] as well as energy storage[239-240]. Different types of POPs have been denoted by various names, including porous polymer networks (PPNs),[4, 241] porous organic frameworks (POFs),[242,243] conjugated microporous polymers (CMPs),[244-245] polymers of intrinsic microporosity (PIMs),[246-247] hypercrosslinked polymers (HCP),[248-249] covalent triazine-based frameworks (CTFs),[250-251] porous aromatic frameworks (PAFs),[22, 252] crystalline covalent organic frameworks (COFs)[16-17] and so on. For convenience, we will use the term POPs to broadly label these materials.

Using POPs as carbon capture materials has the following principal advantages: a) constructed from comparatively rigid monomers, POPs can yield pores with rigid walls, leading to permanent porosity. The surface areas of POPs are comparable to the most porous materials. In particular, PPN-4, made by linking tetrakis(phenyl) subunits using Yamamoto coupling, has demonstrated the highest Brunauer–Emmett–Teller (BET) surface areas (6461 m^2/g) among all POP materials published so far.[4] b) The synthesis of POPs have drawn from an enormous number of modern bond forming methodologies, including boronic acid condensation,[17, 253] metal-catalyzed coupling,[4, 12, 14, 254] imine formation,[15, 255-256] Friedel-Crafts alkylation,[13, 251] and so on. The assembly process of POPs combines merits of the enormous reaction choices and rational design of monomers, leading to numerous structural topologies and diversified porosities. c) POPs, composed of light elements (typically H, B, C, N, and O), are usually lightweight materials, therefore, their gravimetric carbon capture capacities tend to be higher. d) Due to the nature of covalent bonds, POPs usually have very high stability compared with most MOFs, which are linked through coordination bonds. [135, 136] The exceptional chemical and water stability enable their reusability. The combination of favorable properties of large surface area, tunable pore size, high stability and easy functionalization enable POPs as ideal candidates for carbon capture. Although some excellent reviews already documented the synthesis and application of POPs,[3, 257-258] very few review reports have focused on the developments and achievements of POP materials for carbon capture.[193, 259]

This review is intended to provide readers with a comprehensive overview of the considerations associated with carbon capture using POPs. First, various definitions and

terminologies used to evaluate the performance of POPs for carbon capture, including the CO_2 capacity, enthalpy of CO_2 adsorption, selectivity and frequently used regeneration strategies are introduced in Section 2. A detailed correlation study between the structural and chemical features of POPs and their adsorption capacities will also be discussed, focusing on their physical interactions (Section 3) and chemical reactions (Section 4). Ultrahigh-surface-area POPs usually have weak physical interactions with CO_2 molecules, and they could find use in pre-combustion carbon capture, where the processes operate at elevated pressures.[222, 260-262] Chemical functionalization of POPs with polar groups, including nitrogen-rich groups,[263-264] oxygen-rich groups,[265-266] and inorganic ions,[241, 267-270] can be utilized to enhance the average dipole-quadruple interactions with CO_2 with a result of improved CO_2 capacity. Moreover, alkyl-amine functionalized POPs can undergo chemical reactions with CO_2 and therefore tend to have higher adsorption enthalpies and selectivities.[12, 271-273] Such materials have great potential for practical applications in post-combustion carbon capture. Finally, a concise outlook for utilizing POPs for carbon capture will be discussed in Section 5, noting areas in which further work is needed to develop the next-generation POPs for practical applications. The current challenges toward using POPs in CO_2 capture will be outlined clearly so that the relevant scientific fields can move the conversation forward towards practical solutions.

6.2 Carbon capture in porous organic polymers based on physical interactions

POPs have been proven to be the potential materials in carbon capture applications, which can be attributed to the large permanent surface areas, suitable pore size

93

distributions, as well as suitable interactions with carbon dioxide.[274] The CO_2 uptake capacities at 1 bar and 273 K, the CO_2 uptake capacities at 1 bar and 298 K, the CO_2 uptake capacities at 0.15 bar and 298 K, CO_2/N_2 selectivity and heats of adsorption for selected POPs are listed in Table 5. Note that some data have been taken approximately from the figures or curves published in the literature. Many POPs exhibit good performances for carbon capture at 1 bar and 273K/298K. Notably, it is important to address the conditions relevant to the post-combustion carbon capture process of CO_2 (0.15 bar, 40 °C). We urge that these pressure and temperature conditions be implemented as standard conditions in future reports of CO_2 adsorbent testing in order to effectively evaluate their applicability to post-combustion carbon capture and expedite the design and discovery process.

CO_2 adsorption is a well-established CO_2 separation approach used in the chemical and petroleum industries today. Adsorbents typically fall into either of two categories: 1) physical adsorption, which is temperature and pressure dependent (adsorption occurs at high pressures and low temperatures) and 2) chemical adsorption, where adsorption of CO_2 depends on the acid–base neutralization reaction.[275] For the physical adsorption mechanism, the separation of gas mixtures mainly depends on the physical properties of gas molecules, as discussed previously in Section 2.3. Materials that physically adsorb CO_2 usually consume less energy to regenerate because lack of new bond formation between the adsorbate and sorbent, as in the case of chemisorption. Hence, chemical functionalization of POPs with polar groups can be utilized to enhance the average dipole-quadruple interactions with carbon dioxide, leading to higher carbon capture capacity as well as higher selectivity.

94

Table 5. Summary of low pressure CO_2 uptakes, CO_2/N_2 selectivity and heats of adsorption in selected POPs.

POPs	Main functional group	BET (m^2g^{-1})	CO_2(mmol/g) 1bar, 273K	CO_2(mmol/g) 1bar, 298K	CO_2(mmol/g) 0.15bar, 298K	CO_2/N_2 Selectivity# IAST	CO_2/N_2 Selectivity# Henry's law	ΔH_{CO2} (kJmol^{-1})	Ref.
COF-1	None functional	750	2.23						222
COF-5	None functional	1670	1.34						222
COF-6	None functional	750	1.40						222
COF-8	None functional	1350	1.22						222
COF-10	None functional	1760	1.02						222
COF-102	None functional	3620	1.38						222
COF-103	None functional	3530	1.39						222
BILP-1	Benzimidazole	1172	4.27	2.97	0.69		36	26.5	276
BILP-2	Benzimidazole	708	3.38	2.36			71	28.6	277
BILP-3	Benzimidazole	1306	5.11	3.00	1.02		31	28.6	278
BILP-4	Benzimidazole	1135	5.34	3.59			32	28.7	277
BILP-5	Benzimidazole	599	2.91	1.98			36	28.8	277
BILP-6	Benzimidazole	1261	5.00	2.84	1.07		39	28.4	278
BILP-7	Benzimidazole	1122	4.39	2.77			34	27.8	277
BILP-10	Benzimidazole	787	4.09	2.55	0.73	57		38.2	279
BILP-11	Benzimidazole	658	3.09	2.00	0.61	56		32.0	279
BILP-12	Benzimidazole	1497	5.07	3.18	0.72	31		27.6	279
BILP-13	Benzimidazole	677	2.57	1.79	0.43	32		26.7	279
BILP-15	Benzimidazole	448	2.61				63	33	280
BILP-16	Benzimidazole	435	2.60				49	32	280
BILP-15(AC)	Benzimidazole	862	3.41				50	28.9	280
BILP-16(AC)	Benzimidazole	643	3.41				49	31.6	280
BIPLP-1	Bis(imino)pyridine	1580	2.30	1.20	0.25		16	32.2	267
Cu/BF$_4$/ BIPLP-1	Bis(imino)pyridine and CuBF$_4$	380	2.5	1.75	0.53		64	32.3	267
BILP-101	Benzimidazole	536		2.47	0.82	71	80	33	281
TBILP-1	Triazine and benzimidazole	330	2.66	1.77	0.55	62	63	35	282
TBILP-2	Triazine and benzimidazole	1080	5.18	3.32	0.98	43	40	29	282
COP-19	Triazine	640	2.44	1.32	0.40	131.2			283

POPs	Main functional group	BET (m^2g^{-1})	CO_2(mmol/g) 1bar, 273K	CO_2(mmol/g) 1bar, 298K	CO_2(mmol/g) 0.15bar, 298K	CO_2/N_2 Selectivity[#] IAST	CO_2/N_2 Selectivity[#] Henry's law	ΔH_{CO2} (kJmol^{-1})	Ref.
Azo-COP-1	Azo	635	2.45	1.48	0.39	63.7		29.3	[284]
Azo-COP-2	Azo	729	2.50	1.52	0.41	109.6		24.8	[284]
Azo-COP-3	Azo	493	1.91	1.18	0.36	78.6		32.1	[284]
TB-COP-1	Azo	1340	5.19	3.16	0.74	68.9		25.9	[263]
ALP-1	Azo	1235	5.36	3.25		28	27	29.2	[285]
ALP-2	Azo	1065	4.79	2.45		26	27	27.9	[285]
ALP-3	Azo	975	3.77	2.29		35	35	29.6	[285]
ALP-4	Azo	862	3.52	1.84		26	28	28.2	[285]
ALP-6	Azo	698	3.48	2.05	0.64			28.6	[286]
ALP-7	Azo	412	2.32	1.39	0.41			30.7	[286]
POF1B	Hydroxyl	917	4.28	2.05	0.49				[242]
POF2B	Hydroxyl	769	3.52	1.60	0.40				[242]
POF3B	Hydroxyl	608	2.90	1.47	0.36				[242]
NPOF-1-NH$_2$	Aromatic amine	1535	5.84	3.77	1.07	25		32.1	[243]
NPOF-4-NH$_2$	Aromatic amine	554	2.90	1.89		38	40	30.1	[287]
PPN-6	None functional	4023		1.4	0.22*			17	[269]
PPN-6-SO$_3$H	-SO$_3$H	1254		3.6	1.15*	155		30.4	[269]
PPN-6-SO$_3$Li	-SO$_3$Li	1186		3.7	1.45*	414		35.7	[269]
PPN-6-SO$_3$NH$_4$	-SO$_3$NH$_4$	593	7.5	3.7	1.78*		196	40	[241]
PPN-6-CH$_2$Cl	Chloromethyl	1740		1.48	0.25*	13		21	[12]
PPN-6-DETA	Alkyl amine	555		4.31	3.08*	442		55	[12]
PPN-125	Hydroxyl	703		1.87	0.45			25	[272]
PPN-125-DETA	Alkyl amine	229		2.05	1.43			62	[272]
PPN-80	Alkyl amine			1.57	1.02			72	[273]
PPN-81	Alkyl amine			1.87	1.36	4716		54	[273]
COP-97	Melamine	59	2.34	2.09	1.52	779.2		46	[283]
PPN-101	Benzimidazole	1096	2.5	1.45	0.39				[67]

Table 5. Continued 1

POPs	Main functional group	BET (m^2g^{-1})	CO_2(mmol/g) 1bar, 273K	CO_2(mmol/g) 1bar, 298K	CO_2(mmol/g) 0.15bar, 298K	CO_2/N_2 Selectivity[#] IAST	CO_2/N_2 Selectivity[#] Henry's law	ΔH_{CO2} (kJmol^{-1})	Ref.
TAPOP-1	Triazine	930	4.2					27.8	[288]
TAPOP-2	Triazine	940	3.6					34.7	[288]
Fe-POP-1	Porphyrin and Fe^{3+}	875	5.21						[65]
Fe-POP-2	Porphyrin and Fe^{3+}	855	5.10						[65]
Fe-POP-3	Porphyrin and Fe^{3+}	750	2.47						[65]
PFPOP-1	Hydroxyl	570	3.34	1.40	0.49	43.7		26.9	[289]
PFPOP-2	Hydroxyl	630	4.11	1.86	0.55	52.1		30.2	[289]
PFPOP-3	Hydroxyl	530	4.74	2.06	0.60	56.5		32.5	[289]
MAPOP-1	Hydroxyl	310	2.86	1.50	0.36			29.0	[290]
MAPOP-2	Hydroxyl	660	2.77	1.55	0.43			30.6	[290]
MAPOP-3	Hydroxyl	920	2.64	1.57	0.43			31.8	[290]
MAPOP-4	Hydroxyl	820	3.07	1.80	0.45			29.5	[290]
MKPOP-1	Hydroxyl	510	1.98	1.41	0.43			23.5	[291]
MKPOP-2	Hydroxyl	160	1.43	1.07	0.39			18.3	[291]
MKPOP-3	Hydroxyl	590	2.61	1.68	0.45			27.1	[291]
MKPOP-4	Hydroxyl	480	1.93	1.32	0.43			23.6	[291]
PCP-Cl	Pyridinium, Cl$^-$	755	2.31	1.40	0.34	34		28.5	[292]
PCP-BF$_4$	Pyridinium, BF$_4^-$	586	2.20	1.33	0.34	30		31.6	[292]
PCP-PF$_6$	Pyridinium, PF$_6^-$	433	1.78	1.07	0.27	36		30.8	[292]
Polymer 1	Phosphonium	1168	2.18	1.09	0.25		56	35.5	[268]
Polymer 2	Phosphonium	1015	2.80	1.61	0.41		45	30.1	[268]
Polymer 3	Phosphonium	904	2.32	1.45	0.30		36	27.2	[268]
Polymer 4	Phosphonium	852	2.84	1.55	0.41		28	24.2	[268]
Polymer 5	Phosphonium	823	2.57	1.48	0.34		46	25.9	[268]
Polymer 2+6	Phosphonium	770	2.93	1.70	0.45			30.1	[268]
Network A	Non-functional	4077	2.65	1.45	0.20		8.7	23.7	[260]
Network B	Imine	1847	3.29	1.63	0.30		19.5	21.8	[260]
Network C	Triazole	1237	3.86	2.20	0.5		14.2	33.7	[260]
Network D	Non-functional	1213	2.42	1.33	0.25		12.2	26.1	[260]
Network E	Non-functional	1470	2.95	1.77	0.35		9.2	25.4	[260]

Table 5. Continued 2

POPs	Main functional group	BET (m^2g^{-1})	CO_2(mmol/g) 1bar, 273K	CO_2(mmol/g) 1bar, 298K	CO_2(mmol/g) 0.15bar, 298K	CO_2/N_2 Selectivity[#] IAST	CO_2/N_2 Selectivity[#] Henry's law	ΔH_{CO2} (kJmol^{-1})	Ref.
Network F	Aromatic amine	653	1.80	1.08	0.25		12.2	26.7	[260]
Network G	Carbazole	1056	2.15	1.25	0.30		15.1	26.6	[260]
Network-1	Hydroxyl	414	1.85	1.25			16	31	[13]
Network-2	Hydroxyl	538	2.28	1.46			23	31	[13]
Network-3	Hydroxyl	333	1.89	1.24				31	[13]
Network-4	Hydroxyl	1015	3.96	2.27				31	[13]
Network-4R	Hydroxyl	927	3.46	2.21			26	31	[13]
Network-4S	Hydroxyl	981	3.50	2.21				31	[13]
Network-5	Hydroxyl	657	2.79	1.80				31	[13]
Network-6	Hydroxyl	650	2.24	1.41				31	[13]
CMP-1		837	2.05						[265]
CMP-1-COOH	Carboxyl group	522	1.60						[265]
CMP-1-(CH$_3$)$_2$	Methyl group	899	1.62						[265]
CMP-1-(OH)$_2$	Hydroxyl group	1043	1.80						[265]
DA-CMP-1	Aromatic amine	662	2.28	1.35	0.30	60.4	37.1	30	[244]
DA-CMP-2	Aromatic amine	603	1.64	0.95	0.24	63.1	33.1	30	[244]
TCMP-0	Triazine	963	2.38	1.34	0.25		9.6		[245]
TNCMP-2	Triazine	995	2.62	1.45	0.30		7.6		[245]
TCMP-3	Triazine	691	2.25	1.26	0.20		25.2		[245]
TCMP-5	Triazine	494	1.22	0.68	0.15		17.0		[245]
TB-MOP	Aromatic amine	694	4.05	2.57	0.80		50.6		[293]
PAF-1	Non-functional	5600	2.05	1.08				15.6	[262]
PAF-3	Non-functional	2932	3.48	1.82			87	19.2	[262]
PAF-4	Non-functional	2246	2.41	1.15			44	16.2	[262]
PAF-26-COOH	Carboxyl group	717	2.32	1.45	0.33	20		28.1	[270]
PAF-26-COOLi	Inorganic ion	591	2.54	1.61	0.36	24		31.8	[270]
PAF-26-COONa	Inorganic ion	483	2.67	1.61	0.36	53		35.0	[270]

98

Table 5. Continued 4									
POPs	Main functional group	BET (m^2g^{-1})	CO_2(mmol/g) 1bar, 273K	CO_2(mmol/g) 1bar, 298K	CO_2(mmol/g) 0.15bar, 298K	CO_2/N_2 Selectivity[#] IAST	Henry's law	ΔH_{CO2} (kJmol^{-1})	Ref.
PAF-26-COOK	Inorganic ion	430	2.41	1.54	0.40	50		32.6	[270]
PAF-26-COOMg	Inorganic ion	572	2.76	1.67	0.40	73		30.0	[270]
PAF-30	Triazine	540	2.39	1.53	0.52			36.9	[264]
PAF-33	Non-functional	821	2.16	1.25	0.27		19.4	27.4	[294]
PAF-33-NH$_2$	Amino group	370	1.19	0.75	0.33		79.8	32.9	[294]
PAF-33-COOH	Carboxyl group	445	1.94	1.21	0.29		104.3	30.0	[294]
PAF-34	Non-functional	953	2.50	1.39	0.17		26.3	27.2	[294]
PAF-34-OH	Hydroxyl group	771	2.21	1.25	0.27		39.1	30.7	[294]
PAF-35	Non-functional	567	1.77	1.01	0.22		29.9	30.3	[294]
PAF-56P	Triazine	553.4		1.52	0.33	40			[295]
POM1-IM	Imidazolium salt	926	3.16					25.6	[296]
POM2-IM	Imidazolium salt	653	3.30			13		31.1	[296]
POM3-IM	Imidazolium salt	575	3.23					31.5	[296]
POM4-IM	Imidazolium salt	632	2.41						[296]
POM5-IM	Imidazolium salt	50	1.30						[296]
POM6-IM	Imidazolium salt	659	1.25						[296]
PON-1	Non-functional	1422		2.61	0.55				[297]
PON-2	Non-functional	168		0.77	0.27				[297]
PON-3	Non-functional	51		0.86	0.32				[297]
[HO$_2$C]$_{25\%}$-H$_2$P-COF	Carboxyl group	786	2.18	1.32	0.34			38.2	[266]
[HO$_2$C]$_{50\%}$-H$_2$P-COF	Carboxyl group	673	3.05	1.52	0.34			39.6	[266]
[HO$_2$C]$_{75\%}$-H$_2$P-COF	Carboxyl group	482	3.57	1.64	0.34			41.2	[266]
[HO$_2$C]$_{100\%}$-H$_2$P-COF	Carboxyl group	364	3.95	1.73	0.50	77		43.5	[266]
CPP	Triazole and amine	579	3.57	2.27	0.72		94	33.5	[298]
Cage 2	Imine	533	3.00						[299]

POPs	Main functional group	BET (m^2g^{-1})	CO_2(mmol/g) 1bar, 273K	CO_2(mmol/g) 1bar, 298K	CO_2(mmol/g) 0.15bar, 298K	CO_2/N_2 Selectivity[#] IAST	CO_2/N_2 Selectivity[#] Henry's law	ΔH_{CO2} (kJmol^{-1})	Ref.
om-ph-MR	Melamine	256	2.50	1.77	0.86		100	32.2	[300]
SNU-C1-sca	Triazole	830	4.38	3.14	0.75			31.2	[301]
SNW-1	Melamine	821		2.19	0.67	50		35	[302]
TCPF-4(dried)	Aromatic amine	1404	4.66	2.86	0.80		56	30	[303]
TCPF-4 (humidified)	Aromatic amine	1404	3.00	1.75					[303]
TBMID	Aromatic amine	688	3.30	2.20	0.50		58.8	33.5	[304]
PECONF-1	Aromatic amine	499	1.86	1.34		135	51	29	[305]
PECONF-2	Aromatic amine	637	2.85	1.98			44	31	[305]
PECONF-3	Aromatic amine	851	3.49	2.47			41	26	[305]
PECONF-4	Aromatic amine		2.95	1.96			51	34	[305]

Table 5. Continued 5

[#]CO_2/N_2 selectivity at 298 K. *CO_2 uptake at 0.15 bar and 295 K.

6.2.1 Non-functionalized porous organic polymers

To date, a number of different types of coupling reactions and monomers have been successfully applied to synthesize various POPs. POPs with ultrahigh-surface-area usually have very weak physical interactions with CO_2 molecules and are thus applicable as materials in pre-combustion carbon capture. Among them, porous materials constructed from boron-oxygen bonds are among the first-reported and well-studied systems, often known as COFs.[17, 224, 306-308] Diboronic acids undergo condensation reactions, such as cyclotrimerization or reactions with ortho-benzenediol moieties to form six or five-membered rings that lend to network formation.[17] Since the formation of boroxine ring is quite reversible, such COFs typically have good crystallinity with long-range order,

making it possible to precisely design new COFs with atomic level control. Moreover, boroxine ring-based COFs usually have a narrow pore size distribution compared with amorphous porous materials. Unfortunately, the boroxine rings show relatively high sensitivities to moisture, which results in framework decomposition and reformation of boronic acids. As a result, boroxine-linked COFs may not be appropriate materials for CO_2 capture. The introduction of specific functional groups onto the surface of such COFs, either by using pre-synthetic monomer or post-functionalization, may improve their water stability or enable their application in high-pressure CO_2 separation.[309-313]

Unlike the moisture sensitive nature of boroxine rings, polymers based on carbon-carbon bonds are relatively stable. Common strategies, such as Suzuki coupling,[297, 314] Sonogashira reaction,[260, 315-317] Yamamoto reaction,[4, 262, 269, 318-319] Eglinton coupling,[225, 320] and Friedel-Crafts reaction,[321, 322] give rise to the carbon-carbon coupling to produce amorphous solids. One of the current benchmark polymer for carbon capture is PPN-6,[269] also known as PAF-1.[318] The irreversible nature of carbon-carbon bond formation precludes the formation of structures with long-range order. Structural disorder and defects lead to relatively broad powder X-ray diffraction (PXRD) peaks and pore size distributions observed in amorphous polymers. These materials have the potential to be applied in carbon capture due to their extraordinary chemical and thermal stabilities, large surface areas, and low cost.

Several aspects of POPs have been intensively studied and applied in order to guide the design and improve the carbon capture properties of these porous polymers. In general, it has been observed that: 1) Larger surface area will provide more adsorption

sites and 2) proper design of pore size that are compatible with the dimensions of CO_2 molecules will significantly improve the selectivity of POPs over other gaseous components in a mixture.

6.2.1.1 The effect of surface area on carbon capture

High surface area is one of the most notable properties of POPs. While high surface area may have little contribution to adsorption at low pressure,[317, 323] it will dramatically increase the number of adsorption sites for CO_2 at elevated pressures, which is ideal for pre-combustion capture process.[192] At a significantly high pressure, almost all the adsorption sites on the surface are available for CO_2 binding. Additional CO_2 molecules may further condense inside the pores beyond monolayers coverages, creating multiple-layers, and thus further increasing the overall capacity. It has been reported that the amount of excess CO_2 uptake is directly related to the total pore volume as well as the BET surface area.[324] PPN-4, with the highest surface area (6461 m^2 g^{-1}), showed excellent CO_2 adsorption at high pressure (3.89 mmol/g at 295 K, 50 bar).[4] Thus, targeting high surface area polymers is an effective method to synthesizing materials with high CO_2 capacity.

Additionally, the pore properties may also affect the CO_2 capacity, which has been investigated by Jiang and coworkers.[325] The CO_2 adsorption capacities of various COF materials was simulated at high pressure (30 bar) in order to demonstrate the relationship between the CO_2 adsorption capacity and various pore properties, such as density, pore volume, BET surface area, and free volume. Both the gravimetric and volumetric CO_2 capacities demonstrate corresponding trends with all four of the pore-related parameters.

102

Specifically, the CO_2 capacity increases with surface area, porosity, free volume, and decreases with density. As previously mentioned, at high pressure conditions CO_2 binding is maximized, thus an adsorbent with a large free volume and surface area has more space and active sites to accommodate sorbate molecules and hence exhibit enhanced CO_2 uptake. Moreover, 3D COFs tend to have lower density and larger free pore volume, porosity and surface area than 2D and 1D structures (Figure 37). As a result, 3D COFs usually have larger capacities for CO_2 adsorption at high pressures. Based on this study, the four aforementioned pore parameters could be later applied to evaluate and predict the overall theoretical saturated CO_2 capacity in other COF materials.
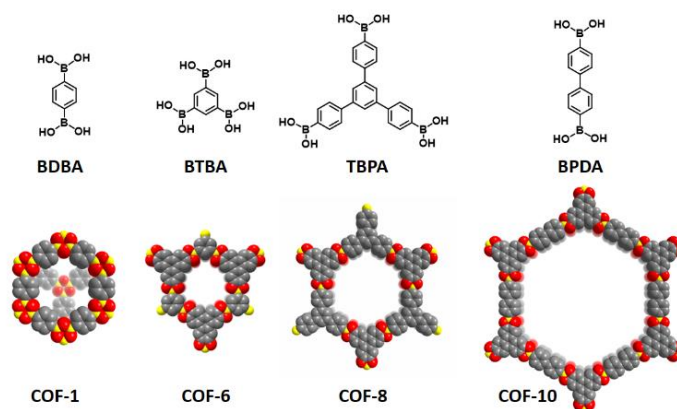
Figure 37. Co-condensation of boronic acid building blocks to give 2D COFs (COF-1, -6, -8, and -10) having systematically designed porous structures. Coloring scheme: C, gray; B, yellow; O, red.
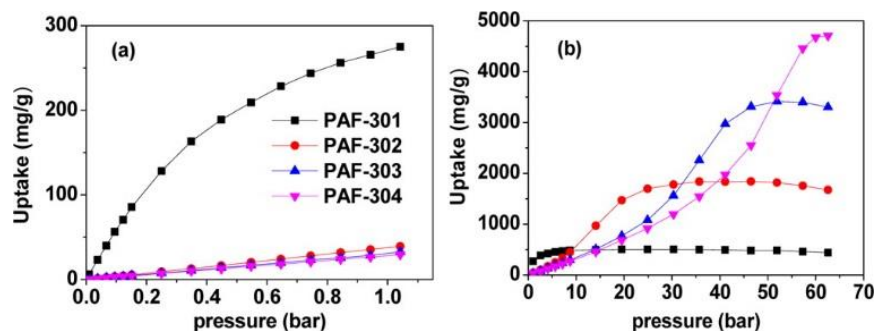
Figure 38. CO_2 adsorption isotherms at 298 K in PAFs: (a) at low pressure; (b) at high pressure. Reprinted from ref.[326]

Theoretically, polymers formed from all carbon-carbon bonds are expected to follow the same trend, which was evidenced by the simulated results of a series of PAF structures.[326] As shown in Figure 38, the CO_2 capacities of a PAF-30X series (X=1, 2, 3, 4, representing the number of phenyl rings in the monomers) showed significant dependence on the linker length at different pressure regions. At low pressure (Figure 38a), the CO_2 adsorptions decreased in the order of PAF-301 > PAF-302 > PAF-303 > PAF-304. This order was exactly opposite to that of the linker lengths but in accord with the isosteric heats, since smaller pores lead to stronger interaction with CO_2 molecules, and isosteric heats dominate the adsorption property at lower pressure. However, structures with larger surface areas start to show higher capacities at high pressure (Figure 38b). Near the high pressure region (p > 55 bar), where CO_2 capacities are approaching the saturated values, and the condition is close to pre-combustion practice, the order of adsorption is entirely opposite to that at low pressure, i.e. PAF-304 > PAF-303 > PAF-302 > PAF-301, indicating that surface area and pore volume dominate the saturated CO_2 capacity. In contrast, Cooper *et al*. reported a negative correlation between surface area and linker

length in a CMP series.[316] Such observations might be caused by possible network interpenetration and increased flexibility of longer linkages.

6.2.1.2 The effect of pore size on carbon capture

Pore structure is one of the key properties to be studied and characterized when considering a given POP for carbon capture. In addition to the functionalities present at the pore surface, the pore size also dramatically affects the adsorption capacity and the selectivity of CO_2 over other gases. By targeting pore sizes near the kinetic diameter of CO_2 (3.3 Å), the number of double or multiple interactions between adsorbed CO_2 and the pore walls can be increased. Such strategy has been successfully used for hydrogen gas storage in different kinds of materials[327], including COFs[308], CMPs[316], PIMs[328] and so on. Due to the distinct differences between the sizes and polarizabilities of CO_2 and other gas molecules,[329] tuning the pore size to around the diameter of CO_2 can lead to enhanced carbon capture performance. In such cases, CO_2 molecules can interact with multiple faces of the pores, while other gas molecules are prevented from forming strong interactions because of their lack of or reduced polarizability. Proper design of microporous structures is one key criteria to improve the selectivity by a kinetic approach.

After the first COF material was reported by Yaghi's group in 2005,[16] the pore sizes in such COFs have been well studied. As mentioned before, the formation of boroxine ring is reversible to some extent, resulting in polymers with certain crystallinity. By applying isoreticular chemistry to COF materials, the pore sizes were enlarged symmetrically, while the relative crystalline properties were well-maintained. On the other

hand, carbon-carbon bond forming reactions are virtually irreversible, producing amorphous solids in most cases. For these reasons, precise control of pore properties in all carbon-carbon bond containing polymers is notably difficult.

6.2.1.3 Polymer sponge

Several other types of POPs have also been reported for carbon capture purposes. Among them, the hyper-cross-linked polymer (also known as "polymer sponge"), reported by Cooper and coworkers, is a unique candidate for pre-combustion CO_2 adsorption (Figure 39).[261] Similar to the carbon-carbon bonds linked polymer, this hyper-cross-linked polymer displays extraordinary stability, even in the presence of a boiling acidic solution. Although the surface area of this polymer is relatively low, the gravimetric CO_2 capacity reached 15.32 mmol/g under dry conditions at 298 K and 40 bar. The flexible nature of this polymer enables CO_2 adsorption via physical swelling, different from that of rigid materials. Performance was further enhanced at high pressures leading to a higher CO_2 capacity and an enhanced CO_2 selectivity over some of the top performing MOFs and inorganic sorbents. Moreover, the adsorption is hardly affected by the presence of water vapor due to the hydrophobicity of this carbon-based network. The CO_2 sorption remains at 13.17 mmol/g under wet conditions at 298K and 40 bar, which is about 86% of their dry CO_2 capacity. By contrast, the MOF sample, HKUST-1, retains only 28% of its dry CO_2 capacity under the same conditions, while zeolite 13x only remains 6%. The low-cost, extraordinary stability, high CO_2 capacity, and excellent selectivity makes the

polymer sponge a promising candidate for pre-combustion carbon capture in industrial settings.
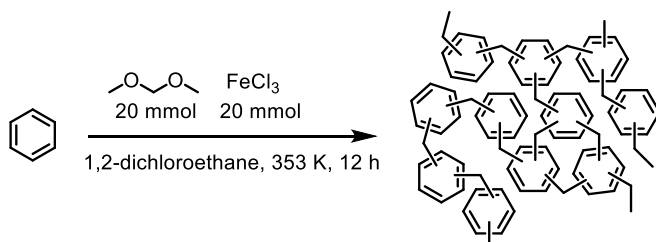
Figure 39. Synthesis of the hyper-cross-linked polymer. Adapted from ref. [261].

6.2.2 Nitrogen-rich porous organic polymers

At this point, it is important to note that targeting high surface area materials may not always be the best approach to improve CO_2 capacity at low pressure. Incorporating specific functional groups in order to enhance CO_2-adsorbent interactions may be an even more effective strategy. Studies have shown that introducing nitrogen sites in POPs has great potential for increasing CO_2 uptake and selectivity of the materials through specific dipole-quadrupole interactions and/or hydrogen bonding. To date, a series of nitrogen-rich functionalities have been incorporated into POPs for higher CO_2 uptake and selectivity, including aromatic amines, imidazole, triazole, triazine, melamine, azo, imine, imide, tetrazole, and so on.

6.2.2.1 Aromatic amine functionalized porous organic polymers

Aromatic amine based POPs refer to polymeric materials containing amine groups, that are directly bound to the aromatic rings of the monomers. These POPs can be classified into three categories: primary, secondary and tertiary aromatic amine based materials.

In primary aromatic amine based POPs, the CO_2 adsorption capacities are often related to the existence of nitrogen functional sites and suitable pore sizes for CO_2. [243-244, 287] For instance, as introducing –NH_2 groups into NPOF-4 to generate NPOF-4-NH_2, the isosteric heat of CO_2 adsorption (Q_{st}) was improved from 23.2 kJ mol^{-1} (NPOF-4) to 30.1 kJ mol^{-1} (NPOF-4-NH_2) (Figure 40).[287] The siginificant enhancement originated from the large quadrupole moment of CO_2 that forms stronger interaction with polar -NH_2 groups. Besides the enhanced CO_2-adsorbent affinity, post-synthetic modification produced narrower pores in NPOF-4-NH_2 than NPOF-4, that lead to higher Q_{st} in NPOF-4-NH_2 by multiple wall interactions.

Similar examples have also been reported in POPs with secondary aromatic amines, such as TBMID,[304] PECONF,[305] and PTPA-3[330]. The existence of secondary aromatic amines groups promotes favorable interactions between polymers and CO_2, thus enhancing the CO_2 uptake. There are two ways to incorporate the secondary amines into POPs. In the cases of PECONF, secondary aromatic amine groups are introduced into the polymer via the reaction between primary amines and halogenated monomers. By removing the generated hydrogen halide, the monomers were cross-link to form networks with a high density of secondary aromatic amine groups. PECONF has CO_2 uptake of 3.50

mmol/g at 273 K and 1 bar. The other way to incorporate the secondary aromatic amine groups into POPs is to employ monomers containing secondary aromatic amine groups in polymerization, which is found in the synthesis of TBMID.[304] Following polymerization via Sonogashira-Hagihara cross-coupling, secondary aromatic amine groups from the isoindigo monomers were successfully embodied within TBMID. As expected, the strong dipole-quadrupole interactions between secondary aromatic amine groups and CO_2 endowed TBMID with high affinity towards CO_2, which was supported by the high isosteric heats of CO_2 adsorption (33.5 kJ mol^{-1}). TBMID also demonstrated a high CO_2 uptake of 3.30 mmol/g at 273K and 1.13 bar with a CO_2/N_2 selectivity of 58.8.
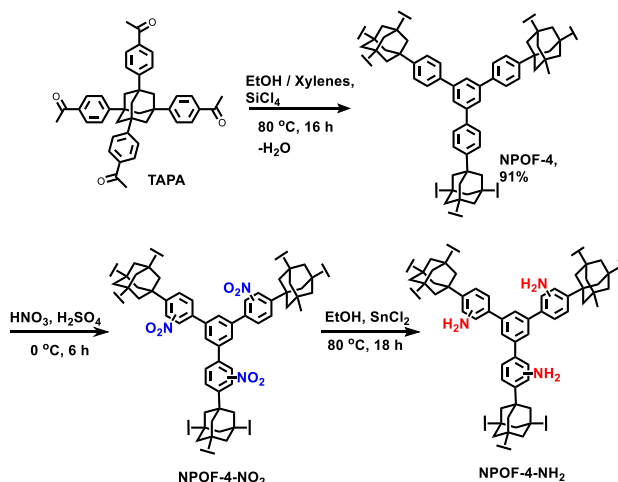
Figure 40. Schematic representation of NPOF-4 synthesis and its post-synthesis modification.

So far, POPs containing tertiary aromatic amine groups have been reported most.[263, 286, 288-290, 293, 303, 331] Among them, a typical example is Tröger's base-derived microporous organic polymers (TB-MOPs) [293]. In the synthesis of TB-MOPs, tertiary

aromatic amines are formed via Trögerization of terminal amines attached to tetrahedral monomers through a one-pot metal-free synthetic approach. The CO_2 adsorption results show 4.05 mmol/g and 2.57 mmol/g at 273 K and 298 K, respectively. Besides the high CO_2 uptake, TB-MOP also exhibits excellent selectivity for CO_2 over N_2, which are 45.2 and 50.6 at 273 and 298 K, respectively. In addition, the heats of adsorption were measured in the range of 24.5-29.5 kJ mol^{-1}, which were relatively high in MOP materials but still lower than the energy of chemisorptive process. The inherent microporosity could also be responsible for the high CO_2 capacity due to multiple wall interactions.

It is worth pointing out that a general trend between the CO_2 uptake of POPs and the types of aromatic amine (primary, secondary or tertiary) cannot be concluded. The CO_2 uptake of POPs is a result of multiple variables, such as inherent pore size, surface area, and density of polar groups. In general, arylamines have less affinity towards CO_2 compared with alkylamines, since the charge density on arylamine nitrogen sites is lower than that of alkylamines. Nevertheless, arylamine incorporated POPs exhibit considerable CO_2 uptakes and could be considered as good CO_2 adsorbents with enhanced stability due to rigidity of aromatic units that promote permanent porosity.

6.2.2.2 Benzimidazole-linked porous organic polymers

El-Kaderi *et al*. reported the synthesis of a series of benzimidazole-linked polymers (BILPs) formed via condensation reactions.[276-278, 280-282, 332] For example, BILP-1, formed by the template-free synthesis from 2,3,6,7,10,11-hexaaminotriphenylene (HATP) and tetrakis(4-formylphenyl)methane (TFPM), exhibits a BET surface area of

1172 m^2 g^{-1} and CO_2 uptake of 2.97 mmol/g at 298 K and 1 bar (Figure 41).[276] Notably, BILP-1 is stable in the presence of 2 M HCl due to the chemical robustness of the imidazole ring. Moreover, BILP-4 shows BET surface area of 1135 m^2 g^{-1} and significantly high CO_2 uptake of 5.34 mmol/g at 273 K and 1 bar.[277] In addition, BILP-101, synthesized from 1,2,4,5-benzenetetramine tetrahydrochloride (TBA) and 1,3,5-triformylbenzene, exhibits a CO_2 uptake of 0.82 mmol/g at 298 K and 0.15 bar and exceptional CO_2 selectivity over N_2 (80) at 298 K.[281] The relatively high CO_2 uptake and selectivity over N_2 and CH_4 by BILPs are most likely because of favorable interactions of the polarizable CO_2 molecules with the framework through dipole-quadrupole interactions and/or hydrogen bonding via proton-free and protonated nitrogen sites of imidazole rings.
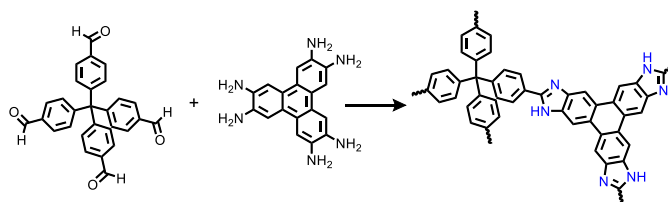
Figure 41. Synthesis of BILP-1. Reprinted from ref. [276].

In order to study the effect of acid on textural properties of BILPs, HCl-free amine building units and diluted acid with variable acid/amine ratios are used in the synthesis (Figure 42).[280] According to the proposed mechanism of imidazole moiety formation, the acid protonates the carbonyl groups of the aldehyde moiety and catalyzes the formation of imine bond. Since imine-bond formation is reversible, acid can be used to control the rate of condensation and thus improve the surface area of the polymers.

After optimizing the amount of HCl used and its concentration, the surface areas of BILP-15 and BILP-16 increased significantly by 92% and 47%. A noticable increase in CO_2 uptake was observed from 2.60 mmol/g to 3.41 mmol/g at 273 K and 1 bar.

In 2014, the El-Kaderi group also reported the synthesis of triazine-based benzimidazole-linked polymers (TBILPs), namely TBILP-1 and TBILP-2, by condensation reactions of 2,4,6-tris(4-formylphenyl)-1,3,5-triazine (TFPT) with 1,2,4,5-benzenetetraamine tetrachloride (BTA) and 2,3,6,7,14,15-hexaaminotriptycene (HATT), respectively.[282] TBILP-1 shows very high selectivity (63) for CO_2 over N_2 t 298K. TBILP-2 exhibits significantly high CO_2 uptake (5.18 mmol/g) at 1 bar and 273 K, which can be attributed to the combined effects of the Lewis basic 1,3,5-triazine and imidazole-building units of the frameworks. Both TBILPs shows the moderate isosteric heats of adsorption for CO_2, which permits high and reversible CO_2 uptake at ambient temperature. In the same year, the Zhou group reported the synthesis of PPN-101 from tetrahedral aldehyde and amine monomer.[67] PPN-101 shows a high BET surface area of 1095 $m^2\,g^{-1}$ and a CO_2 uptake of 5.34 mmol/g at 273 K and 1 bar. The calculated CO_2/N_2 selectivity is 199 due to the presence of benzimidazole units in the framework.
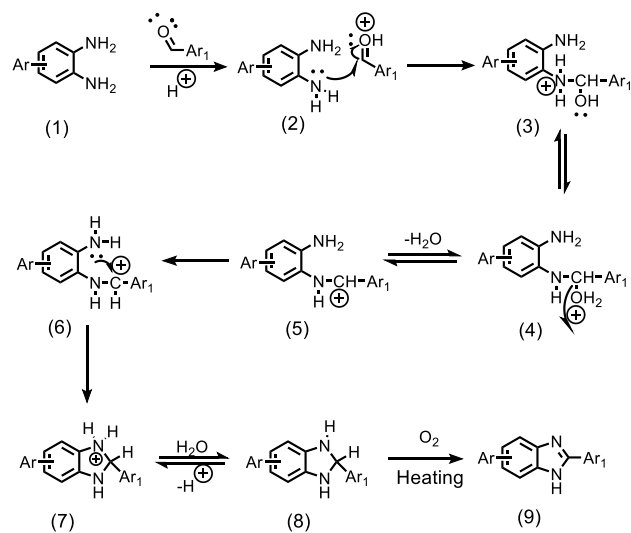
Figure 42. Proposed mechanism of imidazole moiety formation by the acid-catalyzed process. Adapted from ref. [280].

Pyrene-derived BILPs are also known for their high surface areas, chemical stability and N-rich pore walls, which may have a great potential in CO_2 capture and separation. Four novel pyrene-derived BILPs were synthesized by Sekizkardes and coworkers (Figure 43).[279] The BET surface areas of BILP-10, 11, 12, 13 were measured to be 787, 658, 1497, 677 m^2 g^{-1}, respectively. Among them, BILP-12 demonstrated the highest CO_2 uptake of 5.07 mmol/g at 273 K and 1 bar, while BILP-11 had the best selectivity of 56 for CO_2/N_2 at 298 K. Overall, these BILPs are very competitive materials in terms of CO_2 capture and separation.
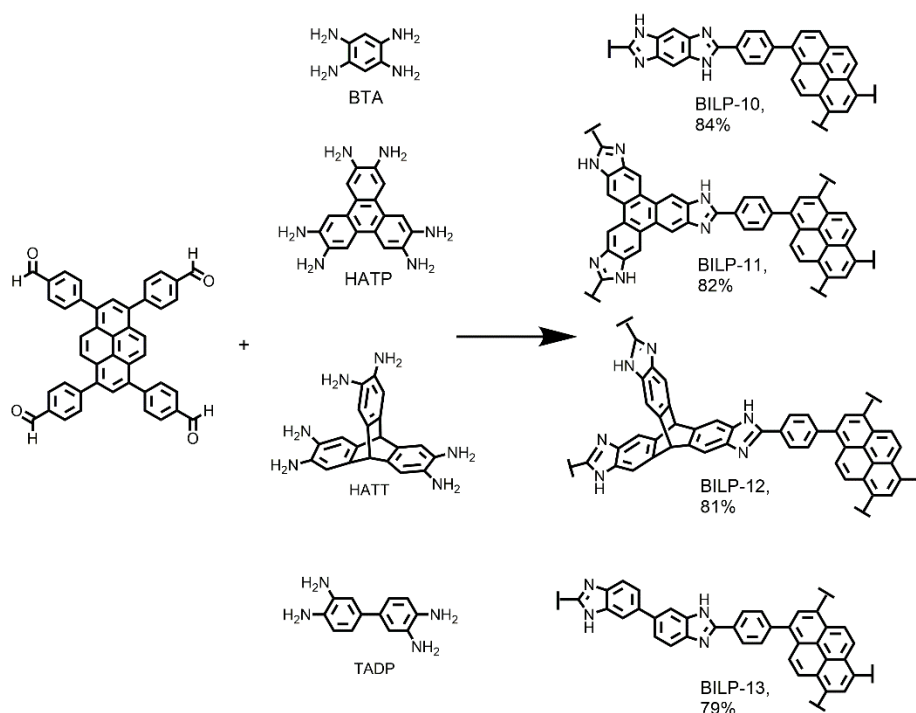
Figure 43. Synthesis of BILP-10, BILP-11, BILP-12, and BILP-13. Adapted from ref. [279].

6.2.2.3 Triazole-linked porous organic polymers

Triazole-linked POPs are usually synthesized by click reactions between azide and alkynyl moieties.[301] For example, Cooper *et al*. reported a series of networks synthesized by click reactions (Figure 44).[260] Among them, network C refers to tetrahedral-based polytriazole, which is formed through click chemistry from tetrahedral monomers. Although the surface area of network C is not the highest among the studied networks, it exhibits the highest CO_2 uptake (2.20 mmol/g) at 298 K and 1 bar. The promising CO_2 uptake performance of network C most likely stems from the electron-rich triazole unit in the network. Moreover, network C has the highest heat of adsorption (33.7 kJ mol^{-1}) at low coverage compared with other networks, which is important for post-combustion

114

carbon capture which occurs in the low pressure regime. In addition, this number is maintained at higher coverage.
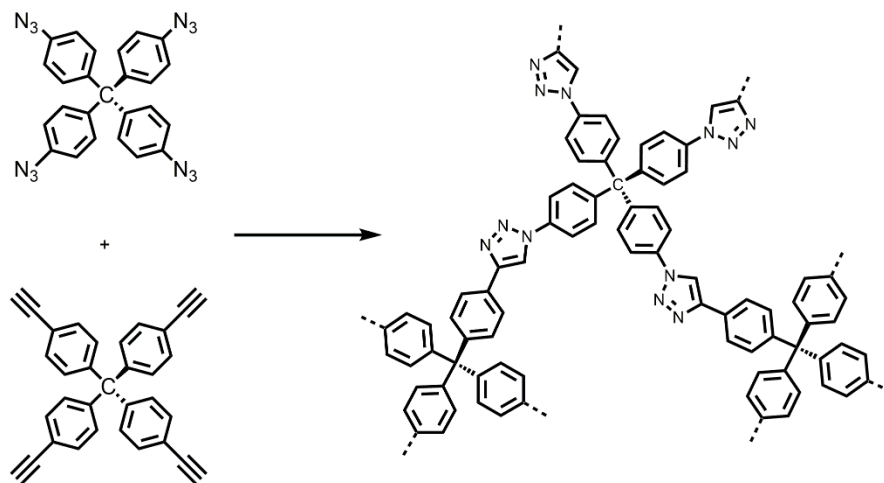
Figure 44. Synthetic route for network C. Adapted from ref. [333].

6.2.2.4 Triazine-linked porous organic polymers

  Introduction of stable electron-withdrawing triazine units into POP systems could be advantageous to both in stability and electronic structure of the POP materials.[334] Triazine-linked POPs were first developed by Thomas and co-workers through ionothermal synthesis reaction.[251] Ordered microporous POPs can be obtained from the trimerization of nitrile units in a melt $ZnCl_2$ at 400 °C. Later, perfluorinated triazine linked framework (FCTF-1) were reported by Han et al for carbon capture.[335] The perfluorinated materials often exhibit hydrophobic and lipophobic characteristics as well as the extraordinary affinity to CO_2. In particular, FCTF-1 has the following advantages: a) the N-rich framework favors CO_2 adsorption, while the electronegativity of F can further

enhance the electrostatic interactions with CO_2; b) The incorporation of F results in smaller pore size (less than 0.5 nm), which can promote the CO_2 adsorption via multiwall interactions as well as enhance CO_2-N_2 separation by kinetic selectivity; c) the hydrophobic nature of F units enables the materials great water stability, and more importantly, FCTF-1 can retain its high CO_2 capture performance even in the presence of water; d) since no strong chemical adsorption is involved, regeneration is facile.

In 2012, the Cooper group reported the synthesis of a series of conjugated microporous polymers based on electron-withdrawing 1,3,5-triazine linkage (TCMPs) by palladium-catalyzed Sonogashira-Hagihara cross-coupling reaction.[245] Although the surface areas of the TCMPs were similar to the corresponding benzene-linked CMPs, the CO_2 capacity was higher. In paticular, TNCMP-2 exhibited high surface area (995 m^2 g^{-1}) and efficient CO_2 uptake (1.45 mmol/g) at 298 K and 1 bar.

In 2015, Zhu *et al*. reported the synthesis of porous aromatic framework PAF-56P via cross-coupling of cyanuric chloride and *p*-terophenyl monomers (Figure 45).[295] PAF-56P exhibits a three dimensional framework with a large pore size of 12.0 Å and a high CO_2 uptake (1.52 mmol/g) at 298 K and 1 bar. When PAF-56P was integrated with glassy polysulfone (PSF Udel P-3500) matrices to make PAF-56P/PSF hollow fiber membranes for CO_2 capture, the membranes showed high selectivity of CO_2 over N_2 (as high as 38.9) due to the abundance of basic nitrogen sites in the PAF-56P framework.
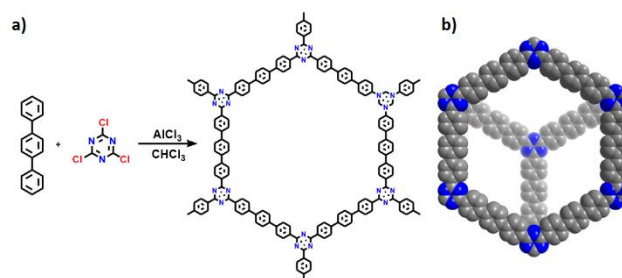
Figure 45. a) Synthesis of PAF-56P and b) PAF-56P stacked structure drawn by materials studio. Adapted from ref.[295].

6.2.2.5 Melamine functionalized porous organic polymers

In 2014, the Zhu group reported the synthesis of N-rich SNW-1 from melamine and terephthalaldehyde monomers linked through C-N bond formation (Figure 46).[302] SNW-1 exhibits a three-dimensional framework with a surface area of 821 m^2 g^{-1} and major pore size around 5 Å.[336] The high CO_2 sorption capacity and selectivity of SNW-1 can be attributed to the microporous properties and existence of abundant N-H groups present within the frameworks. Small pores of SNW-1 are most likely to be highly packed with CO_2 molecules via Van der Waals interactions. The N-H moieties in the SNW-1 can interact strongly with CO_2 molecules, which is favorable for high CO_2 adsorption.
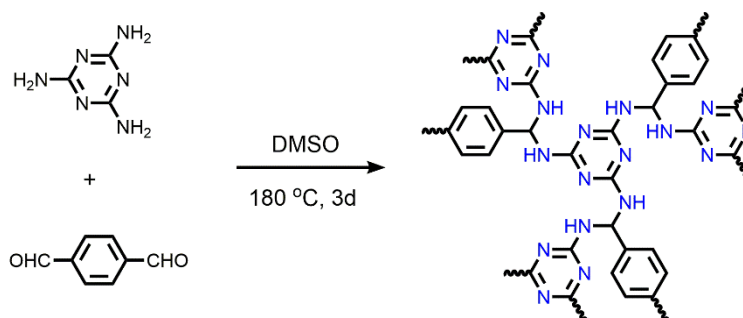
Figure 46. Schematic representation of chemical structure of SNW-1. Adapted from ref. [336].

117
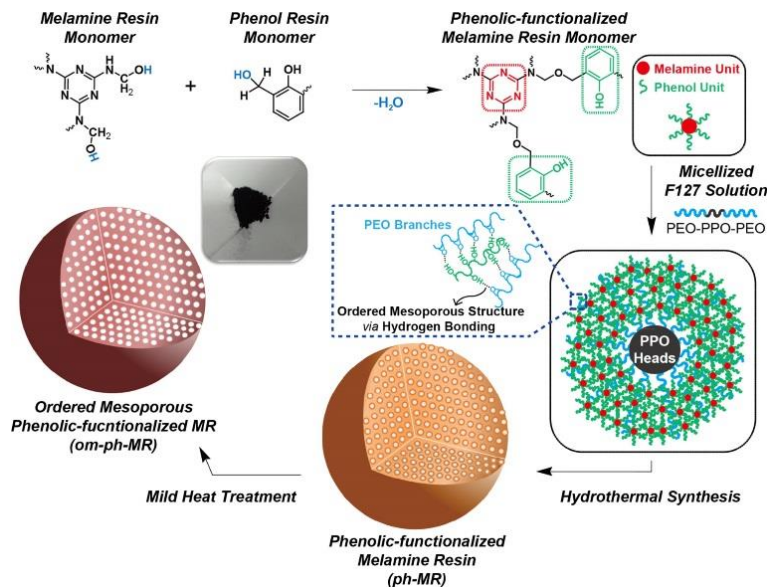
Figure 47. Schematic representation showing the synthetic route of ordered mesoporous phenolic-functionalized melamine resin (om-ph-MR). Reprinted from ref. [300].

Despite the high N con tent, melamin resin (MR) cannot be used for carbon capture due to its nonporous nature. In 2015, Choi and coworkers reported a co-assembling method to make a highly-ordered mesoporous polymeric network with high nitrogen content from nonporous melamine resin monomer (Figure 47).[300] The phenolic resin (PR) units can form hydrogen bonding with a well known surfactant Fluroinc F127 to produce a highly ordered mesoporous copolymer network. The resultant polymer om-ph-MR shows an unexpected increased CO_2 selectivity with temperature rise. The exceptional selectivity is likely because of the abundant nitrogen moieties permitting a high binding affinity with CO_2 plus the presence of the well-defined mesopores (2.5-2.9 nm) facilitating N_2 release at higher temperature.

118

6.2.2.6 Azo-linked porous organic polymers

In 2013, Yavuz and Coskun reported the synthesis of nanoporous azo-COPs by catalyst-free coupling of aromatic nitro and amine moieties under basic conditions (Figure 48).[284] These azo- COPs have BET surface areas up to 729 m^2 g^{-1} and CO_2 uptake up to 2.50 mmol/g at 273 K and 1 bar. Particularly, these azo-COPs exhibit a significant increase in the CO_2 selectivity over N_2 at increased temperature, which is most likely due to the N_2-phobic azo groups in the polymer. Monte Carlo simulations reveal that although N_2 adsorption is enthalpically favorable, the entropy loss upon binding of N_2 molecules leads to N_2 phobicity of azo groups. This work also shows the importance of azo groups in separation of CO_2 and N_2 mixtures efficiently, which is promising for the post-combustion CO_2 separation.
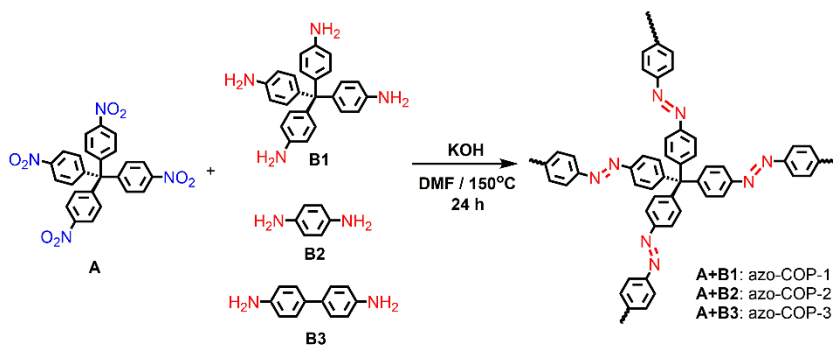
Figure 48. Synthesis route for azo-COPs. Adapted from ref. [284].

In the following year, El-Kaderi *et al*. reported a facile method to synthesize highly porous azo-linked polymers (ALPs) by homocoupling of aniline-like building units catalyzed by copper (I) bromide.[285] Among them, ALP-1 showes a high BET surface area of 1235 m^2 g^{-1} as well as high thermal and chemical stability. In addition, ALP-1 exhibits

119

a remarkable gravimatrical CO_2 uptake (5.36 mmol/g) at 273 K and 1 bar. The azo group can function as the Lewis basic site, while the electron deficient carbon atom in CO_2 can function as Lewis acid, generating enhanced dipole-quadruple interactions between these two metrics.

6.2.2.7 Imine-linked porous organic polymers

Utilizing the strategy of formation of imine bonds is a reversible reaction by dynamic covalent chemistry, crystalline imine-linked COFs were developed by the Yaghi group.[15] The imine linked COFs are good candidates for carbon capture due to the enhanced affinities of nitrogen atoms to CO_2. The imine-based POPs can be synthesized by co-condensation of aldehydes with amines or hydrazides. Many research groups have focused on developing crystalline COFs via novel synthetic strategies, which would greatly promote the development of the imine linked COFs and provide better candidates for practical carbon capture.[299, 337-345]

In 2012, Banerjee and coworkers reported the two imine-linked COFs, TpPa-1 and TpPa-2 for carbon capture (Figure 49).[346] These COFs were synthesized via Schiff base reactions of 1,3,5-triformylphloroglucinol (Tp) with p-phenylenediamine (Pa-1) and 2,5-dimethyl-p-phenylenediamine (Pa-2) under solvothermal conditions. Surprisingly, the enol-imine group underwent irreversible proton tautomerization to form the keto-enamine product. Both TpPa-1 and TpPa-2 showed exceptional acidic stability and water stability. TpPa-2 is stable even in 9N NaOH as TpPa-1 and TpPa-2 demonstrated reversible type-I adsorption isotherms during the N2 uptake measurement with the BET surface areas of

535 m^2 g^{-1} and 339 m^2 g^{-1}, respectively. The CO_2 adsorption of TpPa-1 and TpPa-2 are

3.48 mmol/g and 2.86 mmol/g at 273 K and 1 bar, respectively. Additionally, the synthetic

strategy was applied to other starting materials, such as benzidine (BD), affording TpBD

COFs. Moreover, TpBD can be obtained with solvent free mechanochemical grinding

while maintaining its crystallinity and the porosity.[347] Microwave-assisted solvothermal

method was also employed to synthesize TpPa-1, which exhibited enhanced crystallinity

and porosity with an increased CO_2 uptake of 4.95 mmol/g at 273 K and 1 bar.[348] To

further enhance the stability and crystallinity, Banerjee group discovered that introducing

–OH units adjacent to the –C=N- centers can create intramolecular O-H···N=C hydrogen

bonds.[349] The generated COF, namely DhaTph, also showed improved crystallinity and

chemical stability compared with the COF lacking intramolecular hydrogen bonding. The

CO_2 uptake of DhaTph is 2.91 mmol/g at 273 K and 1 bar.
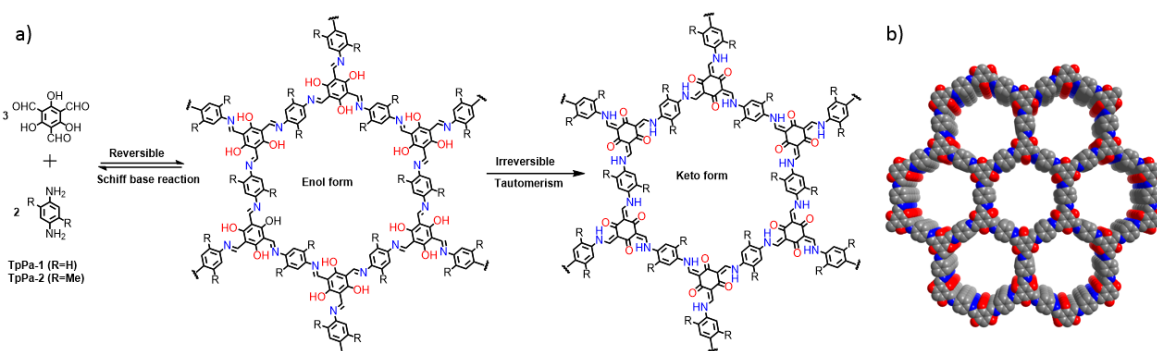
Figure 49. a) Schematic representation of the synthesis of TpPa-1 and TpPa-2 by the combined reversible and irreversible reaction of Tp with Pa-1 and Pa-2, respectively. b) TpPa-1 stacked structure drawn by materials studio.

121
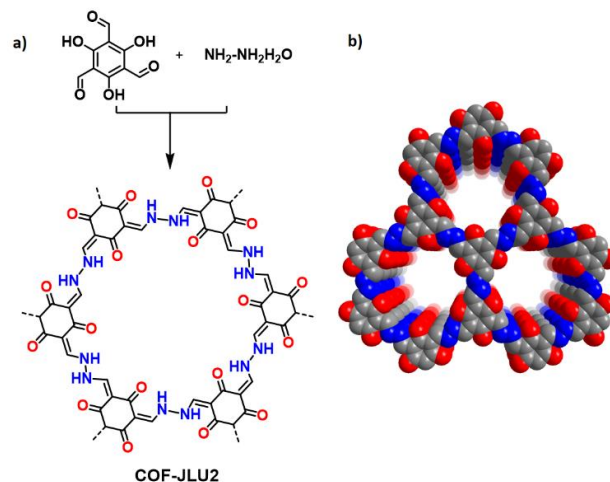
Figure 50. a) Schematic representation of the synthesis of COF-JLU2. b) Top views of the AA stacking structure of COF-JLU2.

An azine-linked COF, namely COF-JLU2, was designed and synthesized by condensation of 1,3,5-triformylphloroglucinol and hydrazine under solvothermal conditions (Figure 50).[350] COF-JLU2 combines the following merits: permanent microporosity, high crystallinity, and good stability. The BET surface area of COF-JLU2 is 410 $m^2 g^{-1}$, while the CO_2 uptake is 4.93 mmol/g at 273K and 1 bar. The CO_2 adsorption capacity is comparable to some excellent POP materials, including CPOP-1 (4.81 mmol/g)[351] and PPF-1 (3.09 mmol/g)[352]. The excellent CO_2 capacity can be attributed to the inherent microporosity and the abundant heteroatom activated sites in the skeleton. The Q_{st} of COF-JLU2 for CO_2 was calculated to be 31 kJ mol^{-1} at low coverage. The selectivity of CO_2/N_2 was 77, which was calculated using Henry's law.

6.2.3 Oxygen-rich porous organic polymers

Another commonly used functional groups in POPs to enhance the CO_2 binding energy by dipole-quadrupole interactions are oxygen-containing moieties, such as the hydroxyl groups and carboxyl groups. These functional groups are highly polar, leading to the strong dipole-quadruple interactions with CO_2.

6.2.3.1 Multi-hydroxyl-containing porous organic polymers

Han's group utilized phenol formaldehyde resin (PF) chemistry to construct three hydroxyl-containing porous organic polymers (PFPOP 1-3, Figure 51).[289] These PFPOP materials are prepared by combining four –OH containing phenol with trialdehydes under catalyst-free conditions. Due to the carbon-carbon bond linkages, these PFPOPs demonstrate high thermal and chemical stability. All of the PFPOPs present Type I BET isotherms, with slight sorption hysteresis and specific surface areas of PFPOP-1, PFPOP-2 and PFPOP-3 are 570, 630, and 530 $m^2 \cdot g^{-1}$, respectively. The microporous properties and internal structures containing abundant hydroxyl groups make these materials suitable for carbon capture. Among them, PFPOP-3 has the highest CO_2 storage capacity of 4.74 mmol/g at 273 K and 1 bar. Meanwhile, PFPOPs show considerable CO_2 over N_2 selectivity (43.7 – 56.5 by IAST) in the flue gas composition (CO_2/N_2 = 15/85) at 273 K and 1.0 bar. Han group further explored this type of chemistry and created a series of mannitol-based acetal–linked POPs (MAPOPs) with decent CO_2 capacities.[290]

Compared to MAPOPs, Li and coworkers extended the aromatic acetyl monomers to more functionalities.[291] The corresponding polymers, namely mannitol-based ketal-

linked porous organic polymers (MKPOPs), demonstrated BET surface areas steaming from 160 to 590 $m^2 \cdot g^{-1}$ with exceptionally relative low CO_2 adsorption capacities (1.43 mmol/g to 2.61 mmol/g at 273 K and 1 bar) and relative low heats of adsorption (18.3 - 27.1 $kJ \cdot mol^{-1}$).
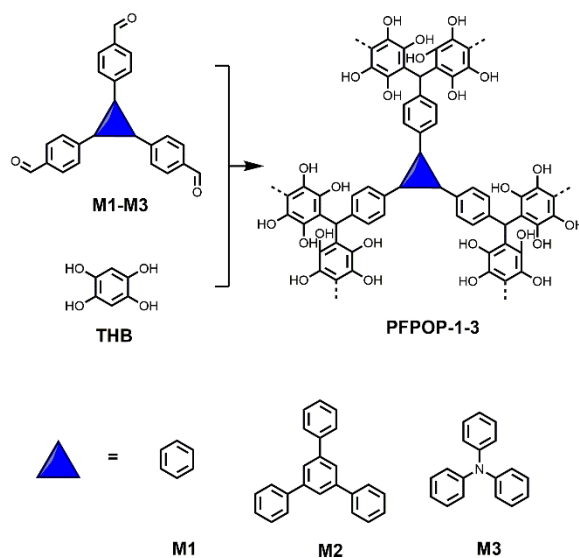
Figure 51. Synthesis of PFPOP-1, PFPOP-2, and PFPOP-3. Adapted from ref. [289].
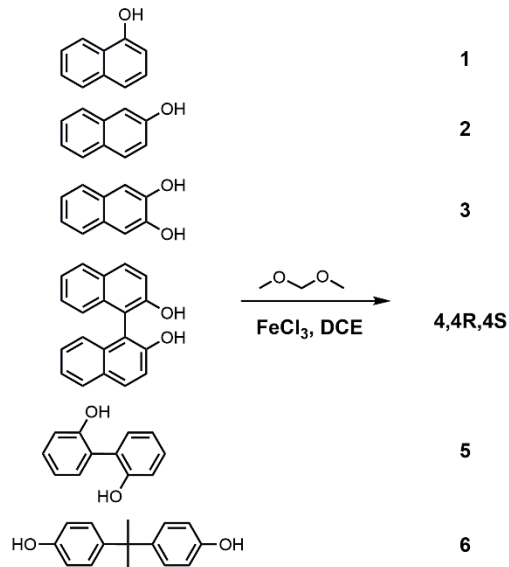
Figure 52. Synthesis of hydroxyl-containing MOP networks via Friedel−Crafts alkylation with FDA at 80 °C for 18 h. Adapted from ref.[13].

Later, a series of alcohol-containing POPs were synthesized by Friedel-Crafts alkylation reaction of aromatic monomers and formaldehyde dimethyl acetal (FDA) (Figure 52).[13] CO_2 adsorptions were measured under both dry and wet conditions. For binaphthol (BINOL) network 1 & 2, naphthalen-1-ol and naphthalen-2-ol were employed as monomers, respectively. The CO_2 uptakes were found to be 1.25 mmol/g and 1.46 mmol/g at 298 K and 1 bar, respectively. For network 4, which utilized 4,4'-bi-1-naphthol, a much higher CO_2 adsorption of 2.27 mmol/g is detected at 298 K and 1 bar. At 273 K, network 4 achieved an even higher CO_2 uptake at 3.96 mmol/g. The CO_2/N_2 selectivity was calculated up to be 26 for network 4R. The authors also found that these BINOL networks, though showing high CO_2 uptake under dry conditions, actually adsorbed less CO_2 in the presence of water, indicating that high CO_2 adsorption capacities under dry

condition does not guarantee high CO_2 adsorptions under more realistic wet conditions.

6.2.3.2 Multi-carboxyl-containing porous organic polymers

Carboxylic acid groups have been reported to trigger a dipolar interaction with carbon dioxide.[200, 265, 353-355] Huang and coworkers successfully synthesized a series of two-dimensional COFs as outstanding CO_2 capture materials through easy channel-wall functionalization (Figure 53).[266] Carboxyl groups were introduced into the framework via a one step, metal-freecatalytic synthesis. The carboxyl groups were located at the termini of the pore surfaces and they have similar acidity to that of the free catalytic synthesis. Those carboxyl groups were located at the terminus of the pore surfaces and they have similar acidities to that of the free carboxylic acid. Moreover, the ratio of carboxyl group was easily tuned by adjusting the amount of 2,5-dihydroxyterephthalaldehyde (DHTA) in the synthetic process. The BET surface area of $[HO_2C]_{x\%}$-H_2P-COF decreased from 786 to 364 $m^2\,g^{-1}$ after the modification, and the isosteric heat increased proportionally with the increasing amounts of carboxylic acid loading. The functionalization of channel walls with carboxylic acid groups significantly enhanced the CO_2 adsorption capacity. The CO_2 adsorption of $[HO_2C]_{100\%}$-H_2P-COF reached to 4.1 mmol g^{-1} at 273 K and 1 bar, which is one of the highest value among all the reported 2D and 3D COFs. The CO_2/N_2 selectivity of-$[HO_2C]_{100\%}$-H_2P-COF was found to be 77 with the IAST methods. The CO_2 capacity of $[HO_2C]_{100\%}$-H_2P-COF was also comparable to those of other top-class members.[356, 357] Furthermore, $[HO_2C]_{100\%}$-H_2P-COF can be recycled for more than ten cycles without significant decline in the uptake capacity, suggesting complete regeneration and excellent

cycling performance.
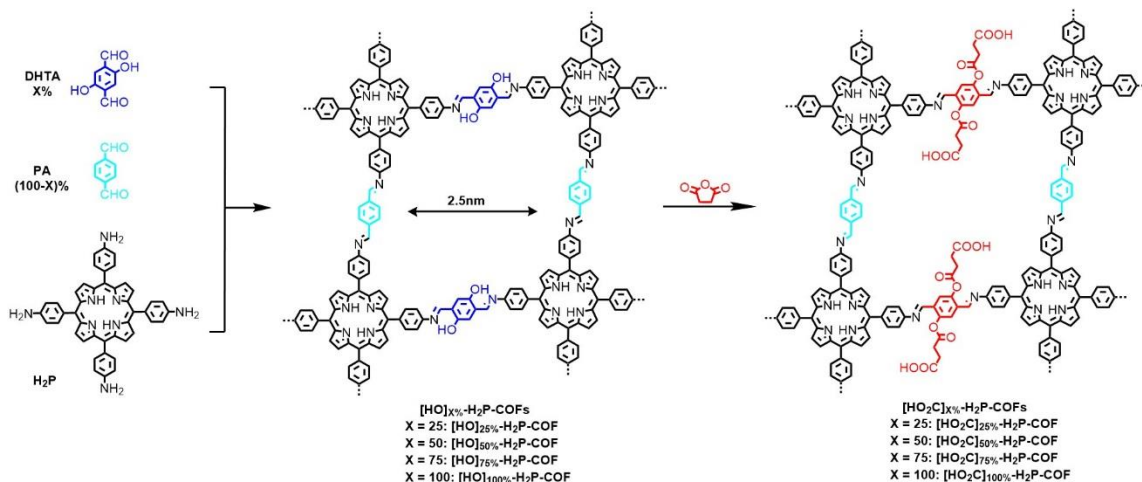
Figure 53. Synthesis of [HO$_2$C]$_{x\%}$-H$_2$P-COFs with channel walls functionalized with carboxylic acid groups through the ring opening reaction of [OH]$_{x\%}$-H$_2$P-COFs with succinic anhydride. Adapted from ref.[266].

6.2.4 Inorganic ions functionalized porous organic polymers
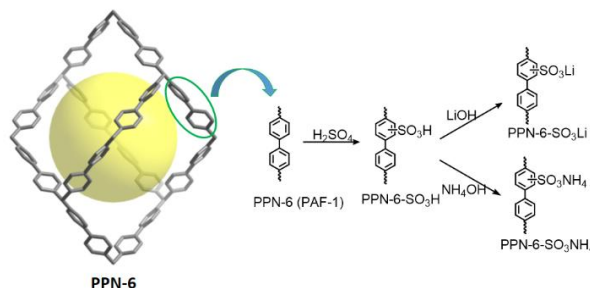
Figure 54. Synthetic route for sulfonate functionalized PPNs.

Since the introduction of polar functionalities has been shown to significantly increase the isosteric heat and CO$_2$/N$_2$ adsorption selectivity,[159, 265, 353] Lu and coworkers were able to graft PPN-6 with CO$_2$-philic groups. PPN-6 was modified by reacting with chlorosulfonic acid to produce PPN-6-SO$_3$H, which was latterly neutralized to PPN-6-

SO$_3$Li (Figure 54).[269] As a result of introducing functional groups into the polymer, the corresponding product PPN-6-SO$_3$H and PPN-6-SO$_3$Li demonstrated reduced BET surface areas of 1254 and 1186 m^2·g^{-1} , respectively. However, both materials have significantly increased gravimetric CO$_2$ uptakes with values of 3.60 mmol/g and 3.70 mmol/g, respectively. The addition of Li$^+$ in the framework promoted the CO$_2$ uptake by providing three open coordination sites to interact with CO$_2$ molecules electrostatically. The significant enhancement by Li$^+$ was also observed in the CO$_2$/N$_2$ selectivity (414 for PPN-6-SO$_3$Li vs. 150 for PPN-6-SO$_3$H) at 295 K and 1 bar. As expected, PPN-6-SO$_3$H and PPN-6-SO$_3$Li showed significantly high heats of adsorption of 30.4 and 35.7 kJ·mol$^-$^{1} at zero loading.

Later, the approach was further extended the use of PPN-6-SO$_3$H by mixing with ammonia hydroxide, where the NH$_4^+$ moieties with reduced basicity could bind to CO$_2$ reversibly (Figure 54). As the result of the incorporation of NH$_4^+$ moieties in the network, the BET surface area further dropped to 593 m^2·g^{-1}. However, PPN-6-SO$_3$NH$_4$ demonstrated the higher CO$_2$ adsorption capacity (1.78 mmol/g) at 0.15 bar and 295 K, with the calculated adsorption enthalpy of 40 kJ·mol^{-1} at zero-loading. This moderate heat capacity made PPN-6-SO$_3$NH$_4$ easier to regenerate compared to other top performing adsorbents. Under the simulated flue gas condition, the IAST adsorption selectivity for PPN-6-SO$_3$NH$_4$ was calculated to be 796 at 313 K and 1 bar. Moreover, the working capacity of PPN-6-SO$_3$NH$_4$ stemmed from 0.47 mmol/g between 40 ^{o}C and 120 ^{o}C, to 1.25 mmol/g between 40 ^{o}C and 150 ^{o}C.

Additionally, Ma and coworkers synthesized another series of carboxylate modified porous aromatic framework (PAF-26-COOH), followed by post-metalation with Li^+, Na^+, K^+, and Mg^{2+} for the purpose of increasing CO_2 capture.[270] After replacement of hydrogen with metal ions, the BET surface area decreased with the increasing ionic radius. However, the incorporation of metal ions led to improved CO_2 adsorption as well as the isosteric heat of adsorption. The Q_{st} of PAF-26-COOH was 28.1 kJ mol^{-1}, while that of PAF-26-COONa reached to 35.0 kJ mol^{-1}. The Q_{st} values for different metal replaced PAF-26-COOM are directly related to the basicities of their compensated alkali or alkaline earth ions. The CO_2/N_2 selectivities were measured by IAST methods, showing that all the functionalized PAF-26 materials had high selectivity.

In order to explore the influences of the ionic charge on CO_2 adsorption, Hu and coworkers used the conjugated cationic triazatriangulenium(TATA) as the skeleton to build two frameworks, TAPOP-1 and TAPOP-2.[288] Both of the polymers were synthesized via FeCl$_3$-promoted oxidative reaction of thiophene-/carbazole-functionalized TATA derivatives (Figure 55). TAPOP-1 and TAPOP-2 demonstrated BET specific surface areas of 930 and 940 m$^2\cdot$g^{-1} with dominantly microporosity. Due to the presence of charges that interact with CO_2 quadrupole moment, these two polymers exhibited relative high CO_2 uptakes with values of 4.20 mmol/g and 3.60 mmol/g at 273 K and 1 bar, respectively. The calculated heats of adsorption were 27.8 and 34.7 kJ$\cdot$mol^{-1}
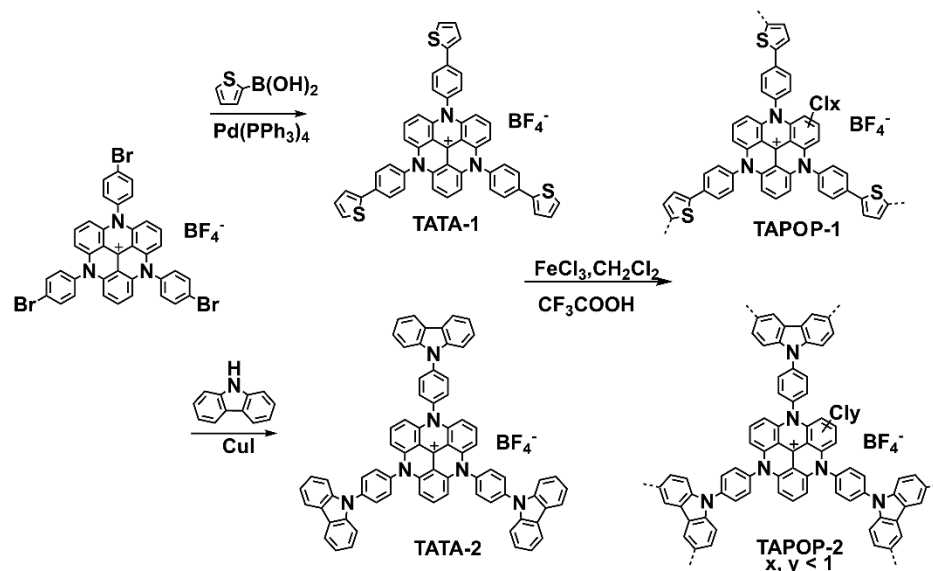
Figure 55. Synthesis of TAPOPs. Adapted from ref.[288].

Buyukcakir and coworkers incorporated 1,1'-bis(4-iodophenyl)-4,4'-bipyridine]-1,1'-diium salts, with counter ions Cl^-, BF_4^-, and PF_6^-, as the precursors to synthesize a series of porous cationic polymers (PCPs).[292] By increasing the ionic radius of the counter ions ($PF_6^- > BF_4^- > Cl^-$), the BET surface area decreased from 755 (Cl^-), 586 (BF_4^-), to 433 (PF_6^-) $m^2 \cdot g^{-1}$. As the introduction of counter ions into the polymers, CO_2 adsorption capacities were not improved compared to the neutral frameworks. However, the isosteric heats of adsorption were found in a range of 28.5 - 31.6 $kJ \cdot mol^{-1}$, which was much higher than the values reported for non-charged POPs with similar structures.[358] The DFT calculation indicated the binding geometries between CO_2 and pyridinium ions were found similar for these three cases. Interestingly, PCP-Cl demonstrated excellent catalytic ability to convert CO_2 into cyclic carbonates due to their nucleophilicity and good leaving ability.

Considering ionic POPs could have strong interactions with CO_2, Wang and coworkers reported several hypercrosslinked phosphonium-embedded polymers (Figure 56).[268] The BET surface area varied from 770 to 1168 $m^2 \cdot g^{-1}$, which could be a result of either the increasing ionic radius or increasing the length of alkyl chains. The DFT studies indicated that the phosphonium units in the polymer had high interaction energies, which was in good agreement with the high CO_2 adsorption capacity. Moreover, the CO_2/N_2 selectivity of these polymers also decreased with increasing anion size, while no significant changes resulted from the length of alkyl chains were observed. In addition, the polymer containing Br$^-$ counter ions and methyl chain demonstrated excellent catalytic activity in the conversion of CO_2 and epoxides into cyclic carbonates, whose efficiency were much higher than the polystyrene resin-support phosphonium catalyst.
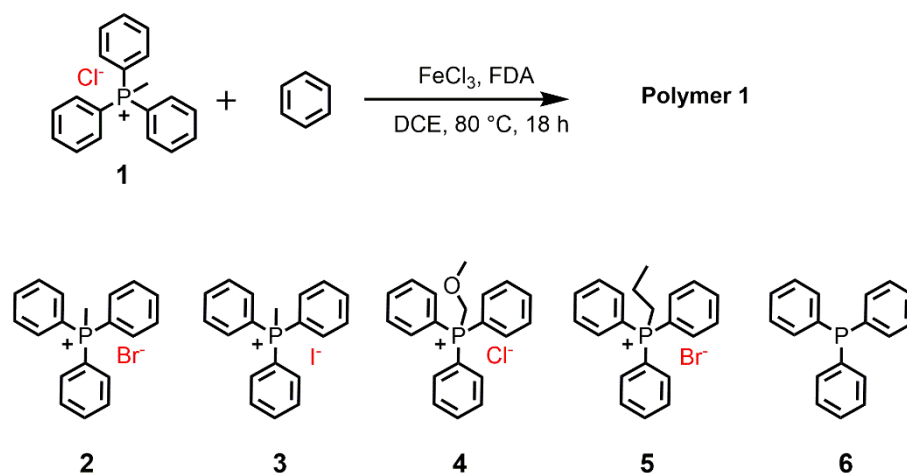
Figure 56. Synthesis of phosphonium–based polymers.

Arab and coworkers introduced the first highly porous bis(imino)pyridine linked

polymer (BIPLP-1) through a bottom-up methods to generate chelating sites in the polymerization process under metal-free conditions (Figure 57).[267] Postsynthetic modification of BIPLP-1 was applied with $Cu(BF_4)_2$ to incorporate BF_4^- and fluorinated ions aiming at increasing the CO_2 adsorption capacity. The BET areas of the polymer were measured to be 1580 $m^2\,g^{-1}$ and 380 $m^2\,g^{-1}$ before and after postsynthetic modification. Though the surface areas were sacrificed for the modifications, the functionalization dramatically enhanced the CO_2 uptake capacity by 200% at 0.15 bar due to the strong CO_2-framework interactions. As a result of the postsynthetic modification, the CO_2 uptake capacity increased by 50% at 1 bar and 298 K. In addition, the CO_2/N_2 selectivity was improved from 16 to 101 at 273 K following functionalization.
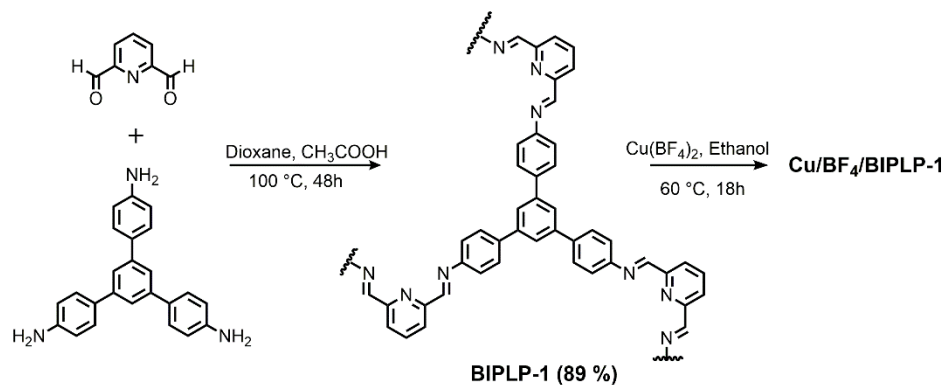
Figure 57. Synthesis of BIPLP-1 and its postsynthetic modification with $Cu(BF_4)_2$.

Wang and coworkers successfully prepared a new series of imidazolium salt-modified porous hypercrosslinked polymer (POM-IMs) by Friedel-Crafts reaction using benzyl halides and modified with N-methylimidazole (Figure 58).[296] The synthetic approach is based on the one-step Friedel–Crafts alkylation between aromatic monomers

and formaldehyde dimethyl acetal. Though POM-IMs' porosities decreased upon functionalization, the CO_2 uptake remained the same or increased slightly. The CO_2 capture capacity was 2.41 – 3.30 mmol/g at 273 K and 1 bar. These materials also demonstrated exceptional water resistance. The CO_2 capture capacities of the POP were maintained after prolonged treatment with hot water (80 ℃, 18 h). Interestingly, these materials, compared to traditional polystyrene resin supported imidazolium salts and the homogeneous imidazolium salts, showed much higher activities for the conversion of CO_2 into various cyclic carbonates, which may be due to the synergistic effect of the porous structure (CO_2 capture) and the functionalized imidazolium salt (CO_2 conversion).
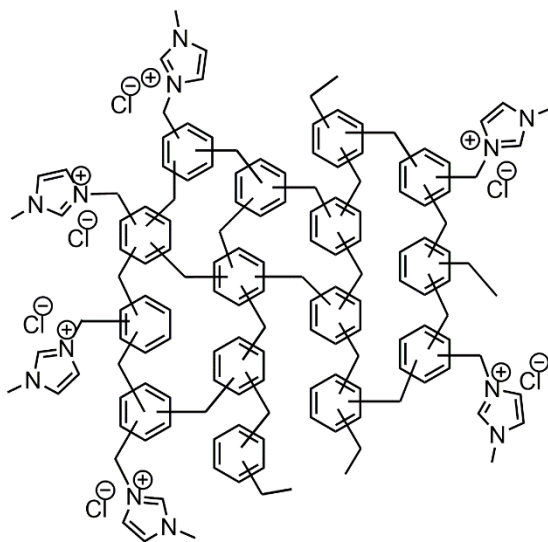
Typical structure of **POM-IM**

Figure 58. The typical structure of POM-IM.

Porphyrin networks with high CO_2 uptake have also been reported.[63] Modak and coworkers used a facile one-pot bottom-up synthesis to achieve a series of porphyrinic Fe-

POPs with exceptionally high CO_2 adsorption capacity.[65] The synthesis involved the crosslinking of repeated porphyrin units through the electrophilic substitution on pyrrole with linear di-aldehydes, phenyl complexes and small amounts of $FeCl_3$. Increasing the length of phenyl linkers, the BET surfaces areas decreased from 875, 855 to 750 $m^2 \cdot g^{-1}$ for Fe-POP-1, -2, and -3. The strong van der Waals force between CO_2 and basic porphyrin subunits of Fe-POP-1 were most likely responsible for its high CO_2 adsorption capacity of 4.32 mmol/g at 273 K and 1 bar.

The Cu(I)-catalyzed click chemistry between alkynes and azides has been widely applied in the synthesis of polymers. Recently, a phthalocyanine-based porous polymer (CPP) was prepared via Cu(I)-catalyzed click reaction that showed a BET surface area of 579 $m^2 \cdot g^{-1}$.[298] CPP also demonstrated very high CO_2 affinity with a value of 3.57 mmol/g (273 K) and 2.27 mmol/g (298 K) at 1 bar. In addition, the adsorption selectivity of CPP was 94 for CO_2/N_2. The calculated heated adsorption was 33.5 $kJ \cdot mol^{-1}$.

6.2.5 Multi-functional porous organic polymers

CMP networks were synthesized via Sonogashira-Hagihara cross-coupling reaction of 1,3,5-triethynylbenzene with either 2,5-dibromobenzoic acid or 2,5-dibromoaniline to yield the corresponding carboxylic acid- and amine-functionalized CMP networks (Figure 59).[265, 267] Based on the BET surface data of CMPs, Dawson and coworkers concluded that the CO_2 adsorption was dependent not only on the surface area and pore volume but also the pore size and functional groups present. In terms of the functional groups, the isosteric heats of CMPs were in the order: $-COOH > -(OH)_2 > -$

$NH_2 > -(CH_3)_2 >$ non-functionalized. This finding indicated that the acidic functional groups may outperform aromatic amino groups in terms of increasing CO_2 capture capacity surprisingly. Compared to other reported systems, the isosteric heat of CMP-1-COOH was higher than activated carbon but lower than some MOFs, such as $HCu(Cu_4Cl)_3(BTTri)_8(en)_5$, which had high heat adsorption of 90 kJ mol^{-1}, reported by Long et al.[159]

CMP-1	R = R' = H
CMP-1-(CH$_3$)$_2$	R = R' = CH$_3$
CMP-1-(OH)$_2$	R = R' = OH
CMP-1-NH$_2$	R = NH$_2$, R' = H
CMP-1-COOH	R = COOH, R' = H
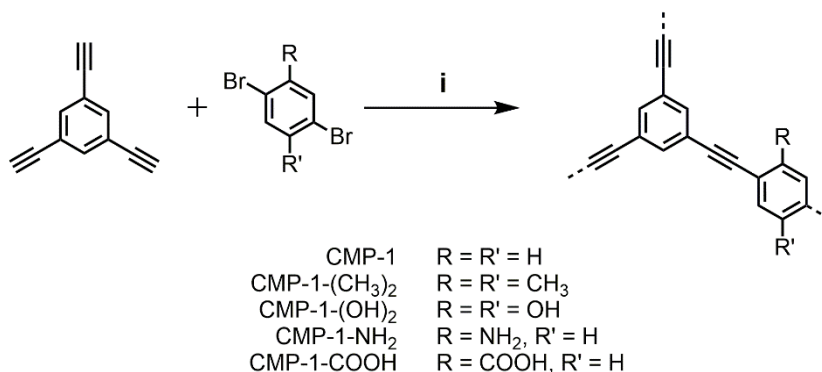
Figure 59. Synthesis of functionalized CMPs using (i) DMF, NEt$_3$, Pd(PPh$_3$)$_4$, CuI, 100 ℃, 72 h. Adapted from ref. [265].

A series of porous aromatic framework (PAF) materials for carbon capture were synthesized by Sonogashira-Hagihara coupling reactions using tri(4-ethynylphenyl)amine and various aryl halides.[294] Yuan and coworkers compared the unmodified PAF with -COOH, -NH$_2$, -OH functionalized PAF in terms of CO_2 adsorption capacity, isosteric heat and CO_2/N_2 selectivity. The results showed that PAF-33-COOH had the highest CO_2 uptake at 1.94 mmol/g among all the samples, which proved that the functionalization effectively improved CO_2 affinity. Based on Henry's law, these PAF materials show high CO_2 over N_2 selectivity, especially for PAF-33-NH$_2$ with an extraordinarily high value of

135

250.5, ranking PAF-33–NH$_2$ among the best porous adsorbents for separating CO$_2$ from N$_2$.

Different strategies have been utilized to carry out the pore surface engineering of POPs, such as quantitative click reactions between the ethynyl units and azide compounds (Figure 60).[359] A variety of functional groups, including ethyl, acetate, hydroxyl, carboxylic acid, and amino groups, have been tethered to the pore walls of parent COFs. The surface area, pore size and pore volume decreased due to the pore surface functionalization. However, the CO$_2$ capacities showed to be highly dependent on the interactions of the functional groups and CO$_2$ molecules. The non-polar ethynyl and ethyl groups interact weekly with CO$_2$, resulting in poor CO$_2$ adsorption capacities when these functional groups were utilized. It was observed that polar ester units could interact with CO$_2$ via dipole-quadrupole interactions. As for carboxylic acid and the hydroxyl functionalized COFs, they interact via dipole-quadrupole and hydrogen bonding interactions, leading to enhanced CO$_2$ capacities. However, the amine groups, which form acid-base pairs with CO$_2$, led to the largest CO$_2$ adsorption capacity among this series of materials. To sum up, both the CO$_2$ capacity and heat of adsorption decreased in the order: EtNH2- > EtOH- > AcOH- > MeOAc- > Et- ~ ethylyl- , which were in the same strength order of the interactions between functional groups and CO$_2$. For the strongly interacting materials, the maximal CO$_2$ capacities occurred when 50% of the available sites were functionalization. This observed phenomenon is the result of a balance between the two contradictory effects of enhanced affinity and decreased porosity. These results

demonstrated that the precise pore surface engineering played a vital role in enhancing the

CO_2 uptake.
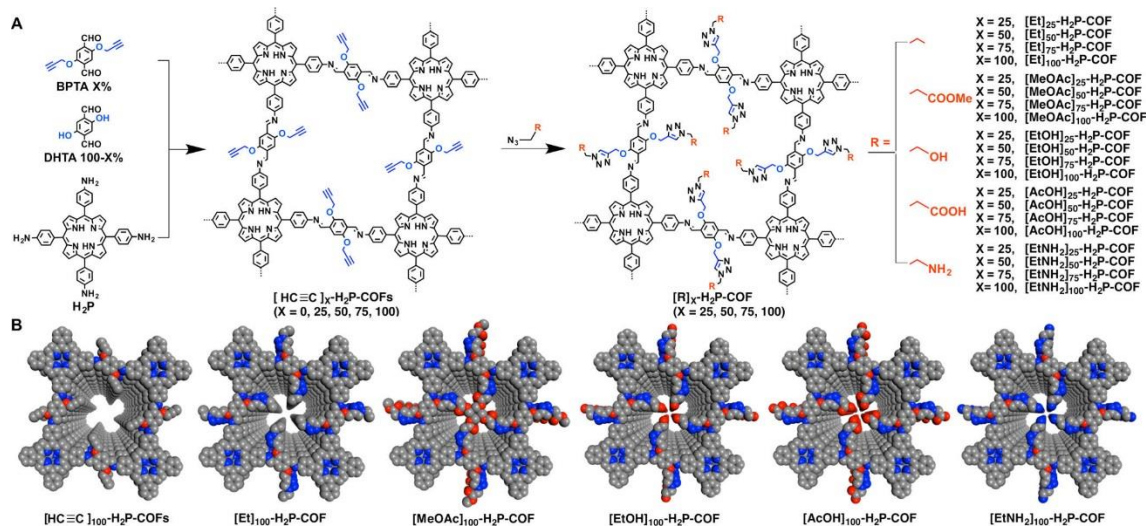
Figure 60. (A) Schematic of Pore Surface Engineering of Imine-Linked COFs with Various Functional Groups via Click Reactions; (B) Pore Structures of COFs with Different Functional Groups (Gray, C; Blue, N; Red, O). Reprinted from ref. [359].

6.3 Carbon capture in porous organic polymers based on chemical reactions

Chemisorption of CO_2 in porous materials involves the reaction between CO_2 with functional groups in the framework. Adsorption is relatively easy in such cases due to the enthalpic favorability, but as such, also disfavors the reverse process, making regeneration a power-intensive process. Amine scrubbing process for CO_2 capture and separation has been well studies since 1930s.[360] Due to the well-understood strong interaction between amine and CO_2, capturing CO_2 by aqueous amine solution is very efficient and it is still considered as one of the record holder for CO_2 uptake. It is worth noting that the mechanisms of the reaction between CO_2 and different alkylamines are slightly different. Reactions between primary and secondary amines and CO_2 generate carbamate, whereas

137

tertiary amines, which have steric bulky nitrogen center form bicarbonate.[361] Taking amine scrubbing as the model, aminated porous materials usually exhibit very large adsorption enthalpies for CO_2 and high CO_2/N_2 selectivity. Amine-tethered POPs are one of the most promising materials for the separation of CO_2 from other gases.[362]

In 2009, PAF-1 (also known as PPN-6), a porous polymer possessing an extremely high BET surface area of 5600 $m^2\,g^{-1}$, was synthesized via the Yamamoto-Ullman cross coupling of tetrakis(4-bromophenyl)methane.[22] Since then, several other similar porous polymers based on other tetrahedral building blocks with high surface areas were reported. [12, 271, 363] These polymers were functionalized with various alkylamines to increase the CO_2 uptake and the CO_2/N_2 selectivity.

Inspired by the impressive CO_2 separation results after incorporation of *N,N*-dimethylethylenediamine in a MOF,[364] PPN-6 was post-synthetically modified with chloromethyl groups.[12] Those chloromethyl groups were later used to tether amine groups, which selectively react with CO_2 (Figure 61). The modified PPN-6 demonstrated not only high CO_2 capacity but also good selectivity over nitrogen, oxygen, and other molecules commonly found in the flue gas. The best performing POP for carbon capture is PPN-6-CH_2DETA with a CO_2 uptake of 4.31 mmol/g at 1 bar and 295 K, and approximately 3.08 mmol/g at 0.15 bar and 295 K. The isosteric heat of adsorption for CO_2 is approximately 55 kJ mol^{-1}, indicating the promising nature of this material for CO_2 separation, especially at higher temperatures.
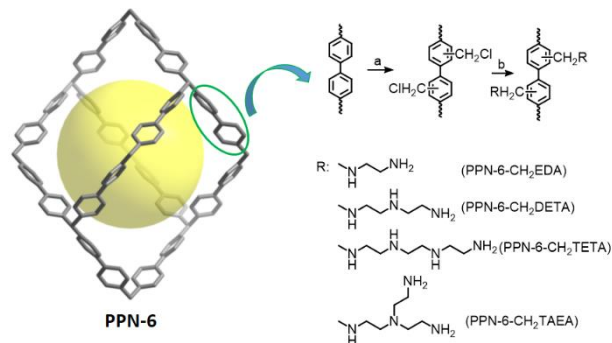
Figure 61. Synthetic route for polyamine-tethered PPNs. a: $CH_3COOH/HCl/H_3PO_4/HCHO$, 90 °C, 3 days; b: amine, 90 °C, 3 days.

In contrast with other top performance CO_2 sorbents such as Mg-MOF-74 which collapse under moist conditions,[365] (this process has since been mitigated somewhat with MOF development to increase water stability[366]) amine-tethered POPs are not only stable to water but also have an improved CO_2 capacity, with a decent regeneration energy. Several groups have researched the mechanisms of CO_2 adsorption and put forward two possible explanations (Figure 62). The first mechanism suggestes that two amine moieties react with one CO_2 to produce a carbamate,[367] which can be further converted to urea with release of water and complication of later CO_2 regeneration.[368] The second mechanism involves one amine group that reacts with one CO_2 molecule and one water molecule to produce a tethered ammonium bicarbonate.

Another approach to amine tethering was demonstrated by preparing PAF-1-CH_2-phthalimide, which was then deprotected by hydrazine to produce PAF-1-CH_2NH_2 (Figure 63).[363] PAF-1-CH_2NH_2 exhibited CO_2 uptake of 4.38 mmol/g at 1 bar and 273 K and 1.52 mmol/g at 0.15 bar and 273 K. The uptake at this pressure may be analogous to the roughly

15% partial pressure of CO_2 in flue gas and thus may be a more relevant parameter for this application. Compared to the CO_2 isosteric heat of adsorption (Q_{st}) of 15.6 kJ mol^{-1} in PAF-1, the amine tetered PAF-1-CH$_2$NH$_2$ increased to 57.6 kJ mol^{-1}. As the sorption sites are filled with only one amine per anchoring site/monomer, the Q_{st} of PAF-1-CH$_2$NH$_2$ decreased quickly after initial loading.
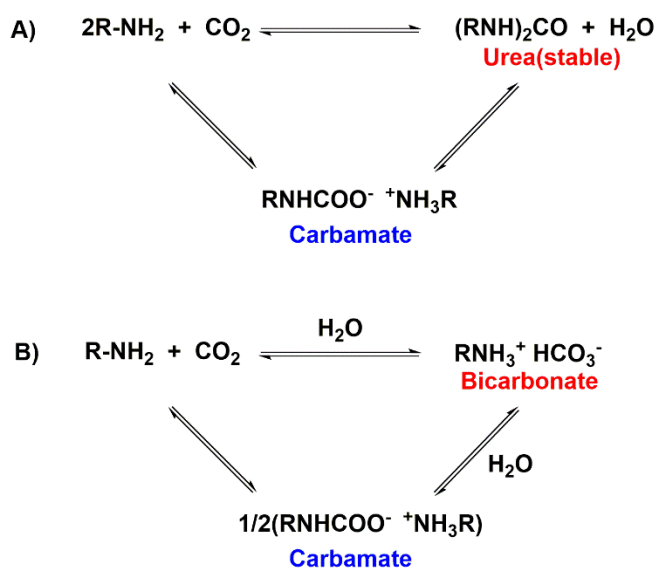
Figure 62. The mechanism of CO_2 adsorpion without moisture (A) and with moisture (B).

Later investigations revealed that PPN-6-CH$_2$DETA had an IAST CO_2/N_2 selectivity of 3.6 x 10^{10} and high overall loading of 1.04 mmol g^{-1}, which were superior to other materials (Table 6).[271] This selectivity value can be understood better by comparing the resultant purity of gases after the mixture separation by these materials. The purity of the desorbed CO_2 from PPN-6-CH$_2$DETA after capture from a gas misture of 0.04% CO_2, 78.96% N_2, and 21% O_2 is 99.999993%. The high selectivity, and the high purity of

seperation, in addition to the low energy required for desorption (the heat of adsoption of 54 kJ mol^{-1}), indicate that this material is by far a top performer for direct air capture for CO_2 and would also be ideal for other CO_2 sorbent applications such as for flue gas capture, and especially for applications requiring maintenance of CO_2 levels in closed atmospheres such as in submarines, spacecraft, and in other scrubber and rebreather technologies.
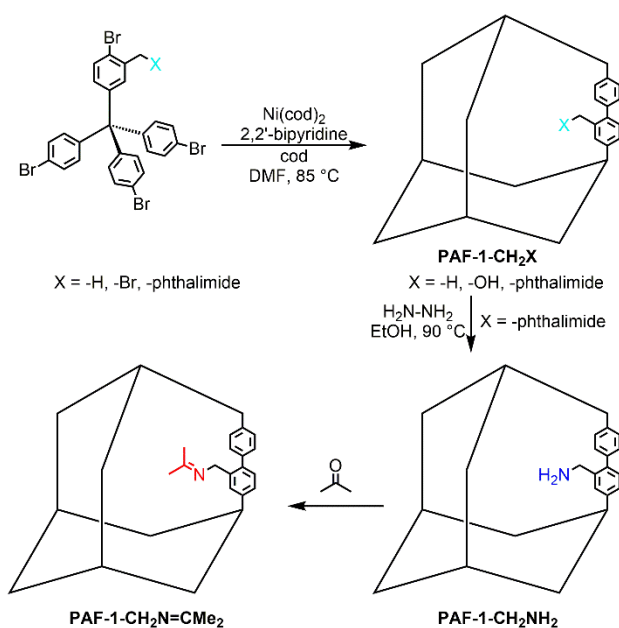
Figure 63. The synthetic procedure for the functionalized PAF-1. The PAF-1 framework is schematically represented as an adamantane cage. Adapted from ref. [363].

Despite their promising performance in carbon capure applications, amine functionalized PAF-1/PPN-6 materials also have a major obstacle to widespread applications. Their synthesis, using Yamamoto polymerization, requires the use of an equimolar amount of bis(1,5-cyclooctadiene)nickel(0) (Ni(COD)$_2$), which is both very

expensive and non-recoverable. This makes the large scale synthesis of these materials non-economical (though still highly promising for some applications such as in scrubbers on submarines and in space). Therefore, synthesis of POPs using other coupling reactions is necessary to lower the cost. PPN-125 (POF1B), synthesized from phloroglucinol (1,3,5-trihydroxybenzene) and terephthalaldehyde, only requires HCl as a catalyst and thus is cheap enough for widespread applications.[242, 272] It also possesses exposed hydroxyl moieties which are easily functionalized with epichlorohydrin and diethylenetriamine (DETA), resulting in an extremely economical synthesis for PPN-125-DETA (Figure 64).

Table 6. Comparison of CO_2 loading, IAST selectivity, and CO_2 purity data for CO_2 capture from "air" containing 400 ppm CO_2.[271]

Material	CO_2 (mmol/g)	N_2[a]		$N_2 + O_2$[a]	
		S_{IAST}	Purity	S_{IAST}	Purity
MgMOF-74[369]	0.16	401	13.8		
Zeolite NaX[369]	0.02	166	6.2		
mmen-CuBTTri[364]	0.05	1239	33.1		
PPN-6-CH$_2$Cl	0.001	11	0.4	11	0.4
mmen-Mg$_2$(dobpdc)[370]	2.05	4.9E04[b]	96.1	4.2E04[b]	94.4
PPN-6-CH$_2$EDA	0.15	5078	67.0	5086	67.0
PPN-6-CH$_2$DETA	1.04	3.8E10	99.9	3.6E10	99.9

[a] balance gas; [b] "Molar selectivity"

However, it has been found that a higher proportion of tetrafunctional monomers compared to bifunctional monomers was found to increase surface area in conjugated POPs, due to a greater amount of cross-linking.[371] This explains why in PPN-125, a BET surface area of only 702 $m^2\,g^{-1}$ was found, as opposed to 6400 $m^2\,g^{-1}$ for PPN-6.[272] After amine loading on PPN-125, a CO_2 uptake of 1.43 mmol/g was found at 298 K and 0.15 bar. The heat of adsorption for PPN-125-DETA is 61 kJ mol^{-1} at zero-coverage, and it remains high even at relatively high loadings. This high enthalpy is close to values calculated to produce adsorbents which consume a minimum amount of energy overall through temperature swing adsorption/desorption when separating CO_2 from air.[372] The high heat of adsorption also suggests a high CO_2 uptake at higher temperature. This is why POF1B, synthesized from the same reactants as PPN-125 under different conditions and investigated for CO_2 uptake with unmodified hydroxyl moieties, has very high CO_2 uptakes at 273K and atmospheric pressure, but low uptakes at 298K and low pressure compared to amine-functionalized polymers.[242]

The low heat capacity of PPN-125-DETA leads reason to why PPN-125-DETA has a low regeneration cost that is only one-third of that of monoethanolamine aqueous solutions, which are currently used for CO_2 capture. Additionally, it was demonstrated to have over 90% capacity retention over 50 cycles of CO_2 adsorption/desorption. As all tests were conducted under dry conditions which could lead to irreversible urea formation, PPN-125-DETA should exhibit both better uptake and higher recyclability under realistic humid conditions that have yet to be tested.
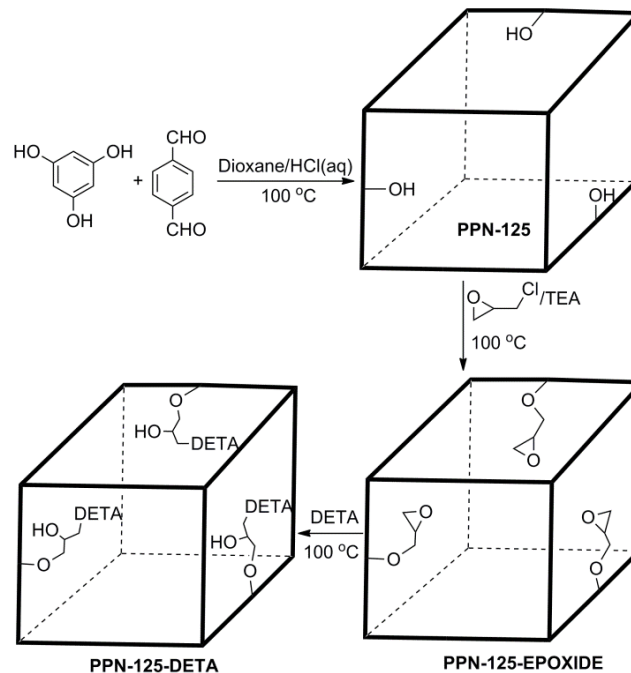
Figure 64. The synthesis of PPN-125-DETA using HCl as a polymerization catalyst, triethylamine(TEA) as a weak base to promote the reaction of the hydroxyl groups with the epichlorohydrin, and diethylenetriamine(DETA) to open the ethylene oxide ring and anchor to the polymer. Reprinted from ref. [272].

Another strategy to incorporate amines into POPs was approached by using them as linkers to form a dimeric polymers. The reaction of 2,4,6-tris(chloromethyl)mesitylene and ethylene diamine produced PPN-80, while the same reaction templated with copolymer P123 produced mesoporous PPN-81 (Figure 65).[273] Templates have been applied to conventional polymers to enhance the porosities.[30] As for porous polymer structures, in spite of the fact that most networks guarantee the intrinsic porosities from the atomic level, using templates is also an efficient and cheap way to tune the porosities. A hiearchical system of pores was formed in PPN-81 and these mesopores not only contributed to the porosity, but also served as channels to improve the diffusion of gas

144

molecules. At zero loading, PPN-81 had a higher heat of adsorption for CO_2 (72 kJ mol^{-1}) than that of PPN-80 (54 kJ mol^{-1}) due to the higher degree of polymerization. In other words, PPN-81 had a higher amine density than PPN-80, and acorrdingly a higher a higher CO_2 uptake at 0.15 atm (approximately 1.87 mmol/g at 295 K vs approximately 1.57 mmol/g for PPN-80). PPN-81 possessed an excellent CO_2/N_2 selectivity at 1 bar (4716), and recyclability (no loss over 6 cycles). The adsorption temperature of 10°C and regeneration (desorption) temperature of 60°C tested would likely be most appropriate for applications such as in rebreathers. Overall, the relative performances between PPN-80, PPN-81, and PPN-125 suggest that a templated version of PPN-125 should be worth investigating.
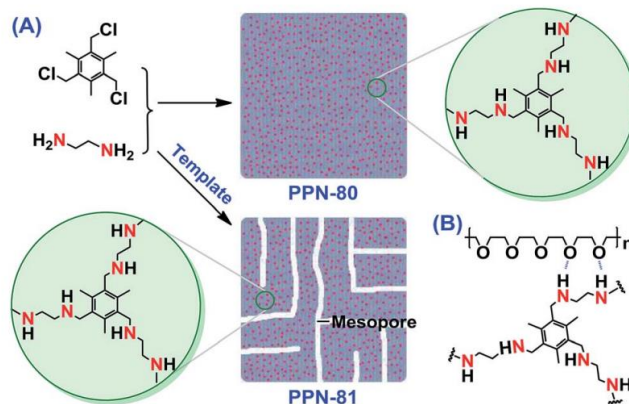
Figure 65. Polymerization of monomers to form PPN-80 in the absence of template and PPN-81 in the presence of template. Reprinted from ref. [273].

PPN-6-DETA and PPN-125-DETA compare favorably to 30% MEA in all tested metrics relative to carbon capture applications (Table 7). Additionally, PPN-125-DETA both has a far lower cost and higher demonstrated stability than other types of sorbent with

145

higher CO_2 uptakes such as mmen-CuBTTri,[364] mmen-Mg_2(dobpdc),[370] or IRMOF-74-III-CH_2NH_2,[366] MIL-101-DETA possesses similar stability and higher CO_2 uptake than PPN-125-DETA at room temperature and 0.15 atm pressure (2.13 mmol/g vs 1.43 mmol/g), but the overall cost of MIL-101-DETA synthesis is likely to be much higher.[373-374] The improvement of approximately 150% in CO_2 uptake under these conditions seen between PPN-80 and PPN-81 suggests that a templated synthesis of PPN-125 could produce a polymer with CO_2 uptake of up to 2.30 mmol/g.

Table 7. Calculated parameters for 30% MEA[375-376], PPN-6-CH_2-DETA[12, 375], and PPN-125-DETA using a temperature swing adsorption/desorption carbon capture method. Values for 30% MEA and PPN-6-CH_2-DETA were taken from the literature.

Parameters	30% MEA	PPN-6-CH_2-DETA[a]	PPN-125-DETA[b]
Working Capacity (mmol/g)	0.83	2.1	0.97
Heat capacity at 40 ℃ (J/g·K)	3.5	1.2	1.0
Δh_{cap} (J/g)	280	84	86
Δh_{ads} (J/g)	100	194	48
Regeneration Energy (J/g)	380	278	134
Working Capacity/Regeneration Energy (mmol/kJ)	2.2	7.5	7.2
Energy Efficiency (kJ/kg$_{CO2}$)	10519	3019	3156

a)desorption temperature is 115 ℃; b) desorption temperature is 120 ℃

Testing of these materials under realistic humid conditions may increase the total CO_2 uptake. A covalent organic polymer (COP-19) synthesized from melamine and terephthaldehyde was impregnated with polyethylamine(PEI) to make COP-97, which

demonstrated a CO_2 uptake of 1.65 mmol/g at 0.15 bar and 298 K with a very high CO_2/N_2 selectivity and good recyclability over 10 cycles.[283] This uptake increased to 2.38 mmol/g, when a moist mixed gas (15% CO_2, 3.8% H_2O) was used at 297K. As the higher temperature facilitates the bicarbonate-forming reaction shown, it further increased to 2.52 mmol/g at 313K.

In contrast, what may be currently considered one of the best solid amine CO_2 flue gas sorbents is a MOF-derived porous carbon monolith saturated with tetraethylenepentamine, TEPA@MDCM.[377] This material showed a CO_2 uptake of 5.6 mmol g^{-1} under "simulated flue gas conditions" of 75°C (348 K) and 0.15 atm CO_2. This material demonstrates a loss of approximately 25% of its CO_2 uptake capacity over 80 adsorption/desorption cycles, and about a 12% mass loss over 90 cycles, indicating slightly less stability than a material like PPN-125-DETA with covalently tethered alkylamines. The uptake also decreased at a lower temperature, presumably due to slower adsorption kinetics in a limited adsorption time in this material with most of the pore volume saturated with amines. TEPA@MDCM may also not be low-cost, due to the necessity of successively synthesizing the MOF, carbonizing it, and impregnating it with alkylamine.

In general, CO_2 uptake by solid alkylamine-based POPs under applicable conditions appears to be dominated by the density of accessible alkylamine sites. An optimal material is inexpensive, highly stable and recyclable and has an extremely high pore volume that is mostly filled with reactive alkylamines providing high uptake and selectivity.

6.4 Concluding remarks and outlooks

In conclusion, there has been significant research progress in the exploration of POPs as potential porous solid adsorbents for carbon capture. Ultrahigh-surface-area POPs can find use in the pre-combustion carbon capture, while the highly functionalized POPs can be utilized in the post-combustion carbon capture. Chemical functionalization of POPs provides abundant binding sites with CO_2 molecules, leading to higher adsorption capacities, especially at lower pressure. The affinities between POP materials and CO_2 molecules can be classified into two categories: physical interactions and chemical reactions. In the case where physical interactions dominate, bond formation is absent/negligible during the adsorption process, and thus the capacity and selectivity at low pressures will be relatively low while the regeneration process will be facile. When chemical bond formation dominates, they usually have very high selectivity, although the regeneration takes more energy. An ideal sorbent for capturing CO_2 from post-combustion capture should have high CO_2 adsorption capacity, high selectivity, minimal regeneration energy, and long-term stability under the operating conditions.

From the foregoing discussions, it is clear that POPs are well on the way to fulfilling most of these criteria. However, there are still some aspects in urgent need of improvement: a), the crystallinity of the POPs. For the majority of the aforementioned examples, the quantity of binding sites occupied by CO_2 molecules is far less than the total calculated binding sites due to the amorphous nature of the POPs that hinders their full accessibility. For example, although large amount of polyamines has been introduced into PPN-6-DETA through post synthetic approaches, those amine chains are not arranged in

order due the amorphous structure of PPN-6 and the flexibility of amine chains, resulting in only one-third utilization of the amine sites. Moreover, amorphous POPs are hard to characterize even by PXRD, which makes it difficult to reveal the structure of POPs and thus challenging to study the mechanism of CO_2 capture. b) For now, the performance of carbon capture materials has mostly been evaluated by single component CO_2 uptake isotherms or the breakthrough experiments using a CO_2/N_2 mixed gas. However, the presence of water and other minor components (O_2, CO, SO_x, NO_x) may have significant consequences on the performances of the materials, which needs more exploration. c) The synthetic cost should be further decreased in order to scale the materials up for industrial application. The expensive catalysts, complicated monomer synthesis as well as the tedious post-functionalization would result in very high cost of the material, making it impractical for real applications. Nevertheless, tremendous efforts have already been made in improving the carbon capture properties of POP materials, and we believe that POPs are capable of serving as next-generation materials for real-world carbon capture applications.

7. CONCLUSION

The exploration of new structures and new applications are of the central value of MOFs/PPNs study. In this dissertation, five independent projects based on various applications using metal-organic frameworks and porous polymer networks have been accomplished. In the first project, utilizing PCN-333(Sc), MIL-100(Sc), MOF-74(Zn), and MOF-74(Mg) as templates, a series of Ti-MOFs were obtained using a stepwise framework templating strategy. The crystallinity of these Ti-MOFs was well maintained throughout, as confirmed from powder X-ray diffraction and gas adsorption measurements. This work provides a systematic strategy to construct Ti-MOFs while highlighting the potential of Ti-MOFs in photocatalytic applications.

Secondly, stable metalloporphyrin based PPN-23 and PPN-24, have been synthesized through a facile one-pot bottom-up approach. PPN-24(Fe) performs great catalytic efficiency as a biomimetic catalyst for the oxidation reaction of ABTS in the presence of H_2O_2.

Thirdly, we have conducted a very comprehensive study on flexible zirconium MOFs, which can be used as switchable catalysts. Single crystal XRD was utilized to confirm the structural transformation. The pore size of these Zr MOFs can be modified by both the predesigned ligand with different functional groups and the post-functionalized strategy by insertion of organic linkers with different sizes. Furthermore, the activity of PCN-700-Me$_2$ as a Lewis acid catalyst can be turned on and off, making it a switchable

catalyst. The discovery of the switchable catalysis within flexible MOFs will open up a field of study intersecting with both crystalline porous materials and switchable catalysts.

Also, MOFs usually exhibit excellent performance for hydrogen adsorption. As way of example, MOFs constructed by carboxylate, azolate or mixed linkers, are discussed. The post-synthetic modifications on MOF materials to increase the hydrogen storage capacities are also carefully illustrated.

Last but not least, intensive efforts have been made to investigate porous organic polymers (POPs) as one type of the most promising candidates for carbon capture. This section provides a critical and in-depth analysis of recent POP research as it pertains to carbon capture. A detailed correlation study between the structural and chemical features of POPs and their adsorption capacities are carefully discussed, mainly focusing on the physical interactions and chemical reactions.

In conclusion, functional porous materials have demonstrated great potential in various applications, especially in heterogeneous catalysis and gas storage. Porous materials with desirable properties can be rationally designed and functionalized for specific applications. This work not only demonstrated several strategies of engineering functional porous materials for different applications, but also shed light on the development of many other functional porous materials and their applications.

REFERENCES

1. Davis, M. E., Ordered porous materials for emerging applications. *Nature* **2002,** *417* (6891), 813-821.

2. Zhou, H.-C.; Long, J. R.; Yaghi, O. M., Introduction to metal–organic frameworks. *Chem. Rev.* **2012,** *112* (2), 673-674.

3. Feng, X.; Ding, X.; Jiang, D., Covalent organic frameworks. *Chem. Soc. Rev.* **2012,** *41* (18), 6010-6022.

4. Yuan, D.; Lu, W.; Zhao, D.; Zhou, H.-C., Highly stable porous polymer networks with exceptionally high gas-uptake capacities. *Adv. Mater.* **2011,** *23* (32), 3723-3725.

5. Deng, H.; Grunder, S.; Cordova, K. E.; Valente, C.; Furukawa, H.; Hmadeh, M.; Gándara, F.; Whalley, A. C.; Liu, Z.; Asahina, S.; Kazumori, H.; O'Keeffe, M.; Terasaki, O.; Stoddart, J. F.; Yaghi, O. M., Large-pore apertures in a series of metal-organic frameworks. *Science* **2012,** *336* (6084), 1018-1023.

6. Suh, M. P.; Park, H. J.; Prasad, T. K.; Lim, D.-W., Hydrogen storage in metal–organic frameworks. *Chem. Rev.* **2012,** *112* (2), 782-835.

7. Li, J.-R.; Kuppler, R. J.; Zhou, H.-C., Selective gas adsorption and separation in metal-organic frameworks. *Chem. Soc. Rev.* **2009,** *38* (5), 1477-1504.

8. Kreno, L. E.; Leong, K.; Farha, O. K.; Allendorf, M.; Van Duyne, R. P.; Hupp, J. T., Metal–organic framework materials as chemical sensors. *Chem. Rev.* **2012,** *112* (2), 1105-1125.

9. Horcajada, P.; Gref, R.; Baati, T.; Allan, P. K.; Maurin, G.; Couvreur, P.; Férey, G.; Morris, R. E.; Serre, C., Metal–organic frameworks in biomedicine. *Chem. Rev.* **2012,** *112* (2), 1232-1268.

10. Lee, J.; Farha, O. K.; Roberts, J.; Scheidt, K. A.; Nguyen, S. T.; Hupp, J. T., Metal-organic framework materials as catalysts. *Chem. Soc. Rev.* **2009,** *38* (5), 1450-1459.

11. Corma, A.; García, H.; Llabrés i Xamena, F. X., Engineering metal organic frameworks for heterogeneous catalysis. *Chem. Rev.* **2010,** *110* (8), 4606-4655.

12. Lu, W.; Sculley, J. P.; Yuan, D.; Krishna, R.; Wei, Z.; Zhou, H.-C., Polyamine-tethered porous polymer networks for carbon dioxide capture from flue gas. *Angew. Chem. Int. Ed.* **2012,** *51* (30), 7480-7484.

13. Dawson, R.; Stevens, L. A.; Drage, T. C.; Snape, C. E.; Smith, M. W.; Adams, D. J.; Cooper, A. I., Impact of water coadsorption for carbon dioxide capture in microporous polymer sorbents. *J. Am. Chem. Soc.* **2012,** *134* (26), 10741-10744.

14. Stockel, E.; Wu, X.; Trewin, A.; Wood, C. D.; Clowes, R.; Campbell, N. L.; Jones, J. T. A.; Khimyak, Y. Z.; Adams, D. J.; Cooper, A. I., High surface area amorphous microporous poly(aryleneethynylene) networks using tetrahedral carbon- and silicon-centred monomers. *Chem. Commun.* **2009,** (2), 212-214.

15. Uribe-Romo, F. J.; Hunt, J. R.; Furukawa, H.; Klöck, C.; O'Keeffe, M.; Yaghi, O. M., A crystalline imine-linked 3-d porous covalent organic framework. *J. Am. Chem. Soc.* **2009,** *131* (13), 4570-4571.

16. Côté, A. P.; Benin, A. I.; Ockwig, N. W.; O'Keeffe, M.; Matzger, A. J.; Yaghi, O. M., Porous, crystalline, covalent organic frameworks. *Science* **2005,** *310* (5751), 1166-1170.

17. El-Kaderi, H. M.; Hunt, J. R.; Mendoza-Cortés, J. L.; Côté, A. P.; Taylor, R. E.; O'Keeffe, M.; Yaghi, O. M., Designed synthesis of 3D covalent organic frameworks. *Science* **2007,** *316* (5822), 268-272.

18. Rosi, N. L.; Eckert, J.; Eddaoudi, M.; Vodak, D. T.; Kim, J.; O'Keeffe, M.; Yaghi, O. M., Hydrogen storage in microporous metal-organic frameworks. *Science* **2003,** *300* (5622), 1127-1129.

19. Yaghi, O. M.; O'Keeffe, M.; Ockwig, N. W.; Chae, H. K.; Eddaoudi, M.; Kim, J., Reticular synthesis and the design of new materials. *Nature* **2003,** *423* (6941), 705-714.

20. Seo, J. S.; Whang, D.; Lee, H.; Jun, S. I.; Oh, J.; Jeon, Y. J.; Kim, K., A homochiral metal-organic porous material for enantioselective separation and catalysis. *Nature* **2000,** *404* (6781), 982-986.

21.   Kreno, L. E.; Leong, K.; Farha, O. K.; Allendorf, M.; Van Duyne, R. P.; Hupp, J. T., Metal–organic framework materials as chemical sensors. *Chem. Rev.* **2011,** *112* (2), 1105-1125.

22.   Ben, T.; Ren, H.; Ma, S.; Cao, D.; Lan, J.; Jing, X.; Wang, W.; Xu, J.; Deng, F.; Simmons, J. M.; Qiu, S.; Zhu, G., Targeted synthesis of a porous aromatic framework with high stability and exceptionally high surface area. *Angew. Chem. Int. Ed.* **2009,** *48* (50), 9457-9460.

23.   Vaesen, S.; Guillerm, V.; Yang, Q.; Wiersum, A. D.; Marszalek, B.; Gil, B.; Vimont, A.; Daturi, M.; Devic, T.; Llewellyn, P. L.; Serre, C.; Maurin, G.; De Weireld, G., A robust amino-functionalized titanium(iv) based MOF for improved separation of acid gases. *Chem. Commun.* **2013,** *49* (86), 10082-10084.

24.   Feng, D.; Gu, Z.-Y.; Li, J.-R.; Jiang, H.-L.; Wei, Z.; Zhou, H.-C., Zirconium-Metalloporphyrin PCN-222: Mesoporous metal–organic frameworks with ultrahigh stability as biomimetic catalysts. *Angew. Chem. Int. Ed.* **2012,** *124* (41), 10453-10456.

25.   Shustova, N. B.; Cozzolino, A. F.; Dincă, M., Conformational locking by design: relating strain energy with luminescence and stability in rigid metal–organic frameworks. *J. Am. Chem. Soc.* **2012,** *134* (48), 19596-19599.

26.   Férey, G.; Mellot-Draznieks, C.; Serre, C.; Millange, F.; Dutour, J.; Surblé, S.; Margiolaki, I., A chromium terephthalate-based solid with unusually large pore volumes and surface area. *Science* **2005,** *309* (5743), 2040-2042.

27.   Gándara, F.; Furukawa, H.; Lee, S.; Yaghi, O. M., High methane storage capacity in aluminum metal–organic frameworks. *J. Am. Chem. Soc.* **2014,** *136* (14), 5271-5274.

28.   Cavka, J. H.; Jakobsen, S.; Olsbye, U.; Guillou, N.; Lamberti, C.; Bordiga, S.; Lillerud, K. P., A new zirconium inorganic building brick forming metal organic frameworks with exceptional stability. *J. Am. Chem. Soc.* **2008,** *130* (42), 13850-13851.

29.   Feng, D.; Chung, W.-C.; Wei, Z.; Gu, Z.-Y.; Jiang, H.-L.; Chen, Y.-P.; Darensbourg, D. J.; Zhou, H.-C., Construction of ultrastable porphyrin zr metal–organic frameworks through linker elimination. *J. Am. Chem. Soc.* **2013,** *135* (45), 17105-17110.

30.   Morris, W.; Volosskiy, B.; Demir, S.; Gándara, F.; McGrier, P. L.; Furukawa, H.; Cascio, D.; Stoddart, J. F.; Yaghi, O. M., Synthesis, structure, and metalation of two new highly porous zirconium metal–organic frameworks. *Inorg. Chem.* **2012,** *51* (12), 6443-6445.

31.   Serre, C.; Groves, J. A.; Lightfoot, P.; Slawin, A. M. Z.; Wright, P. A.; Stock, N.; Bein, T.; Haouas, M.; Taulelle, F.; Férey, G., Synthesis, structure and properties of related microporous n,n'-piperazinebismethylenephosphonates of aluminum and titanium. *Chem. Mater.* **2006,** *18* (6), 1451-1457.

32.   Dan-Hardi, M.; Serre, C.; Frot, T.; Rozes, L.; Maurin, G.; Sanchez, C.; Férey, G., A new photoactive crystalline highly porous titanium(iv) dicarboxylate. *J. Am. Chem. Soc.* **2009,** *131* (31), 10857-10859.

33.   Fu, Y.; Sun, D.; Chen, Y.; Huang, R.; Ding, Z.; Fu, X.; Li, Z., An amine-functionalized titanium metal–organic framework photocatalyst with visible-light-induced activity for CO_2 reduction. *Angew. Chem. Int. Ed.* **2012,** *51* (14), 3364-3367.

34.   Hendon, C. H.; Tiana, D.; Fontecave, M.; Sanchez, C.; D'arras, L.; Sassoye, C.; Rozes, L.; Mellot-Draznieks, C.; Walsh, A., Engineering the optical response of the titanium-MIL-125 metal–organic framework through ligand functionalization. *J. Am. Chem. Soc.* **2013,** *135* (30), 10942-10945.

35.   Nasalevich, M. A.; Goesten, M. G.; Savenije, T. J.; Kapteijn, F.; Gascon, J., Enhancing optical absorption of metal-organic frameworks for improved visible light photocatalysis. *Chem. Commun.* **2013,** *49* (90), 10575-10577.

36.   Gao, J.; Miao, J.; Li, P.-Z.; Teng, W. Y.; Yang, L.; Zhao, Y.; Liu, B.; Zhang, Q., A p-type Ti(IV)-based metal-organic framework with visible-light photo-response. *Chem. Commun.* **2014,** *50* (29), 3786-3788.

37.   Feng, D.; Wang, K.; Wei, Z.; Chen, Y.-P.; Simon, C. M.; Arvapally, R. K.; Martin, R. L.; Bosch, M.; Liu, T.-F.; Fordham, S.; Yuan, D.; Omary, M. A.; Haranczyk, M.; Smit, B.; Zhou, H.-C., Kinetically tuned dimensional augmentation as a versatile synthetic route towards robust metal–organic frameworks. *Nat. Commun.* **2014,** *5*.

38.   Rozes, L.; Sanchez, C., Titanium oxo-clusters: precursors for a Lego-like construction of nanostructured hybrid materials. *Chem. Soc. Rev.* **2011,** *40* (2), 1006-1030.

39.   Cohen, S. M., Postsynthetic methods for the functionalization of metal–organic frameworks. *Chem. Rev.* **2011,** *112* (2), 970-1000.

40.   Wang, Z.; Cohen, S. M., Postsynthetic modification of metal-organic frameworks. *Chem. Soc. Rev.* **2009,** *38* (5), 1315-1329.

41.   Dincă, M.; Long, J. R., High-enthalpy hydrogen adsorption in cation-exchanged variants of the microporous metal−organic framework $Mn_3[(Mn_4Cl)_3(BTT)_8(CH_3OH)_{10}]_2$. *J. Am. Chem. Soc.* **2007,** *129* (36), 11172-11176.

42.   Brozek, C. K.; Dinca, M., Cation exchange at the secondary building units of metal-organic frameworks. *Chem. Soc. Rev.* **2014,** *43* (16), 5456-5467.

43.   Mitchell, L.; Gonzalez-Santiago, B.; Mowat, J. P. S.; Gunn, M. E.; Williamson, P.; Acerbi, N.; Clarke, M. L.; Wright, P. A., Remarkable Lewis acid catalytic performance of the scandium trimesate metal organic framework MIL-100(Sc) for C-C and C[double bond, length as m-dash]N bond-forming reactions. *Catal. Sci. Tech.* **2013,** *3* (3), 606-617.

44.   Geier, S. J.; Mason, J. A.; Bloch, E. D.; Queen, W. L.; Hudson, M. R.; Brown, C. M.; Long, J. R., Selective adsorption of ethylene over ethane and propylene over propane in the metal-organic frameworks M_2(dobdc) (M = Mg, Mn, Fe, Co, Ni, Zn). *Chem. Sci.* **2013,** *4* (5), 2054-2061.

45.   Miyake, H.; Tsukube, H., Coordination chemistry strategies for dynamic helicates: time-programmable chirality switching with labile and inert metal helicates. *Chem. Soc. Rev.* **2012,** *41* (21), 6977-6991.

46.   Song, X.; Kim, T. K.; Kim, H.; Kim, D.; Jeong, S.; Moon, H. R.; Lah, M. S., Post-synthetic modifications of framework metal ions in isostructural metal−organic frameworks: core−shell heterostructures via selective transmetalations. *Chem. Mater.* **2012,** *24* (15), 3065-3073.

47.   Song, X.; Jeong, S.; Kim, D.; Lah, M. S., Transmetalations in two metal-organic frameworks with different framework flexibilities: kinetics and core-shell heterostructure. *CrystEngComm* **2012,** *14* (18), 5753-5756.

48.   Cozzolino, A. F.; Brozek, C. K.; Palmer, R. D.; Yano, J.; Li, M.; Dincă, M., Ligand Redox non-innocence in the stoichiometric oxidation of mn_2(2,5-dioxidoterephthalate) (Mn-MOF-74). *J. Am. Chem. Soc.* **2014,** *136* (9), 3334-3337.

49.   Mansuy, D., A brief history of the contribution of metalloporphyrin models to cytochrome P450 chemistry and oxidation catalysis. *Comptes Rendus Chimie* **2007,** *10* (4–5), 392-413.

50.   Simonneaux, G.; Le Maux, P.; Ferrand, Y.; Rault-Berthelot, J., Asymmetric heterogeneous catalysis by metalloporphyrins. *Coord. Chem. Rev.* **2006,** *250* (17–18), 2212-2221.

51.   Che, C.-M.; Lo, V. K.-Y.; Zhou, C.-Y.; Huang, J.-S., Selective functionalisation of saturated C-H bonds with metalloporphyrin catalysts. *Chem. Soc. Rev.* **2011,** *40* (4), 1950-1975.

52.   Bruice, T. C., Reactions of hydroperoxides with metallotetraphenylporphyrins in aqueous solutions. *Acc. Chem. Res.* **1991,** *24* (8), 243-249.

53.   Alkordi, M. H.; Liu, Y.; Larsen, R. W.; Eubank, J. F.; Eddaoudi, M., Zeolite-like metal−organic frameworks as platforms for applications: on metalloporphyrin-based catalysts. *J. Am. Chem. Soc.* **2008,** *130* (38), 12639-12641.

54.   Groves, J. T.; Adhyam, D. V., Hydroxylation by cytochrome P-450 and metalloporphyrin models. Evidence for allylic rearrangement. *J. Am. Chem. Soc.* **1984,** *106* (7), 2177-2181.

55.   Lu, H.; Zhang, X. P., Catalytic C-H functionalization by metalloporphyrins: recent developments and future directions. *Chem. Soc. Rev.* **2011,** *40* (4), 1899-1909.

56.   Xue, T.; Jiang, S.; Qu, Y.; Su, Q.; Cheng, R.; Dubin, S.; Chiu, C.-Y.; Kaner, R.; Huang, Y.; Duan, X., Graphene-supported hemin as a highly active biomimetic oxidation catalyst. *Angew. Chem. Int. Ed.* **2012,** *51* (16), 3822-3825.

57.   Wang, Q.; Yang, Z.; Zhang, X.; Xiao, X.; Chang, C. K.; Xu, B., A supramolecular-hydrogel-encapsulated hemin as an artificial enzyme to mimic peroxidase. *Angew. Chem. Int. Ed.* **2007,** *46* (23), 4285-4289.

58.   Leal, O.; Anderson, D. L.; Bowman, R. G.; Basolo, F.; Burwell, R. L., Reversible adsorption of oxygen on silica gel modified by imidazole-attached iron tetraphenylporphyrin. *J. Am. Chem. Soc.* **1975,** *97* (18), 5125-5129.

59.   Li, Z.; Xia, C.-G.; Zhang, X.-M., Preparation and catalysis of DMY and MCM-41 encapsulated cationic Mn(III)–porphyrin complex. *J. Mol. Catal. A: Chem.* **2002,** *185* (1–2), 47-56.

60.   Lee, C. Y.; Farha, O. K.; Hong, B. J.; Sarjeant, A. A.; Nguyen, S. T.; Hupp, J. T., Light-harvesting metal–organic frameworks (MOFs): efficient strut-to-strut energy transfer in bodipy and porphyrin-based MOFs. *J. Am. Chem. Soc.* **2011,** *133* (40), 15858-15861.

61.   Fateeva, A.; Chater, P. A.; Ireland, C. P.; Tahir, A. A.; Khimyak, Y. Z.; Wiper, P. V.; Darwent, J. R.; Rosseinsky, M. J., A water-stable porphyrin-based metal–organic framework active for visible-light photocatalysis. *Angew. Chem.* **2012,** *124* (30), 7558-7562.

62.   Wang, X.-S.; Chrzanowski, M.; Yuan, D.; Sweeting, B. S.; Ma, S., Covalent heme framework as a highly active heterogeneous biomimetic oxidation catalyst. *Chem. Mater.* **2014,** *26* (4), 1639-1644.

63.   Shultz, A. M.; Farha, O. K.; Hupp, J. T.; Nguyen, S. T., Synthesis of catalytically active porous organic polymers from metalloporphyrin building blocks. *Chem. Sci.* **2011,** *2* (4), 686-689.

64.   Chen, L.; Yang, Y.; Jiang, D., CMPs as scaffolds for constructing porous catalytic frameworks: a built-in heterogeneous catalyst with high activity and selectivity based on nanoporous metalloporphyrin polymers. *J. Am. Chem. Soc.* **2010,** *132* (26), 9138-9143.

65.   Modak, A.; Nandi, M.; Mondal, J.; Bhaumik, A., Porphyrin based porous organic polymers: novel synthetic strategy and exceptionally high CO_2 adsorption capacity. *Chem. Commun.* **2012,** *48* (2), 248-250.

66.   Van Arman, S. A., 2-Methyl-2-propanol as solvent for o-iodoxybenzoic acid (IBX) oxidation of 1˚ alcohols to aldehydes. *Tetrahedron Lett.* **2009,** *50* (33), 4693-4695.

67.   Zhang, M.; Perry, Z.; Park, J.; Zhou, H.-C., Stable benzimidazole-incorporated porous polymer network for carbon capture with high efficiency and low cost. *Polymer* **2014,** *55* (1), 335-339.

68.   Feng, D.; Gu, Z. Y.; Li, J. R.; Jiang, H. L.; Wei, Z.; Zhou, H. C., Zirconium-metalloporphyrin PCN-222: mesoporous metal-organic frameworks with ultrahigh stability as biomimetic catalysts. *Angew. Chem. Int. Ed. Engl.* **2012,** *51* (41), 10307-10.

69.   Larsen, R. W.; Wojtas, L.; Perman, J.; Musselman, R. L.; Zaworotko, M. J.; Vetromile, C. M., Mimicking heme enzymes in the solid state: metal–organic materials with selectively encapsulated heme. *J. Am. Chem. Soc.* **2011,** *133* (27), 10356-10359.

70.   Chen, Y.; Hoang, T.; Ma, S., Biomimetic catalysis of a porous iron-based metal–metalloporphyrin framework. *Inorg. Chem.* **2012,** *51* (23), 12600-12602.

71.   Noble, R. W.; Gibson, Q. H., The reaction of ferrous horseradish peroxidase with hydrogen peroxide. *J. Biol. Chem.* **1970,** *245* (9), 2409-2413.

72.   Traut, T., Enzyme activity: allosteric regulation. In *eLS*, John Wiley & Sons, Ltd: 2001.

73.   Kovbasyuk, L.; Krämer, R., Allosteric supramolecular receptors and catalysts. *Chem. Rev.* **2004,** *104* (6), 3161-3188.

74.   Blanco, V.; Leigh, D. A.; Marcos, V., Artificial switchable catalysts. *Chem. Soc. Rev.* **2015,** *44* (15), 5341-70.

75.   Tian, X.; Cassani, C.; Liu, Y.; Moran, A.; Urakawa, A.; Galzerano, P.; Arceo, E.; Melchiorre, P., Diastereodivergent asymmetric sulfa-michael additions of α-branched enones using a single chiral organic catalyst. *J. Am. Chem. Soc.* **2011,** *133* (44), 17934-17941.

76.   Arseniyadis, S.; Valleix, A.; Wagner, A.; Mioskowski, C., Kinetic resolution of amines: a highly enantioselective and chemoselective acetylating agent with a unique solvent-induced reversal of stereoselectivity. *Angew. Chem. Int. Ed.* **2004,** *43* (25), 3314-3317.

77.   Long, J. R.; Yaghi, O. M., The pervasive chemistry of metal-organic frameworks. *Chem. Soc. Rev.* **2009,** *38* (5), 1213-1214.

78.   Stegbauer, L.; Schwinghammer, K.; Lotsch, B. V., A hydrazone-based covalent organic framework for photocatalytic hydrogen production. *Chem. Sci.* **2014,** *5* (7), 2789-2793.

79.   Horike, S.; Shimomura, S.; Kitagawa, S., Soft porous crystals. *Nat. Chem.* **2009,** *1* (9), 695-704.

80.   Sarkisov, L.; Martin, R. L.; Haranczyk, M.; Smit, B., On the flexibility of metal-organic frameworks. *J. Am. Chem. Soc.* **2014,** *136* (6), 2228-31.

81.   Uemura, K.; Matsuda, R.; Kitagawa, S., Flexible microporous coordination polymers. *J. Solid State Chem.* **2005,** *178* (8), 2420-2429.

82.   Nagarkar, S. S.; Desai, A. V.; Ghosh, S. K., Stimulus-responsive metal-organic frameworks. *Chem Asian J.* **2014,** *9* (9), 2358-76.

83.   Wang, X.; Eckert, J.; Liu, L.; Jacobson, A. J., Breathing and twisting: an investigation of framework deformation and guest packing in single crystals of a microporous vanadium benzenedicarboxylate. *Inorg. Chem.* **2011,** *50* (5), 2028-36.

84.   Liu, D.; Liu, T.-F.; Chen, Y.-P.; Zou, L.; Feng, D.; Wang, K.; Zhang, Q.; Yuan, S.; Zhong, C.; Zhou, H.-C., A reversible crystallinity-preserving phase transition in metal–organic frameworks: discovery, mechanistic studies, and potential applications. *J. Am. Chem. Soc.* **2015,** *137* (24), 7740-7746.

85.   Yanai, N.; Uemura, T.; Inoue, M.; Matsuda, R.; Fukushima, T.; Tsujimoto, M.; Isoda, S.; Kitagawa, S., Guest-to-host transmission of structural changes for stimuli-responsive adsorption property. *J. Am. Chem. Soc.* **2012,** *134* (10), 4501-4504.

86.   Serre, C.; Millange, F.; Thouvenot, C.; Noguès, M.; Marsolier, G.; Louër, D.; Férey, G., Very large breathing effect in the first nanoporous chromium(III)-based solids: MIL-53 or $Cr^{III}(OH) \cdot \{O_2C-C_6H_4-CO_2\} \cdot \{HO_2C-C_6H_4-CO_2H\}_x \cdot H_2O_y$. *J. Am. Chem. Soc.* **2002,** *124* (45), 13519-13526.

87.   Llewellyn, P. L.; Bourrelly, S.; Serre, C.; Filinchuk, Y.; Férey, G., How hydration drastically improves adsorption selectivity for co2 over ch4 in the flexible chromium terephthalate MIL-53. *Angew. Chem.* **2006,** *118* (46), 7915-7918.

88.   Mason, J. A.; Oktawiec, J.; Taylor, M. K.; Hudson, M. R.; Rodriguez, J.; Bachman, J. E.; Gonzalez, M. I.; Cervellino, A.; Guagliardi, A.; Brown, C. M.; Llewellyn, P. L.; Masciocchi, N.; Long, J. R., Methane storage in flexible metal–organic frameworks with intrinsic thermal management. *Nature* **2015,** *527* (7578), 357-361.

89.   McDonald, T. M.; Mason, J. A.; Kong, X.; Bloch, E. D.; Gygi, D.; Dani, A.; Crocella, V.; Giordanino, F.; Odoh, S. O.; Drisdell, W. S.; Vlaisavljevich, B.;

Dzubak, A. L.; Poloni, R.; Schnell, S. K.; Planas, N.; Lee, K.; Pascal, T.; Wan, L. F.; Prendergast, D.; Neaton, J. B.; Smit, B.; Kortright, J. B.; Gagliardi, L.; Bordiga, S.; Reimer, J. A.; Long, J. R., Cooperative insertion of CO_2 in diamine-appended metal-organic frameworks. *Nature* **2015,** *519* (7543), 303-308.

90.   Wei, Y.-S.; Chen, K.-J.; Liao, P.-Q.; Zhu, B.-Y.; Lin, R.-B.; Zhou, H.-L.; Wang, B.-Y.; Xue, W.; Zhang, J.-P.; Chen, X.-M., Turning on the flexibility of isoreticular porous coordination frameworks for drastically tunable framework breathing and thermal expansion. *Chem. Sci.* **2013,** *4* (4), 1539.

91.   Furukawa, H.; Gándara, F.; Zhang, Y.-B.; Jiang, J.; Queen, W. L.; Hudson, M. R.; Yaghi, O. M., Water adsorption in porous metal–organic frameworks and related materials. *J. Am. Chem. Soc.* **2014,** *136* (11), 4369-4381.

92.   Deria, P.; Mondloch, J. E.; Tylianakis, E.; Ghosh, P.; Bury, W.; Snurr, R. Q.; Hupp, J. T.; Farha, O. K., Perfluoroalkane functionalization of NU-1000 via solvent-assisted ligand incorporation: synthesis and CO_2 adsorption studies. *J. Am. Chem. Soc.* **2013,** *135* (45), 16801-16804.

93.   Yuan, S.; Lu, W.; Chen, Y.-P.; Zhang, Q.; Liu, T.-F.; Feng, D.; Wang, X.; Qin, J.; Zhou, H.-C., Sequential linker installation: precise placement of functional groups in multivariate metal–organic frameworks. *J. Am. Chem. Soc.* **2015,** *137* (9), 3177-3180.

94.   Beyzavi, M. H.; Klet, R. C.; Tussupbayev, S.; Borycz, J.; Vermeulen, N. A.; Cramer, C. J.; Stoddart, J. F.; Hupp, J. T.; Farha, O. K., A hafnium-based metal–organic framework as an efficient and multifunctional catalyst for facile CO_2 fixation and regioselective and enantioretentive epoxide activation. *J. Am. Chem. Soc.* **2014,** *136* (45), 15861-15864.

95.   Sawano, T.; Thacker, N. C.; Lin, Z.; McIsaac, A. R.; Lin, W., Robust, Chiral, and porous BINAP-based metal–organic frameworks for highly enantioselective cyclization reactions. *J. Am. Chem. Soc.* **2015,** *137* (38), 12241-12248.

96.   Deria, P.; Gómez-Gualdrón, D. A.; Bury, W.; Schaef, H. T.; Wang, T. C.; Thallapally, P. K.; Sarjeant, A. A.; Snurr, R. Q.; Hupp, J. T.; Farha, O. K., Ultraporous, water stable, and breathing zirconium-based metal–organic frameworks with ftw topology. *J. Am. Chem. Soc.* **2015,** *137* (40), 13183-13190.

97. Zhang, Q.; Su, J.; Feng, D.; Wei, Z.; Zou, X.; Zhou, H.-C., Piezofluorochromic metal–organic framework: a microscissor lift. *J. Am. Chem. Soc.* **2015,** *137* (32), 10064-10067.

98. Feng, D.; Gu, Z.-Y.; Li, J.-R.; Jiang, H.-L.; Wei, Z.; Zhou, H.-C., Zirconium-metalloporphyrin PCN-222: mesoporous metal–organic frameworks with ultrahigh stability as biomimetic catalysts. *Angew. Chem. Int. Ed.* **2012,** *51* (41), 10307-10310.

99. Hughes, J. T.; Navrotsky, A., MOF-5: enthalpy of formation and energy landscape of porous materials. *J. Am. Chem. Soc.* **2011,** *133* (24), 9184-9187.

100. Mondloch, J. E.; Katz, M. J.; Planas, N.; Semrouni, D.; Gagliardi, L.; Hupp, J. T.; Farha, O. K., Are Zr6-based MOFs water stable? Linker hydrolysis vs. capillary-force-driven channel collapse. *Chem. Commun.* **2014,** *50* (64), 8944-8946.

101. Delgado-Friedrichs, O.; O'Keeffe, M.; Yaghi, O. M., Three-periodic nets and tilings: edge-transitive binodal structures. *Acta Crystallogr. Sect. A: Found. Crystallogr.* **2006,** *62* (5), 350-355.

102. Furukawa, H.; Kim, J.; Ockwig, N. W.; O'Keeffe, M.; Yaghi, O. M., Control of vertex geometry, structure dimensionality, functionality, and pore metrics in the reticular synthesis of crystalline metal−organic frameworks and polyhedra. *J. Am. Chem. Soc.* **2008,** *130* (35), 11650-11661.

103. Inokuma, Y.; Yoshioka, S.; Ariyoshi, J.; Arai, T.; Hitora, Y.; Takada, K.; Matsunaga, S.; Rissanen, K.; Fujita, M., X-ray analysis on the nanogram to microgram scale using porous complexes. *Nature* **2013,** *495* (7442), 461-466.

104. Bloch, W. M.; Burgun, A.; Coghlan, C. J.; Lee, R.; Coote, M. L.; Doonan, C. J.; Sumby, C. J., Capturing snapshots of post-synthetic metallation chemistry in metal–organic frameworks. *Nat. Chem.* **2014,** *6* (10), 906-912.

105. Chen, L.; Mowat, J. P.; Fairen-Jimenez, D.; Morrison, C. A.; Thompson, S. P.; Wright, P. A.; Duren, T., Elucidating the breathing of the metal-organic framework MIL-53(Sc) with ab initio molecular dynamics simulations and in situ X-ray powder diffraction experiments. *J. Am. Chem. Soc.* **2013,** *135* (42), 15763-73.

106. Yoon, H. J.; Kuwabara, J.; Kim, J.-H.; Mirkin, C. A., Allosteric supramolecular triple-layer catalysts. *Science* **2010,** *330* (6000), 66-69.

107. Serre, C.; Mellot-Draznieks, C.; Surblé, S.; Audebrand, N.; Filinchuk, Y.; Férey, G., Role of solvent-host interactions that lead to very large swelling of hybrid frameworks. *Science* **2007,** *315* (5820), 1828-1831.

108. Simmons, G., Single-crystal elastic constants and calculated aggregate properties. *J. Grad. Res. Center* **1965,** *34* (1-2), 269 pp.

109. Horcajada, P.; Salles, F.; Wuttke, S.; Devic, T.; Heurtaux, D.; Maurin, G.; Vimont, A.; Daturi, M.; David, O.; Magnier, E.; Stock, N.; Filinchuk, Y.; Popov, D.; Riekel, C.; Ferey, G.; Serre, C., How linker's modification controls swelling properties of highly flexible iron(III) dicarboxylates MIL-88. *J. Am. Chem. Soc.* **2011,** *133* (44), 17839-47.

110. Lescouet, T.; Kockrick, E.; Bergeret, G.; Pera-Titus, M.; Aguado, S.; Farrusseng, D., Homogeneity of flexible metal-organic frameworks containing mixed linkers. *J. Mater. Chem.* **2012,** *22* (20), 10287-10293.

111. Zhang, Y.-B.; Furukawa, H.; Ko, N.; Nie, W.; Park, H. J.; Okajima, S.; Cordova, K. E.; Deng, H.; Kim, J.; Yaghi, O. M., Introduction of functionality, selection of topology, and enhancement of gas adsorption in multivariate metal–organic framework-177. *J. Am. Chem. Soc.* **2015,** *137* (7), 2641-2650.

112. Yot, P. G.; Ma, Q.; Haines, J.; Yang, Q.; Ghoufi, A.; Devic, T.; Serre, C.; Dmitriev, V.; Ferey, G.; Zhong, C.; Maurin, G., Large breathing of the MOF MIL-47(VIV) under mechanical pressure: a joint experimental-modelling exploration. *Chem. Sci.* **2012,** *3* (4), 1100-1104.

113. Deria, P.; Bury, W.; Hupp, J. T.; Farha, O. K., Versatile functionalization of the NU-1000 platform by solvent-assisted ligand incorporation. *Chem. Commun.* **2014,** *50* (16), 1965-1968.

114. Deria, P.; Bury, W.; Hod, I.; Kung, C.-W.; Karagiaridi, O.; Hupp, J. T.; Farha, O. K., MOF functionalization via solvent-assisted ligand incorporation: phosphonates vs carboxylates. *Inorg. Chem.* **2015,** *54* (5), 2185-2192.

115. Jiang, J.; Gándara, F.; Zhang, Y.-B.; Na, K.; Yaghi, O. M.; Klemperer, W. G., Superacidity in sulfated metal–organic framework-808. *J. Am. Chem. Soc.* **2014,** *136* (37), 12844-12847.

116. Schlapbach, L.; Zuttel, A., Hydrogen-storage materials for mobile applications. *Nature* **2001,** *414* (6861), 353-358.

117. Orimo, S.-i.; Nakamori, Y.; Eliseo, J. R.; Züttel, A.; Jensen, C. M., Complex Hydrides for hydrogen storage. *Chem. Rev.* **2007,** *107* (10), 4111-4132.

118. Cheng, H.-M.; Yang, Q.-H.; Liu, C., Hydrogen storage in carbon nanotubes. *Carbon* **2001,** *39* (10), 1447-1454.

119. Baughman, R. H.; Zakhidov, A. A.; de Heer, W. A., Carbon nanotubes--the route toward applications. *Science* **2002,** *297* (5582), 787-792.

120. Germain, J.; Fréchet, J. M. J.; Svec, F., Nanoporous polymers for hydrogen storage. *Small* **2009,** *5* (10), 1098-1111.

121. Zou, L.; Feng, D.; Liu, T.-F.; Chen, Y.-P.; Fordham, S.; Yuan, S.; Tian, J.; Zhou, H.-C., Facile one-pot synthesis of porphyrin based porous polymer networks (PPNs) as biomimetic catalysts. *Chem. Commun.* **2015,** *51* (19), 4005-4008.

122. Weitkamp, J.; Fritz, M.; Ernst, S., Zeolites as media for hydrogen storage. *International Journal of Hydrogen Energy* **1995,** *20* (12), 967-970.

123. Dong, J.; Wang, X.; Xu, H.; Zhao, Q.; Li, J., Hydrogen storage in several microporous zeolites. *International Journal of Hydrogen Energy* **2007,** *32* (18), 4998-5004.

124. Czaja, A. U.; Trukhan, N.; Muller, U., Industrial applications of metal-organic frameworks. *Chem. Soc. Rev.* **2009,** *38* (5), 1284-1293.

125. Yuan, S.; Liu, T.-F.; Feng, D.; Tian, J.; Wang, K.; Qin, J.; Zhang, Q.; Chen, Y.-P.; Bosch, M.; Zou, L.; Teat, S. J.; Dalgarno, S. J.; Zhou, H.-C., A single crystalline porphyrinic titanium metal-organic framework. *Chem. Sci.* **2015,** *6* (7), 3926-3930.

126. Goldsmith, J.; Wong-Foy, A. G.; Cafarella, M. J.; Siegel, D. J., Theoretical limits of hydrogen storage in metal–organic frameworks: opportunities and trade-offs. *Chem. Mater.* **2013,** *25* (16), 3373-3382.

127. Dincă, M.; Long, J. R., Hydrogen storage in microporous metal–organic frameworks with exposed metal sites. *Angew. Chem. Int. Ed.* **2008,** *47* (36), 6766-6779.

128. Ren, J.; Langmi, H. W.; North, B. C.; Mathe, M., Review on processing of metal–organic framework (MOF) materials towards system integration for hydrogen storage. *International Journal of Energy Research* **2015,** *39* (5), 607-620.

129. Dincă, M.; Dailly, A.; Liu, Y.; Brown, C. M.; Neumann, D. A.; Long, J. R., Hydrogen storage in a microporous metal−organic framework with exposed Mn^{2+} coordination sites. *J. Am. Chem. Soc.* **2006,** *128* (51), 16876-16883.

130. Farha, O. K.; Özgür Yazaydın, A.; Eryazici, I.; Malliakas, C. D.; Hauser, B. G.; Kanatzidis, M. G.; Nguyen, S. T.; Snurr, R. Q.; Hupp, J. T., De novo synthesis of a metal–organic framework material featuring ultrahigh surface area and gas storage capacities. *Nat. Chem.* **2010,** *2* (11), 944-948.

131. Rowsell, J. L. C.; Millward, A. R.; Park, K. S.; Yaghi, O. M., Hydrogen sorption in functionalized metal−organic frameworks. *J. Am. Chem. Soc.* **2004,** *126* (18), 5666-5667.

132. Ma, S.; Zhou, H.-C., Gas storage in porous metal-organic frameworks for clean energy applications. *Chem. Commun.* **2010,** *46* (1), 44-53.

133. Collins, D. J.; Zhou, H.-C., Hydrogen storage in metal-organic frameworks. *J. Mater. Chem.* **2007,** *17* (30), 3154-3160.

134. Rowsell, J. L. C.; Yaghi, O. M., Strategies for hydrogen storage in metal–organic frameworks. *Angew. Chem. Int. Ed.* **2005,** *44* (30), 4670-4679.

135. Brunauer, S.; Deming, L. S.; Deming, W. E.; Teller, E., On a theory of the van der waals adsorption of gases. *J. Am. Chem. Soc.* **1940,** *62* (7), 1723-1732.

136. Düren, T.; Millange, F.; Férey, G.; Walton, K. S.; Snurr, R. Q., Calculating geometric surface areas as a characterization tool for metal−organic frameworks. *J. Phy. Chem. C* **2007,** *111* (42), 15350-15356.

137. Walton, K. S.; Snurr, R. Q., Applicability of the BET method for determining surface areas of microporous metal−organic frameworks. *J. Am. Chem. Soc.* **2007,** *129* (27), 8552-8556.

138. Salem, M. M. K.; Braeuer, P.; Szombathely, M. v.; Heuchel, M.; Harting, P.; Quitzsch, K.; Jaroniec, M., Thermodynamics of high-pressure adsorption of argon, nitrogen, and methane on microporous adsorbents. *Langmuir* **1998,** *14* (12), 3376-3389.

139.   Kaye, S. S.; Dailly, A.; Yaghi, O. M.; Long, J. R., Impact of preparation and handling on the hydrogen storage properties of $Zn_4O(1,4$-benzenedicarboxylate$)_3$ (MOF-5). *J. Am. Chem. Soc.* **2007,** *129* (46), 14176-14177.

140.   Myers, A.; Calles, J.; Calleja, G., Comparison of molecular simulation of adsorption with experiment. *Adsorption* **1997,** *3* (2), 107-115.

141.   Bae, Y.-S.; Snurr, R. Q., Optimal isosteric heat of adsorption for hydrogen storage and delivery using metal–organic frameworks. *Micro. Meso. Mater.* **2010,** *132* (1–2), 300-303.

142.   Schmitz, B.; Müller, U.; Trukhan, N.; Schubert, M.; Férey, G.; Hirscher, M., Heat of adsorption for hydrogen in microporous high-surface-area materials. *ChemPhysChem* **2008,** *9* (15), 2181-2184.

143.   Wong-Foy, A. G.; Matzger, A. J.; Yaghi, O. M., Exceptional H_2 saturation uptake in microporous metal−organic frameworks. *J. Am. Chem. Soc.* **2006,** *128* (11), 3494-3495.

144.   Dailly, A.; Vajo, J. J.; Ahn, C. C., Saturation of hydrogen sorption in Zn benzenedicarboxylate and Zn Naphthalenedicarboxylate. *J. Phy. Chem. B* **2006,** *110* (3), 1099-1101.

145.   Sabo, M.; Henschel, A.; Frode, H.; Klemm, E.; Kaskel, S., Solution infiltration of palladium into MOF-5: synthesis, physisorption and catalytic properties. *J. Mater. Chem.* **2007,** *17* (36), 3827-3832.

146.   Chui, S. S.-Y.; Lo, S. M.-F.; Charmant, J. P. H.; Orpen, A. G.; Williams, I. D., A chemically functionalizable nanoporous material $[Cu_3(TMA)_2(H_2O)_3]_n$. *Science* **1999,** *283* (5405), 1148-1150.

147.   Panella, B.; Hirscher, M.; Pütter, H.; Müller, U., Hydrogen adsorption in metal–organic frameworks: Cu-MOFs and Zn-MOFs compared. *Adv. Funct. Mater.* **2006,** *16* (4), 520-524.

148.   Batten, S. R.; Robson, R., Interpenetrating nets: ordered, periodic entanglement. *Angew. Chem. In. Ed.* **1998,** *37* (11), 1460-1494.

149.   Frost, H.; Düren, T.; Snurr, R. Q., Effects of surface area, free volume, and heat of adsorption on hydrogen uptake in metal−organic frameworks. *J. Phys. Chem. B* **2006,** *110* (19), 9565-9570.

150. Ferey, G.; Latroche, M.; Serre, C.; Millange, F.; Loiseau, T.; Percheron-Guegan, A., Hydrogen adsorption in the nanoporous metal-benzenedicarboxylate $M(OH)(O_2C-C_6H_4-CO_2)$ (M = Al^{3+}, Cr^{3+}), MIL-53. *Chem. Commun.* **2003,** (24), 2976-2977.

151. Latroche, M.; Surblé, S.; Serre, C.; Mellot-Draznieks, C.; Llewellyn, P. L.; Lee, J.-H.; Chang, J.-S.; Jhung, S. H.; Férey, G., Hydrogen storage in the giant-pore metal–organic frameworks MIL-100 and MIL-101. *Angew. Chem. In. Ed.* **2006,** *45* (48), 8227-8231.

152. Férey, G.; Serre, C.; Mellot-Draznieks, C.; Millange, F.; Surblé, S.; Dutour, J.; Margiolaki, I., A hybrid solid with giant pores prepared by a combination of targeted chemistry, simulation, and powder diffraction. *Angew. Chem. In. Ed.* **2004,** *43* (46), 6296-6301.

153. Llewellyn, P. L.; Bourrelly, S.; Serre, C.; Vimont, A.; Daturi, M.; Hamon, L.; De Weireld, G.; Chang, J.-S.; Hong, D.-Y.; Kyu Hwang, Y.; Hwa Jhung, S.; Férey, G., High uptakes of CO_2 and CH_4 in mesoporous metal—organic frameworks MIL-100 and MIL-101. *Langmuir* **2008,** *24* (14), 7245-7250.

154. Phan, A.; Doonan, C. J.; Uribe-Romo, F. J.; Knobler, C. B.; O'Keeffe, M.; Yaghi, O. M., Synthesis, structure, and carbon dioxide capture properties of zeolitic imidazolate frameworks. *Acc. Chem. Res.* **2010,** *43* (1), 58-67.

155. Zhao, D.; Yuan, D.; Zhou, H.-C., The current status of hydrogen storage in metal-organic frameworks. *Energy Environ. Sci.* **2008,** *1* (2), 222-235.

156. Wu, H.; Zhou, W.; Yildirim, T., Hydrogen storage in a prototypical zeolitic imidazolate framework-8. *J. Am. Chem. Soc.* **2007,** *129* (17), 5314-5315.

157. Park, K. S.; Ni, Z.; Côté, A. P.; Choi, J. Y.; Huang, R.; Uribe-Romo, F. J.; Chae, H. K.; O'Keeffe, M.; Yaghi, O. M., Exceptional chemical and thermal stability of zeolitic imidazolate frameworks. *Proceedings of the National Academy of Sciences* **2006,** *103* (27), 10186-10191.

158. Ortiz, A. U.; Boutin, A.; Fuchs, A. H.; Coudert, F.-X., Investigating the pressure-induced amorphization of zeolitic imidazolate framework ZIF-8: mechanical instability due to shear mode softening. *J. Phys. Chem. Lett.* **2013,** *4* (11), 1861-1865.

159. Demessence, A.; D'Alessandro, D. M.; Foo, M. L.; Long, J. R., Strong CO_2 binding in a water-stable, triazolate-bridged metal−organic framework functionalized with ethylenediamine. *J. Am. Chem. Soc.* **2009,** *131* (25), 8784-8786.

160. Nouar, F.; Eubank, J. F.; Bousquet, T.; Wojtas, L.; Zaworotko, M. J.; Eddaoudi, M., Supermolecular building blocks (sbbs) for the design and synthesis of highly porous metal-organic frameworks. *J. Am. Chem. Soc.* **2008,** *130* (6), 1833-1835.

161. Liu, T.-F.; Zou, L.; Feng, D.; Chen, Y.-P.; Fordham, S.; Wang, X.; Liu, Y.; Zhou, H.-C., Stepwise synthesis of robust metal–organic frameworks via postsynthetic metathesis and oxidation of metal nodes in a single-crystal to single-crystal transformation. *J. Am. Chem. Soc.* **2014,** *136* (22), 7813-7816.

162. Zou, L.; Feng, D.; Liu, T.-F.; Chen, Y.-P.; Yuan, S.; Wang, K.; Wang, X.; Fordham, S.; Zhou, H.-C., A versatile synthetic route for the preparation of titanium metal-organic frameworks. *Chem. Sci.* **2016**.

163. Lian, X.; Feng, D.; Chen, Y.-P.; Liu, T.-F.; Wang, X.; Zhou, H.-C., The preparation of an ultrastable mesoporous Cr(iii)-MOF via reductive labilization. *Chem. Sci.* **2015,** *6* (12), 7044-7048.

164. Hwang, Y. K.; Hong, D.-Y.; Chang, J.-S.; Jhung, S. H.; Seo, Y.-K.; Kim, J.; Vimont, A.; Daturi, M.; Serre, C.; Férey, G., Amine grafting on coordinatively unsaturated metal centers of MOFs: consequences for catalysis and metal encapsulation. *Angew. Chem. In. Ed.* **2008,** *47* (22), 4144-4148.

165. Meilikhov, M.; Yusenko, K.; Esken, D.; Turner, S.; Van Tendeloo, G.; Fischer, R. A., Metals@MOFs – loading MOFs with metal nanoparticles for hybrid functions. *Eur. J. Inorg. Chem.* **2010,** *2010* (24), 3701-3714.

166. Cheon, Y. E.; Suh, M. P., Enhanced hydrogen storage by palladium nanoparticles fabricated in a redox-active metal–organic framework. *Angew. Chem. In. Ed.* **2009,** *48* (16), 2899-2903.

167. Farha, O. K.; Mulfort, K. L.; Hupp, J. T., An example of node-based postassembly elaboration of a hydrogen-sorbing, metal−organic framework material. *Inorg. Chem.* **2008,** *47* (22), 10223-10225.

168. Park, H. J.; Cheon, Y. E.; Suh, M. P., Post-synthetic reversible incorporation of organic linkers into porous metal–organic frameworks through single-crystal-to-

single-crystal transformations and modification of gas-sorption properties. *Chem. Eur. J.* **2010,** *16* (38), 11662-11669.

169.   Wang, Z.; Tanabe, K. K.; Cohen, S. M., Tuning hydrogen sorption properties of metal–organic frameworks by postsynthetic covalent modification. *Chem. Eur. J.* **2010,** *16* (1), 212-217.

170.   Han, S. S.; Goddard, W. A., Lithium-doped metal-organic frameworks for reversible H_2 storage at ambient temperature. *J. Am. Chem. Soc.* **2007,** *129* (27), 8422-8423.

171.   Mavrandonakis, A.; Tylianakis, E.; Stubos, A. K.; Froudakis, G. E., Why Li doping in MOFs enhances H_2 storage capacity? A multi-scale theoretical study. *J. Phys. Chem. C* **2008,** *112* (18), 7290-7294.

172.   Férey, G.; Millange, F.; Morcrette, M.; Serre, C.; Doublet, M.-L.; Grenèche, J.-M.; Tarascon, J.-M., Mixed-valence Li/Fe-based metal–organic frameworks with both reversible redox and sorption properties. *Angew. Chem. In. Ed.* **2007,** *46* (18), 3259-3263.

173.   Zhang, Y.; Scanlon, L. G.; Rottmayer, M. A.; Balbuena, P. B., Computational investigation of adsorption of molecular hydrogen on lithium-doped corannulene. *J. Phys. Chem. B* **2006,** *110* (45), 22532-22541.

174.   Blomqvist, A.; Araújo, C. M.; Srepusharawoot, P.; Ahuja, R., Li-decorated metal–organic framework 5: A route to achieving a suitable hydrogen storage medium. *Proceedings of the National Academy of Sciences* **2007,** *104* (51), 20173-20176.

175.   Mulfort, K. L.; Hupp, J. T., Alkali metal cation effects on hydrogen uptake and binding in metal-organic frameworks. *Inorg. Chem.* **2008,** *47* (18), 7936-7938.

176.   Mulfort, K. L.; Hupp, J. T., Chemical reduction of metal−organic framework materials as a method to enhance gas uptake and binding. *J. Am. Chem. Soc.* **2007,** *129* (31), 9604-9605.

177.   Li, Y.; Yang, R. T., Significantly enhanced hydrogen storage in metal−organic frameworks via spillover. *J. Am. Chem. Soc.* **2006,** *128* (3), 726-727.

178.   Li, Y.; Yang, R. T., Hydrogen storage in metal−organic frameworks by bridged hydrogen spillover. *J. Am. Chem. Soc.* **2006,** *128* (25), 8136-8137.

179. Li, Y.; Yang, R. T., Gas adsorption and storage in metal−organic framework MOF-177. *Langmuir* **2007,** *23* (26), 12937-12944.

180. Raupach, M. R.; Marland, G.; Ciais, P.; Le Quéré, C.; Canadell, J. G.; Klepper, G.; Field, C. B., Global and regional drivers of accelerating CO_2 emissions. *Proceedings of the National Academy of Sciences* **2007,** *104* (24), 10288-10293.

181. Earth System Research Laboratory: http://www.esrl.noaa.gov/gmd/ccgg/trends/index.html, 2011.

182. R. K. Pachauri, A. Reisinger, IPCC Fifth Assessment Report, Intergovernmental Panel on Climate Change, 2014.

183. U.S. Environmental Protection Agency, http://www.epa.gov/climatechange/ccs/, assessed: June 2015.

184. Markewitz, P.; Kuckshinrichs, W.; Leitner, W.; Linssen, J.; Zapp, P.; Bongartz, R.; Schreiber, A.; Muller, T. E., Worldwide innovations in the development of carbon capture technologies and the utilization of CO_2. *Energy Environ. Sci.***2012,** *5* (6), 7281-7305.

185. Smith, H. J.; Fahrenkamp-Uppenbrink, J.; Coontz, R., Clearing the air. *Science* **2009,** *325* (5948), 1641-1641.

186. Jacobson, M. Z., Review of solutions to global warming, air pollution, and energy security. *Energy Environ. Sci.***2009,** *2* (2), 148-173.

187. Leung, D. Y. C.; Caramanna, G.; Maroto-Valer, M. M., An overview of current status of carbon dioxide capture and storage technologies. *Renewable and Sustainable Energy Reviews* **2014,** *39*, 426-443.

188. Li, J.-R.; Ma, Y.; McCarthy, M. C.; Sculley, J.; Yu, J.; Jeong, H.-K.; Balbuena, P. B.; Zhou, H.-C., Carbon dioxide capture-related gas adsorption and separation in metal-organic frameworks. *Coord. Chem. Rev.* **2011,** *255* (15–16), 1791-1823.

189. Sumida, K.; Rogow, D. L.; Mason, J. A.; McDonald, T. M.; Bloch, E. D.; Herm, Z. R.; Bae, T.-H.; Long, J. R., Carbon dioxide capture in metal–organic frameworks. *Chem. Rev.* **2012,** *112* (2), 724-781.

190. Jassim, M. S.; Rochelle, G. T., Innovative absorber/stripper configurations for CO_2 capture by aqueous monoethanolamine. *Industrial & Engineering Chemistry Research* **2006,** *45* (8), 2465-2472.

191. Lee, K. B.; Sircar, S., Removal and recovery of compressed CO_2 from flue gas by a novel thermal swing chemisorption process. *AIChE Journal* **2008,** *54* (9), 2293-2302.

192. Figueroa, J. D.; Fout, T.; Plasynski, S.; McIlvried, H.; Srivastava, R. D., Advances in CO_2 capture technology—The U.S. department of energy's carbon sequestration program. *Int. J. Greenhouse Gas Control* **2008,** *2* (1), 9-20.

193. Dawson, R.; Cooper, A. I.; Adams, D. J., Chemical functionalization strategies for carbon dioxide capture in microporous organic polymers. *Poly. Intert.* **2013,** *62* (3), 345-352.

194. Kather, A.; Scheffknecht, G., The oxycoal process with cryogenic oxygen supply. *Naturwissenschaften* **2009,** *96* (9), 993-1010.

195. Kakaras, E.; Koumanakos, A.; Doukelis, A.; Giannakopoulos, D.; Vorrias, I., Oxyfuel boiler design in a lignite-fired power plant. *Fuel* **2007,** *86* (14), 2144-2150.

196. Passé-Coutrin, N.; Jeanne-Rose, V.; Ouensanga, A., Textural analysis for better correlation of the char yield of pyrolysed lignocellulosic materials. *Fuel* **2005,** *84* (16), 2131-2134.

197. Tagliabue, M.; Farrusseng, D.; Valencia, S.; Aguado, S.; Ravon, U.; Rizzo, C.; Corma, A.; Mirodatos, C., Natural gas treating by selective adsorption: Material science and chemical engineering interplay. *Chem. Eng. J.* **2009,** *155* (3), 553-566.

198. Hwang, C.-C.; Tour, J. J.; Kittrell, C.; Espinal, L.; Alemany, L. B.; Tour, J. M., Capturing carbon dioxide as a polymer from natural gas. *Nat. Commun.* **2014,** *5*.

199. Goeppert, A.; Czaun, M.; Surya Prakash, G. K.; Olah, G. A., Air as the renewable carbon source of the future: an overview of CO_2 capture from the atmosphere. *Energy Environ. Sci.***2012,** *5* (7), 7833-7853.

200. Rochelle, G. T., Amine scrubbing for CO_2 capture. *Science* **2009,** *325* (5948), 1652-1654.

201. Zhang, Y.; Freeman, B.; Rochelle, G., Absorber modeling for NGCC carbon capture with aqueous piperazine. *Faraday Discuss.* **2016**.

202. Walters, M. S.; Edgar, T. F.; Rochelle, G. T., Regulatory control of amine scrubbing for CO_2 capture from power plants. *Industrial & Engineering Chemistry Research* **2016**.

203. Wang, Z.; Mitch, W. A., Influence of dissolved metals on n-nitrosamine formation under amine-based CO_2 capture conditions. *Environ. Sci. Technol.* **2015,** *49* (19), 11974-81.

204. Fostas, B. I.; Gangstad, A.; Nenseter, B.; Pedersen, S.; Sjovoll, M.; Sorensen, A. L., Effects of NOx in the flue gas degradation of MEA. *10th International Conference on Greenhouse Gas Control Technologies* **2011,** *4* (0), 1566-1573.

205. Sculley, J. P.; Verdegaal, W. M.; Lu, W.; Wriedt, M.; Zhou, H. C., High-throughput analytical model to evaluate materials for temperature swing adsorption processes. *Adv. Mater.* **2013,** *25* (29), 3957-61.

206. Haszeldine, R. S., Carbon capture and storage: how green can black be? *Science* **2009,** *325* (5948), 1647-1652.

207. Peeters, A. N. M.; Faaij, A. P. C.; Turkenburg, W. C., Techno-economic analysis of natural gas combined cycles with post-combustion CO_2 absorption, including a detailed evaluation of the development potential. *Int. J. Greenhouse Gas Control* **2007,** *1* (4), 396-417.

208. Oyenekan, B. A.; Rochelle, G. T., Alternative stripper configurations for CO_2 capture by aqueous amines. *AIChE Journal* **2007,** *53* (12), 3144-3154.

209. Freeman, S. A.; Dugas, R.; Van Wagener, D. H.; Nguyen, T.; Rochelle, G. T., Carbon dioxide capture with concentrated, aqueous piperazine. *Int. J. Greenhouse Gas Control* **2010,** *4* (2), 119-124.

210. Wang, Q.; Luo, J.; Zhong, Z.; Borgna, A., CO_2 capture by solid adsorbents and their applications: current status and new trends. *Energy Environ. Sci.***2011,** *4* (1), 42-55.

211. Morris, R. E.; Wheatley, P. S., Gas storage in nanoporous materials. *Angew. Chem. In. Ed.* **2008,** *47* (27), 4966-4981.

212.	D'Alessandro, D. M.; Smit, B.; Long, J. R., Carbon dioxide capture: prospects for new materials. *Angew. Chem. In. Ed.* **2010,** *49* (35), 6058-6082.

213.	Xiang, Z.; Mercado, R.; Huck, J. M.; Wang, H.; Guo, Z.; Wang, W.; Cao, D.; Haranczyk, M.; Smit, B., Systematic tuning and multifunctionalization of covalent organic polymers for enhanced carbon capture. *J. Am. Chem. Soc.* **2015,** *137* (41), 13301-13307.

214.	Jiang, J.; Yu, J.; Corma, A., Extra-large-pore zeolites: bridging the gap between micro and mesoporous structures. *Angew. Chem. In. Ed.* **2010,** *49* (18), 3120-3145.

215.	Chahbani, M. H.; Tondeur, D., Predicting the final pressure in the equalization step of PSA cycles. *Sep. Purif. Technol.* **2010,** *71* (2), 225-232.

216.	Plaza, M. G.; García, S.; Rubiera, F.; Pis, J. J.; Pevida, C., Post-combustion CO_2 capture with a commercial activated carbon: Comparison of different regeneration strategies. *Chemical Engineering Journal* **2010,** *163* (1–2), 41-47.

217.	Zelenak, V.; Halamova, D.; Gaberova, L.; Bloch, E.; Llewellyn, P., Amine-modified SBA-12 mesoporous silica for carbon dioxide capture: Effect of amine basicity on sorption properties. *Micropor. Mesopor. Mat.* **2008,** *116* (1–3), 358-364.

218.	Didas, S. A.; Choi, S.; Chaikittisilp, W.; Jones, C. W., Amine–oxide hybrid materials for CO_2 capture from ambient air. *Acc. Chem. Res.* **2015,** *48* (10), 2680-2687.

219.	McDonald, T. M.; Lee, W. R.; Mason, J. A.; Wiers, B. M.; Hong, C. S.; Long, J. R., Capture of carbon dioxide from air and flue gas in the alkylamine-appended metal–organic framework mmen-Mg_2(dobpdc). *J. Am. Chem. Soc.* **2012,** *134* (16), 7056-7065.

220.	Choi, S.; Drese, J. H.; Jones, C. W., Adsorbent materials for carbon dioxide capture from large anthropogenic point sources. *ChemSusChem* **2009,** *2* (9), 796-854.

221.	Herzog, H., Meldon, J., and Hatton A., Advanced post-combustion CO_2 capture, Massachusetts Institute of Technology, Boston, MA, 2009.

222.	Furukawa, H.; Yaghi, O. M., Storage of hydrogen, methane, and carbon dioxide in highly porous covalent organic frameworks for clean energy applications. *J. Am. Chem. Soc.* **2009,** *131* (25), 8875-8883.

223. Kenarsari, S. D.; Yang, D.; Jiang, G.; Zhang, S.; Wang, J.; Russell, A. G.; Wei, Q.; Fan, M., Review of recent advances in carbon dioxide separation and capture. *RSC Adv.* **2013,** *3* (45), 22739-22773.

224. Wu, D.; Xu, F.; Sun, B.; Fu, R.; He, H.; Matyjaszewski, K., Design and preparation of porous polymers. *Chem. Rev.* **2012,** *112* (7), 3959-4015.

225. Lu, W.; Yuan, D.; Zhao, D.; Schilling, C. I.; Plietzsch, O.; Muller, T.; Bräse, S.; Guenther, J.; Blümel, J.; Krishna, R.; Li, Z.; Zhou, H.-C., Porous polymer networks: synthesis, porosity, and applications in gas storage/separation. *Chem. Mater.* **2010,** *22* (21), 5964-5972.

226. Hentze, H. P.; Antonietti, M., Template synthesis of porous organic polymers. *Current Opinion in Solid State and Materials Science* **2001,** *5* (4), 343-353.

227. Vyas, V. S.; Haase, F.; Stegbauer, L.; Savasci, G.; Podjaski, F.; Ochsenfeld, C.; Lotsch, B. V., A tunable azine covalent organic framework platform for visible light-induced hydrogen generation. *Nat. Commun.* **2015,** *6*.

228. Dogru, M.; Bein, T., Covalent organic frameworks: Growing honeycombs on graphene. *Nat. Nano.* **2011,** *6* (6), 333-335.

229. Doonan, C. J.; Tranchemontagne, D. J.; Glover, T. G.; Hunt, J. R.; Yaghi, O. M., Exceptional ammonia uptake by a covalent organic framework. *Nat. Chem.* **2010,** *2* (3), 235-238.

230. Yu, J.-T.; Chen, Z.; Sun, J.; Huang, Z.-T.; Zheng, Q.-Y., Cyclotricatechylene based porous crystalline material: Synthesis and applications in gas storage. *J. Mater. Chem.* **2012,** *22* (12), 5369-5373.

231. Oh, H.; Kalidindi, S. B.; Um, Y.; Bureekaew, S.; Schmid, R.; Fischer, R. A.; Hirscher, M., A cryogenically flexible covalent organic framework for efficient hydrogen isotope separation by quantum sieving. *Angew. Chem. In. Ed.* **2013,** *52* (50), 13219-13222.

232. Ma, H.; Ren, H.; Meng, S.; Yan, Z.; Zhao, H.; Sun, F.; Zhu, G., A 3D microporous covalent organic framework with exceedingly high C_3H_8/CH_4 and C_2 hydrocarbon/CH_4 selectivity. *Chem. Commun.* **2013,** *49* (84), 9773-9775.

233. Sanders, S. N.; Kumarasamy, E.; Pun, A. B.; Trinh, M. T.; Choi, B.; Xia, J.; Taffet, E. J.; Low, J. Z.; Miller, J. R.; Roy, X.; Zhu, X. Y.; Steigerwald, M. L.; Sfeir, M.

Y.; Campos, L. M., Quantitative intramolecular singlet fission in bipentacenes. *J. Am. Chem. Soc.* **2015,** *137* (28), 8965-8972.

234.   Wan, S.; Gándara, F.; Asano, A.; Furukawa, H.; Saeki, A.; Dey, S. K.; Liao, L.; Ambrogio, M. W.; Botros, Y. Y.; Duan, X.; Seki, S.; Stoddart, J. F.; Yaghi, O. M., Covalent organic frameworks with high charge carrier mobility. *Chem. Mater.* **2011,** *23* (18), 4094-4097.

235.   Ding, S.-Y.; Gao, J.; Wang, Q.; Zhang, Y.; Song, W.-G.; Su, C.-Y.; Wang, W., Construction of covalent organic framework for catalysis: Pd/COF-LZU1 in suzuki–miyaura coupling reaction. *J. Am. Chem. Soc.* **2011,** *133* (49), 19816-19822.

236.   Chandra, S.; Kundu, T.; Kandambeth, S.; BabaRao, R.; Marathe, Y.; Kunjir, S. M.; Banerjee, R., Phosphoric acid loaded Azo (−N═N−) based covalent organic framework for proton conduction. *J. Am. Chem. Soc.* **2014,** *136* (18), 6570-6573.

237.   Das, G.; Biswal, B. P.; Kandambeth, S.; Venkatesh, V.; Kaur, G.; Addicoat, M.; Heine, T.; Verma, S.; Banerjee, R., Chemical sensing in two dimensional porous covalent organic nanosheets. *Chem. Sci.* **2015,** *6* (7), 3931-3939.

238.   Fang, Q.; Wang, J.; Gu, S.; Kaspar, R. B.; Zhuang, Z.; Zheng, J.; Guo, H.; Qiu, S.; Yan, Y., 3D porous crystalline polyimide covalent organic frameworks for drug delivery. *J. Am. Chem. Soc.* **2015,** *137* (26), 8352-8355.

239.   Xu, F.; Xu, H.; Chen, X.; Wu, D.; Wu, Y.; Liu, H.; Gu, C.; Fu, R.; Jiang, D., Radical covalent organic frameworks: a general strategy to immobilize open-accessible polyradicals for high-performance capacitive energy storage. *Angew. Chem. In. Ed.* **2015,** *54* (23), 6814-6818.

240.   DeBlase, C. R.; Silberstein, K. E.; Truong, T.-T.; Abruña, H. D.; Dichtel, W. R., β-ketoenamine-linked covalent organic frameworks capable of pseudocapacitive energy storage. *J. Am. Chem. Soc.* **2013,** *135* (45), 16821-16824.

241.   Lu, W.; Verdegaal, W. M.; Yu, J.; Balbuena, P. B.; Jeong, H.-K.; Zhou, H.-C., Building multiple adsorption sites in porous polymer networks for carbon capture applications. *Energy Environ. Sci.* **2013,** *6* (12), 3559-3564.

242.   Katsoulidis, A. P.; Kanatzidis, M. G., Phloroglucinol based microporous polymeric organic frameworks with −OH functional groups and high CO_2 capture capacity. *Chem. Mater.* **2011,** *23* (7), 1818-1824.

243.   Islamoglu, T.; Kim, T.; Kahveci, Z.; El-Kadri, O. M.; El-Kaderi, H. M., Systematic postsynthetic modification of nanoporous organic frameworks for enhanced CO_2 capture from flue gas and landfill gas. *J. Phys. Chem. C* **2016,** *120* (5), 2592-2599.

244.   Wang, X.; Zhao, Y.; Wei, L.; Zhang, C.; Jiang, J.-X., Nitrogen-rich conjugated microporous polymers: impact of building blocks on porosity and gas adsorption. *J. Mater. Chem. A* **2015,** *3* (42), 21185-21193.

245.   Ren, S.; Dawson, R.; Laybourn, A.; Jiang, J.-x.; Khimyak, Y.; Adams, D. J.; Cooper, A. I., Functional conjugated microporous polymers: from 1,3,5-benzene to 1,3,5-triazine. *Polym. Chem.* **2012,** *3* (4), 928-934.

246.   Budd, P. M.; Butler, A.; Selbie, J.; Mahmood, K.; McKeown, N. B.; Ghanem, B.; Msayib, K.; Book, D.; Walton, A., The potential of organic polymer-based hydrogen storage materials. *Phys. Chem. Chem. Phys.* **2007,** *9* (15), 1802-1808.

247.   Mason, C. R.; Maynard-Atem, L.; Al-Harbi, N. M.; Budd, P. M.; Bernardo, P.; Bazzarelli, F.; Clarizia, G.; Jansen, J. C., Polymer of intrinsic microporosity incorporating thioamide functionality: preparation and gas transport properties. *Macromolecules* **2011,** *44* (16), 6471-6479.

248.   Wood, C. D.; Tan, B.; Trewin, A.; Niu, H.; Bradshaw, D.; Rosseinsky, M. J.; Khimyak, Y. Z.; Campbell, N. L.; Kirk, R.; Stöckel, E.; Cooper, A. I., Hydrogen storage in microporous hypercrosslinked organic polymer networks. *Chem. Mater.* **2007,** *19* (8), 2034-2048.

249.   Lee, J.-Y.; Wood, C. D.; Bradshaw, D.; Rosseinsky, M. J.; Cooper, A. I., Hydrogen adsorption in microporous hypercrosslinked polymers. *Chem. Commun.* **2006,** (25), 2670-2672.

250.   Kuhn, P.; Thomas, A.; Antonietti, M., Toward tailorable porous organic polymer networks: a high-temperature dynamic polymerization scheme based on aromatic nitriles. *Macromolecules* **2009,** *42* (1), 319-326.

251.   Kuhn, P.; Antonietti, M.; Thomas, A., Porous, covalent triazine-based frameworks prepared by ionothermal synthesis. *Angew. Chem. In. Ed.* **2008,** *47* (18), 3450-3453.

252.   Ren, H.; Ben, T.; Wang, E.; Jing, X.; Xue, M.; Liu, B.; Cui, Y.; Qiu, S.; Zhu, G., Targeted synthesis of a 3D porous aromatic framework for selective sorption of benzene. *Chem. Commun.* **2010,** *46* (2), 291-293.

253.   Hunt, J. R.; Doonan, C. J.; LeVangie, J. D.; Côté, A. P.; Yaghi, O. M., Reticular synthesis of covalent organic borosilicate frameworks. *J. Am. Chem. Soc.* **2008,** *130* (36), 11872-11873.

254.   Frank, W.; Pautzsch, T.; Klemm, E., Bipyridinylene-based conjugated polymer containing a ruthenium(ii) bipyridine metal complex synthesized by suzuki coupling. *Macromolecular Chemistry and Physics* **2001,** *202* (12), 2535-2537.

255.   Zhou, T.-Y.; Xu, S.-Q.; Wen, Q.; Pang, Z.-F.; Zhao, X., One-step construction of two different kinds of pores in a 2D covalent organic framework. *J. Am. Chem. Soc.* **2014,** *136* (45), 15885-15888.

256.   Zhang, Y.-B.; Su, J.; Furukawa, H.; Yun, Y.; Gándara, F.; Duong, A.; Zou, X.; Yaghi, O. M., Single-crystal structure of a covalent organic framework. *J. Am. Chem. Soc.* **2013,** *135* (44), 16336-16339.

257.   Waller, P. J.; Gándara, F.; Yaghi, O. M., Chemistry of covalent organic frameworks. *Acc. Chem. Res.* **2015,** *48* (12), 3053-3063.

258.   Ding, S.-Y.; Wang, W., Covalent organic frameworks (COFs): from design to applications. *Chem. Soc. Rev.* **2013,** *42* (2), 548-568.

259.   Zeng, Y.; Zou, R.; Zhao, Y., Covalent organic frameworks for CO_2 capture. *Adv. Mater.* **2016,** *28* (15), 2855-2873.

260.   Dawson, R.; Stockel, E.; Holst, J. R.; Adams, D. J.; Cooper, A. I., Microporous organic polymers for carbon dioxide capture. *Energy Environ. Sci.* **2011,** *4* (10), 4239-4245.

261.   Woodward, R. T.; Stevens, L. A.; Dawson, R.; Vijayaraghavan, M.; Hasell, T.; Silverwood, I. P.; Ewing, A. V.; Ratvijitvech, T.; Exley, J. D.; Chong, S. Y.; Blanc, F.; Adams, D. J.; Kazarian, S. G.; Snape, C. E.; Drage, T. C.; Cooper, A. I., Swellable, water- and acid-tolerant polymer sponges for chemoselective carbon dioxide capture. *J. Am. Chem. Soc.* **2014,** *136* (25), 9028-9035.

262.   Ben, T.; Pei, C.; Zhang, D.; Xu, J.; Deng, F.; Jing, X.; Qiu, S., Gas storage in porous aromatic frameworks (PAFs). *Energy Environ. Sci.* **2011,** *4* (10), 3991-3999.

263. Byun, J.; Je, S.-H.; Patel, H. A.; Coskun, A.; Yavuz, C. T., Nanoporous covalent organic polymers incorporating Troger's base functionalities for enhanced CO_2 capture. *J. Mater. Chem. A* **2014,** *2* (31), 12507-12512.

264. Zhao, H.; Jin, Z.; Su, H.; Zhang, J.; Yao, X.; Zhao, H.; Zhu, G., Target synthesis of a novel porous aromatic framework and its highly selective separation of CO_2/CH_4. *Chem. Commun.* **2013,** *49* (27), 2780-2782.

265. Dawson, R.; Adams, D. J.; Cooper, A. I., Chemical tuning of CO_2 sorption in robust nanoporous organic polymers. *Chem. Sci.* **2011,** *2* (6), 1173-1177.

266. Huang, N.; Chen, X.; Krishna, R.; Jiang, D., Two-dimensional covalent organic frameworks for carbon dioxide capture through channel-wall functionalization. *Angew. Chem. Int. Ed.* **2015,** *54* (10), 2986-2990.

267. Arab, P.; Verlander, A.; El-Kaderi, H. M., Synthesis of a highly porous bis(imino)pyridine-linked polymer and its postsynthetic modification with inorganic fluorinated ions for selective CO_2 capture. *J. Phys. Chem. C* **2015,** *119* (15), 8174-8182.

268. Wang, J.; Wei Yang, J. G.; Yi, G.; Zhang, Y., Phosphonium salt incorporated hypercrosslinked porous polymers for CO_2 capture and conversion. *Chem. Commun.* **2015,** *51* (86), 15708-15711.

269. Lu, W.; Yuan, D.; Sculley, J.; Zhao, D.; Krishna, R.; Zhou, H.-C., Sulfonate-grafted porous polymer networks for preferential co2 adsorption at low pressure. *J. Am. Chem. Soc.* **2011,** *133* (45), 18126-18129.

270. Ma, H.; Ren, H.; Zou, X.; Meng, S.; Sun, F.; Zhu, G., Post-metalation of porous aromatic frameworks for highly efficient carbon capture from $CO_2 + N_2$ and $CH_4 + N_2$ mixtures. *Polym. Chem.* **2014,** *5* (1), 144-152.

271. Lu, W.; Sculley, J. P.; Yuan, D.; Krishna, R.; Zhou, H.-C., Carbon dioxide capture from air using amine-grafted porous polymer networks. *J. Phys. Chem. C* **2013,** *117* (8), 4057-4061.

272. Lu, W.; Bosch, M.; Yuan, D.; Zhou, H.-C., Cost-effective synthesis of amine-tethered porous materials for carbon capture. *ChemSusChem* **2015,** *8* (3), 433-438.

273. Sun, L.-B.; Li, A.-G.; Liu, X.-D.; Liu, X.-Q.; Feng, D.; Lu, W.; Yuan, D.; Zhou, H.-C., Facile fabrication of cost-effective porous polymer networks for highly selective CO_2 capture. *J. Mater. Chem. A* **2015,** *3* (7), 3252-3256.

274. Ben-Mansour, R.; Habib, M. A.; Bamidele, O. E.; Basha, M.; Qasem, N. A. A.; Peedikakkal, A.; Laoui, T.; Ali, M., Carbon capture by physical adsorption: Materials, experimental investigations and numerical modeling and simulations – A review. *Applied Energy* **2016,** *161*, 225-255.

275. Cavenati, S.; Grande, C. A.; Rodrigues, A. E., Removal of carbon dioxide from natural gas by vacuum pressure swing adsorption. *Energy & Fuels* **2006,** *20* (6), 2648-2659.

276. Rabbani, M. G.; El-Kaderi, H. M., Template-free synthesis of a highly porous benzimidazole-linked polymer for CO_2 capture and H_2 storage. *Chem. Mater.* **2011,** *23* (7), 1650-1653.

277. Rabbani, M. G.; El-Kaderi, H. M., Synthesis and characterization of porous benzimidazole-linked polymers and their performance in small gas storage and selective uptake. *Chem. Mater.* **2012,** *24* (8), 1511-1517.

278. Rabbani, M. G.; Reich, T. E.; Kassab, R. M.; Jackson, K. T.; El-Kaderi, H. M., High CO_2 uptake and selectivity by triptycene-derived benzimidazole-linked polymers. *Chem. Commun.* **2012,** *48* (8), 1141-1143.

279. Sekizkardes, A. K.; Islamoglu, T.; Kahveci, Z.; El-Kaderi, H. M., Application of pyrene-derived benzimidazole-linked polymers to CO_2 separation under pressure and vacuum swing adsorption settings. *J. Mater. Chem. A* **2014,** *2* (31), 12492-12500.

280. Altarawneh, S.; İslamoğlu, T.; Sekizkardes, A. K.; El-Kaderi, H. M., Effect of acid-catalyzed formation rates of benzimidazole-linked polymers on porosity and selective CO_2 capture from gas mixtures. *Environ. Sci. Technol.* **2015,** *49* (7), 4715-4723.

281. Sekizkardes, A. K.; Culp, J. T.; Islamoglu, T.; Marti, A.; Hopkinson, D.; Myers, C.; El-Kaderi, H. M.; Nulwala, H. B., An ultra-microporous organic polymer for high performance carbon dioxide capture and separation. *Chem. Commun.* **2015,** *51* (69), 13393-13396.

179

282. Sekizkardes, A. K.; Altarawneh, S.; Kahveci, Z.; İslamoğlu, T.; El-Kaderi, H. M., Highly selective CO_2 capture by triazine-based benzimidazole-linked polymers. *Macromolecules* **2014,** *47* (23), 8328-8334.

283. Patel, H. A.; Yavuz, C. T., Highly optimized CO_2 capture by inexpensive nanoporous covalent organic polymers and their amine composites. *Faraday Discussions* **2015,** *183* (0), 401-412.

284. Patel, H. A.; Hyun Je, S.; Park, J.; Chen, D. P.; Jung, Y.; Yavuz, C. T.; Coskun, A., Unprecedented high-temperature CO_2 selectivity in N2-phobic nanoporous covalent organic polymers. *Nat. Commun.* **2013,** *4*, 1357.

285. Arab, P.; Rabbani, M. G.; Sekizkardes, A. K.; İslamoğlu, T.; El-Kaderi, H. M., Copper(I)-catalyzed synthesis of nanoporous azo-linked polymers: impact of textural properties on gas storage and selective carbon dioxide capture. *Chem. Mater.* **2014,** *26* (3), 1385-1392.

286. Arab, P.; Parrish, E.; Islamoglu, T.; El-Kaderi, H. M., Synthesis and evaluation of porous azo-linked polymers for carbon dioxide capture and separation. *J. Mater. Chem. A* **2015,** *3* (41), 20586-20594.

287. Islamoglu, T.; Gulam Rabbani, M.; El-Kaderi, H. M., Impact of post-synthesis modification of nanoporous organic frameworks on small gas uptake and selective CO2 capture. *J. Mater. Chem. A* **2013,** *1* (35), 10259-10266.

288. Hu, X.-M.; Chen, Q.; Sui, Z.-Y.; Zhao, Z.-Q.; Bovet, N.; Laursen, B. W.; Han, B.-H., Triazatriangulenium-based porous organic polymers for carbon dioxide capture. *RSC Adv.* **2015,** *5* (109), 90135-90143.

289. Jia, S.-H.; Ding, X.; Yu, H.-T.; Han, B.-H., Multi-hydroxyl-containing porous organic polymers based on phenol formaldehyde resin chemistry with high carbon dioxide capture capacity. *RSC Adv.* **2015,** *5* (87), 71095-71101.

290. Ding, X.; Li, H.; Zhao, Y.-C.; Han, B.-H., Mannitol-based acetal-linked porous organic polymers for selective capture of carbon dioxide over methane. *Polym. Chem.* **2015,** *6* (29), 5305-5312.

291. Li, H.; Ding, X.; Zhao, Y.-C.; Han, B.-H., Preparation of mannitol-based ketal-linked porous organic polymers and their application for selective capture of carbon dioxide. *Polymer* **2016,** *89*, 112-118.

292. Buyukcakir, O.; Je, S. H.; Choi, D. S.; Talapaneni, S. N.; Seo, Y.; Jung, Y.; Polychronopoulou, K.; Coskun, A., Porous cationic polymers: the impact of counteranions and charges on CO2 capture and conversion. *Chem. Commun.* **2016,** *52* (5), 934-937.

293. Zhu, X.; Do-Thanh, C.-L.; Murdock, C. R.; Nelson, K. M.; Tian, C.; Brown, S.; Mahurin, S. M.; Jenkins, D. M.; Hu, J.; Zhao, B.; Liu, H.; Dai, S., Efficient CO_2 capture by a 3D porous polymer derived from tröger's base. *ACS Macro Letters* **2013,** *2* (8), 660-663.

294. Yuan, R.; Ren, H.; Yan, Z.; Wang, A.; Zhu, G., Robust tri(4-ethynylphenyl)amine-based porous aromatic frameworks for carbon dioxide capture. *Polym. Chem.* **2014,** *5* (7), 2266-2272.

295. Meng, L.; Zou, X.; Guo, S.; Ma, H.; Zhao, Y.; Zhu, G., Self-supported fibrous porous aromatic membranes for efficient CO_2/N_2 separations. *ACS Applied Materials & Interfaces* **2015,** *7* (28), 15561-15569.

296. Wang, J.; Sng, W.; Yi, G.; Zhang, Y., Imidazolium salt-modified porous hypercrosslinked polymers for synergistic CO_2 capture and conversion. *Chem. Commun.* **2015,** *51* (60), 12076-12079.

297. Jeon, H. J.; Choi, J. H.; Lee, Y.; Choi, K. M.; Park, J. H.; Kang, J. K., Highly selective CO_2-capturing polymeric organic network structures. *Advanced Energy Materials* **2012,** *2* (2), 225-228.

298. Neti, V. S. P. K.; Wang, J.; Deng, S.; Echegoyen, L., High and selective CO_2 adsorption by a phthalocyanine nanoporous polymer. *J. Mater. Chem. A* **2015,** *3* (19), 10284-10288.

299. Tozawa, T.; Jones, J. T. A.; Swamy, S. I.; Jiang, S.; Adams, D. J.; Shakespeare, S.; Clowes, R.; Bradshaw, D.; Hasell, T.; Chong, S. Y.; Tang, C.; Thompson, S.; Parker, J.; Trewin, A.; Bacsa, J.; Slawin, A. M. Z.; Steiner, A.; Cooper, A. I., Porous organic cages. *Nat. Mater.* **2009,** *8* (12), 973-978.

300. Lee, J. H.; Lee, H. J.; Lim, S. Y.; Kim, B. G.; Choi, J. W., Combined CO_2-philicity and ordered mesoporosity for highly selective CO_2 capture at high temperatures. *J. Am. Chem. Soc.* **2015,** *137* (22), 7210-7216.

301. Xie, L.-H.; Suh, M. P., High CO_2-capture ability of a porous organic polymer bifunctionalized with carboxy and triazole groups. *Chem. Eur. J.* **2013,** *19* (35), 11590-11597.

302. Gao, X.; Zou, X.; Ma, H.; Meng, S.; Zhu, G., Highly selective and permeable porous organic framework membrane for CO_2 capture. *Adv. Mater.* **2014,** *26* (22), 3644-3648.

303. Gu, C.; Liu, D.; Huang, W.; Liu, J.; Yang, R., Synthesis of covalent triazine-based frameworks with high CO_2 adsorption and selectivity. *Polym. Chem.* **2015,** *6* (42), 7410-7417.

304. Zhao, Y.; Wang, X.; Zhang, C.; Xie, F.; Kong, R.; Jiang, J.-X., Isoindigo-based microporous organic polymers for carbon dioxide capture. *RSC Adv.* **2015,** *5* (121), 100322-100329.

305. Mohanty, P.; Kull, L. D.; Landskron, K., Porous covalent electron-rich organonitridic frameworks as highly selective sorbents for methane and carbon dioxide. *Nat. Commun.* **2011,** *2*, 401.

306. Côté, A. P.; El-Kaderi, H. M.; Furukawa, H.; Hunt, J. R.; Yaghi, O. M., Reticular synthesis of microporous and mesoporous 2D covalent organic frameworks. *J. Am. Chem. Soc.* **2007,** *129* (43), 12914-12915.

307. Mastalerz, M., The next generation of shape-persistant zeolite analogues: covalent organic frameworks. *Angew. Chem. In. Ed.* **2008,** *47* (3), 445-447.

308. Tilford, R. W.; Mugavero, S. J.; Pellechia, P. J.; Lavigne, J. J., Tailoring microporosity in covalent organic frameworks. *Adv. Mater.* **2008,** *20* (14), 2741-2746.

309. Bunck, D. N.; Dichtel, W. R., Internal functionalization of three-dimensional covalent organic frameworks. *Angew. Chem. In. Ed.* **2012,** *51* (8), 1885-1889.

310. Brucks, S. D.; Bunck, D. N.; Dichtel, W. R., Functionalization of 3D covalent organic frameworks using monofunctional boronic acids. *Polymer* **2014,** *55* (1), 330-334.

311. Lanni, L. M.; Tilford, R. W.; Bharathy, M.; Lavigne, J. J., Enhanced hydrolytic stability of self-assembling alkylated two-dimensional covalent organic frameworks. *J. Am. Chem. Soc.* **2011,** *133* (35), 13975-13983.

312. Bunck, D. N.; Dichtel, W. R., Postsynthetic functionalization of 3D covalent organic frameworks. *Chem. Commun.* **2013,** *49* (24), 2457-2459.

313. Kalidindi, S. B.; Wiktor, C.; Ramakrishnan, A.; We; Schneemann, A.; Van Tendeloo, G.; Fischer, R. A., Lewis base mediated efficient synthesis and solvation-like host-guest chemistry of covalent organic framework-1. *Chem. Commun.* **2013,** *49* (5), 463-465.

314. Yuan, Y.; Sun, F.; Ren, H.; Jing, X.; Wang, W.; Ma, H.; Zhao, H.; Zhu, G., Targeted synthesis of a porous aromatic framework with a high adsorption capacity for organic molecules. *J. Mater. Chem.* **2011,** *21* (35), 13498-13502.

315. Jiang, J.-X.; Su, F.; Trewin, A.; Wood, C. D.; Campbell, N. L.; Niu, H.; Dickinson, C.; Ganin, A. Y.; Rosseinsky, M. J.; Khimyak, Y. Z.; Cooper, A. I., Conjugated microporous poly(aryleneethynylene) networks. *Angew. Chem. In. Ed.* **2007,** *46* (45), 8574-8578.

316. Jiang, J.-X.; Su, F.; Trewin, A.; Wood, C. D.; Niu, H.; Jones, J. T. A.; Khimyak, Y. Z.; Cooper, A. I., Synthetic control of the pore dimension and surface area in conjugated microporous polymer and copolymer networks. *J. Am. Chem. Soc.* **2008,** *130* (24), 7710-7720.

317. Dawson, R.; Laybourn, A.; Khimyak, Y. Z.; Adams, D. J.; Cooper, A. I., High surface area conjugated microporous polymers: the importance of reaction solvent choice. *Macromolecules* **2010,** *43* (20), 8524-8530.

318. Xu, Y.; Jin, S.; Xu, H.; Nagai, A.; Jiang, D., Conjugated microporous polymers: design, synthesis and application. *Chem. Soc. Rev.* **2013,** *42* (20), 8012-8031.

319. Zhang, C.; Liu, Y.; Li, B.; Tan, B.; Chen, C.-F.; Xu, H.-B.; Yang, X.-L., Triptycene-based microporous polymers: synthesis and their gas storage properties. *ACS Macro Let.* **2012,** *1* (1), 190-193.

320. Lu, W.; Wei, Z.; Yuan, D.; Tian, J.; Fordham, S.; Zhou, H.-C., Rational design and synthesis of porous polymer networks: toward high surface area. *Chem. Mater.* **2014,** *26* (15), 4589-4597.

321. Wood, C. D.; Tan, B.; Trewin, A.; Su, F.; Rosseinsky, M. J.; Bradshaw, D.; Sun, Y.; Zhou, L.; Cooper, A. I., Microporous organic polymers for methane storage. *Adv. Mater.* **2008,** *20* (10), 1916-1921.

322. Du, N.; Park, H. B.; Robertson, G. P.; Dal-Cin, M. M.; Visser, T.; Scoles, L.; Guiver, M. D., Polymer nanosieve membranes for CO_2-capture applications. *Nat. Mater.* **2011,** *10* (5), 372-375.

323. Wilmer, C. E.; Farha, O. K.; Bae, Y.-S.; Hupp, J. T.; Snurr, R. Q., Structure-property relationships of porous materials for carbon dioxide separation and capture. *Energy Environ. Sci.***2012,** *5* (12), 9849-9856.

324. Cansado, I. P. P.; Carrott, M. R.; Carrott, P. J. M., Influence of degassing temperature on the performance of carbon molecular sieves for separations involving O_2, N_2, CO_2, and CH_4. *Energy & Fuels* **2006,** *20* (2), 766-770.

325. Babarao, R.; Jiang, J., Exceptionally high CO_2 storage in covalent-organic frameworks: Atomistic simulation study. *Energy Environ. Sci.***2008,** *1* (1), 139-143.

326. Yang, Z.; Peng, X.; Cao, D., Carbon dioxide capture by PAFs and an efficient strategy to fast screen porous materials for gas separation. *J. Phys. Chem. C* **2013,** *117* (16), 8353-8364.

327. Weder, C., Hole control in microporous polymers. *Angew. Chem. In. Ed.* **2008,** *47* (3), 448-450.

328. Ghanem, B. S.; Hashem, M.; Harris, K. D. M.; Msayib, K. J.; Xu, M.; Budd, P. M.; Chaukura, N.; Book, D.; Tedds, S.; Walton, A.; McKeown, N. B., Triptycene-based polymers of intrinsic microporosity: organic materials that can be tailored for gas adsorption. *Macromolecules* **2010,** *43* (12), 5287-5294.

329. Presser, V.; McDonough, J.; Yeon, S.-H.; Gogotsi, Y., Effect of pore size on carbon dioxide sorption by carbide derived carbon. *Energy Environ. Sci.***2011,** *4* (8), 3059-3066.

330. Liao, Y.; Weber, J.; Faul, C. F. J., Conjugated microporous polytriphenylamine networks. *Chem. Commun.* **2014,** *50* (59), 8002-8005.

331. Wang, D.; Li, L.; Yang, W.; Zuo, Y.; Feng, S.; Liu, H., POSS-based luminescent porous polymers for carbon dioxide sorption and nitroaromatic explosives detection. *RSC Adv.* **2014,** *4* (104), 59877-59884.

332. Rabbani, M. G.; Sekizkardes, A. K.; El-Kadri, O. M.; Kaafarani, B. R.; El-Kaderi, H. M., Pyrene-directed growth of nanoporous benzimidazole-linked nanofibers

and their application to selective CO_2 capture and separation. *J. Mater. Chem.* **2012,** *22* (48), 25409-25417.

333.   Holst, J. R.; Stöckel, E.; Adams, D. J.; Cooper, A. I., High surface area networks from tetrahedral monomers: metal-catalyzed coupling, thermal polymerization, and "click" chemistry. *Macromolecules* **2010,** *43* (20), 8531-8538.

334.   Gomes, R.; Bhanja, P.; Bhaumik, A., A triazine-based covalent organic polymer for efficient CO2 adsorption. *Chem. Commun.* **2015,** *51* (49), 10050-10053.

335.   Zhao, Y.; Yao, K. X.; Teng, B.; Zhang, T.; Han, Y., A perfluorinated covalent triazine-based framework for highly selective and water-tolerant CO_2 capture. *Energy Environ. Sci.***2013,** *6* (12), 3684-3692.

336.   Schwab, M. G.; Fassbender, B.; Spiess, H. W.; Thomas, A.; Feng, X.; Müllen, K., Catalyst-free preparation of melamine-based microporous polymer networks through schiff base chemistry. *J. Am. Chem. Soc.* **2009,** *131* (21), 7216-7217.

337.   Kandambeth, S.; Venkatesh, V.; Shinde, D. B.; Kumari, S.; Halder, A.; Verma, S.; Banerjee, R., Self-templated chemically stable hollow spherical covalent organic framework. *Nat. Commun.* **2015,** *6*.

338.   Kaleeswaran, D.; Vishnoi, P.; Murugavel, R., [3+3] Imine and [small beta]-ketoenamine tethered fluorescent covalent-organic frameworks for CO_2 uptake and nitroaromatic sensing. *J. Mater. Chem. C* **2015,** *3* (27), 7159-7171.

339.   Gao, Q.; Bai, L.; Zhang, X.; Wang, P.; Li, P.; Zeng, Y.; Zou, R.; Zhao, Y., Synthesis of microporous nitrogen-rich covalent-organic framework and its application in CO_2 capture. *Chinese Journal of Chemistry* **2015,** *33* (1), 90-94.

340.   Zhu, Y.; Zhang, W., Reversible tuning of pore size and CO_2 adsorption in azobenzene functionalized porous organic polymers. *Chem. Sci.* **2014,** *5* (12), 4957-4961.

341.   Rabbani, M. G.; Sekizkardes, A. K.; Kahveci, Z.; Reich, T. E.; Ding, R.; El-Kaderi, H. M., A 2D mesoporous imine-linked covalent organic framework for high pressure gas storage applications. *Chem. Eur. J.* **2013,** *19* (10), 3324-3328.

342.   Li, Z.; Feng, X.; Zou, Y.; Zhang, Y.; Xia, H.; Liu, X.; Mu, Y., A 2D azine-linked covalent organic framework for gas storage applications. *Chem. Commun.* **2014,** *50* (89), 13825-13828.

343. de la Peña Ruigómez, A.; Rodríguez-San-Miguel, D.; Stylianou, K. C.; Cavallini, M.; Gentili, D.; Liscio, F.; Milita, S.; Roscioni , O. M.; Ruiz-González, M. L.; Carbonell, C.; Maspoch, D.; Mas-Ballesté, R.; Segura, J. L.; Zamora, F., Direct on-surface patterning of a crystalline laminar covalent organic framework synthesized at room temperature. *Chem. Eur. J.* **2015,** *21* (30), 10666-10670.

344. Yan, X.; Cook, T. R.; Pollock, J. B.; Wei, P.; Zhang, Y.; Yu, Y.; Huang, F.; Stang, P. J., Responsive supramolecular polymer metallogel constructed by orthogonal coordination-driven self-assembly and host/guest interactions. *J. Am. Chem. Soc.* **2014,** *136* (12), 4460-4463.

345. Zeng, Y.; Zou, R.; Luo, Z.; Zhang, H.; Yao, X.; Ma, X.; Zou, R.; Zhao, Y., Covalent organic frameworks formed with two types of covalent bonds based on orthogonal reactions. *J. Am. Chem. Soc.* **2015,** *137* (3), 1020-1023.

346. Kandambeth, S.; Mallick, A.; Lukose, B.; Mane, M. V.; Heine, T.; Banerjee, R., Construction of crystalline 2D covalent organic frameworks with remarkable chemical (acid/base) stability via a combined reversible and irreversible route. *J. Am. Chem. Soc.* **2012,** *134* (48), 19524-19527.

347. Biswal, B. P.; Chandra, S.; Kandambeth, S.; Lukose, B.; Heine, T.; Banerjee, R., Mechanochemical synthesis of chemically stable isoreticular covalent organic frameworks. *J. Am. Chem. Soc.* **2013,** *135* (14), 5328-5331.

348. Wei, H.; Chai, S.; Hu, N.; Yang, Z.; Wei, L.; Wang, L., The microwave-assisted solvothermal synthesis of a crystalline two-dimensional covalent organic framework with high CO2 capacity. *Chem. Commun.* **2015,** *51* (61), 12178-12181.

349. Kandambeth, S.; Shinde, D. B.; Panda, M. K.; Lukose, B.; Heine, T.; Banerjee, R., Enhancement of chemical stability and crystallinity in porphyrin-containing covalent organic frameworks by intramolecular hydrogen bonds. *Angew. Chem. Int. Ed.* **2013,** *52* (49), 13052-13056.

350. Li, Z.; Zhi, Y.; Feng, X.; Ding, X.; Zou, Y.; Liu, X.; Mu, Y., An azine-linked covalent organic framework: synthesis, characterization and efficient gas storage. *Chem. Eur. J.* **2015,** *21* (34), 12079-12084.

351. Chen, Q.; Luo, M.; Hammershøj, P.; Zhou, D.; Han, Y.; Laursen, B. W.; Yan, C.-G.; Han, B.-H., Microporous polycarbazole with high specific surface area for gas storage and separation. *J. Am. Chem. Soc.* **2012,** *134* (14), 6084-6087.

352. Zhu, Y.; Long, H.; Zhang, W., Imine-linked porous polymer frameworks with high small gas (H_2, CO_2, CH_4, C_2H_2) uptake and CO_2/N_2 selectivity. *Chem. Mater.* **2013,** *25* (9), 1630-1635.

353. Torrisi, A.; Bell, R. G.; Mellot-Draznieks, C., Functionalized MOFs for enhanced CO_2 capture. *Cryst. Growth Des.* **2010,** *10* (7), 2839-2841.

354. Hicks, J. C.; Drese, J. H.; Fauth, D. J.; Gray, M. L.; Qi, G.; Jones, C. W., Designing adsorbents for CO_2 capture from flue gas-hyperbranched aminosilicas capable of capturing CO_2 reversibly. *J. Am. Chem. Soc.* **2008,** *130* (10), 2902-2903.

355. Gadzikwa, T.; Farha, O. K.; Mulfort, K. L.; Hupp, J. T.; Nguyen, S. T., A Zn-based, pillared paddlewheel MOF containing free carboxylic acids via covalent post-synthesis elaboration. *Chem. Commun.* **2009,** (25), 3720-3722.

356. Jiang, H.-L.; Feng, D.; Liu, T.-F.; Li, J.-R.; Zhou, H.-C., Pore surface engineering with controlled loadings of functional groups via click chemistry in highly stable metal–organic frameworks. *J. Am. Chem. Soc.* **2012,** *134* (36), 14690-14693.

357. Wang, L.; Yang, R. T., Significantly increased CO_2 adsorption performance of nanostructured templated carbon by tuning surface area and nitrogen doping. *J. Phys. Chem. C* **2012,** *116* (1), 1099-1106.

358. Yang, Z.-Z.; Zhao, Y.; Zhang, H.; Yu, B.; Ma, Z.; Ji, G.; Liu, Z., Fluorinated microporous organic polymers: design and applications in CO_2 adsorption and conversion. *Chem. Commun.* **2014,** *50* (90), 13910-13913.

359. Huang, N.; Krishna, R.; Jiang, D., Tailor-made pore surface engineering in covalent organic frameworks: systematic functionalization for performance screening. *J. Am. Chem. Soc.* **2015,** *137* (22), 7079-7082.

360. Blanchon le Bouhelec, E.; Mougin, P.; Barreau, A.; Solimando, R., Rigorous modeling of the acid gas heat of absorption in alkanolamine solutions. *Energy & Fuels* **2007,** *21* (4), 2044-2055.

361. da Silva, E. F.; Svendsen, H. F., Computational chemistry study of reactions, equilibrium and kinetics of chemical CO_2 absorption. *Int. J. Greenhouse Gas Control* **2007,** *1* (2), 151-157.

362. Sreenivasulu, B.; Sreedhar, I.; Suresh, P.; Raghavan, K. V., Development trends in porous adsorbents for carbon capture. *Environ. Sci. Technol.* **2015,** *49* (21), 12641-12661.

363. Garibay, S. J.; Weston, M. H.; Mondloch, J. E.; Colon, Y. J.; Farha, O. K.; Hupp, J. T.; Nguyen, S. T., Accessing functionalized porous aromatic frameworks (PAFs) through a de novo approach. *Crystengcomm* **2013,** *15* (8), 1515-1519.

364. McDonald, T. M.; D'Alessandro, D. M.; Krishna, R.; Long, J. R., Enhanced carbon dioxide capture upon incorporation of N,N-dimethylethylenediamine in the metal-organic framework CuBTTri. *Chem. Sci.* **2011,** *2* (10), 2022-2028.

365. DeCoste, J. B.; Peterson, G. W.; Schindler, B. J.; Killops, K. L.; Browe, M. A.; Mahle, J. J., The effect of water adsorption on the structure of the carboxylate containing metal-organic frameworks Cu-BTC, Mg-MOF-74, and UiO-66. *J. Mater. Chem. A* **2013,** *1* (38), 11922-11932.

366. Fracaroli, A. M.; Furukawa, H.; Suzuki, M.; Dodd, M.; Okajima, S.; Gándara, F.; Reimer, J. A.; Yaghi, O. M., Metal–organic frameworks with precisely designed interior for carbon dioxide capture in the presence of water. *J. Am. Chem. Soc.* **2014,** *136* (25), 8863-8866.

367. Planas, N.; Dzubak, A. L.; Poloni, R.; Lin, L.-C.; McManus, A.; McDonald, T. M.; Neaton, J. B.; Long, J. R.; Smit, B.; Gagliardi, L., The mechanism of carbon dioxide adsorption in an alkylamine-functionalized metal–organic framework. *J. Am. Chem. Soc.* **2013,** *135* (20), 7402-7405.

368. Sayari, A.; Belmabkhout, Y., Stabilization of amine-containing CO_2 adsorbents: dramatic effect of water vapor. *J. Am. Chem. Soc.* **2010,** *132* (18), 6312-6314.

369. Mason, J. A.; Sumida, K.; Herm, Z. R.; Krishna, R.; Long, J. R., Evaluating metal-organic frameworks for post-combustion carbon dioxide capture via temperature swing adsorption. *Energy Environ. Sci.* **2011,** *4* (8), 3030-3040.

370. McDonald, T. M.; Lee, W. R.; Mason, J. A.; Wiers, B. M.; Hong, C. S.; Long, J. R., Capture of carbon dioxide from air and flue gas in the alkylamine-appended metal-organic framework mmen-Mg_2(dobpdc). *J Am Chem Soc* **2012,** *134* (16), 7056-65.

371. Abbott, L. J.; Colina, C. M., Porosity and ring formation in conjugated microporous polymers. *Journal of Chemical & Engineering Data* **2014,** *59* (10), 3177-3182.

372. Pirngruber, G. D.; Guillou, F.; Gomez, A.; Clausse, M., A theoretical analysis of the energy consumption of post-combustion CO_2 capture processes by temperature swing adsorption using solid sorbents. *Int. J. Greenhouse Gas Control* **2013,** *14*, 74-83.

373. Lin, Y.; Kong, C.; Chen, L., Direct synthesis of amine-functionalized MIL-101(Cr) nanoparticles and application for CO_2 capture. *RSC Adv.* **2012,** *2* (16), 6417-6419.

374. Kim, S.-N.; Yang, S.-T.; Kim, J.; Park, J.-E.; Ahn, W.-S., Post-synthesis functionalization of MIL-101 using diethylenetriamine: a study on adsorption and catalysis. *CrystEngComm* **2012,** *14* (12), 4142-4147.

375. Sculley, J. P.; Verdegaal, W. M.; Lu, W.; Wriedt, M.; Zhou, H.-C., High-throughput analytical model to evaluate materials for temperature swing adsorption processes. *Adv. Mater.* **2013,** *25* (29), 3957-3961.

376. Dugas, R. E.; Rochelle, G. T., Modeling CO_2 absorption into concentrated aqueous monoethanolamine and piperazine. *Chem. Eng. Sci.* **2011,** *66* (21), 5212-5218.

377. Gadipelli, S.; Patel, H. A.; Guo, Z., An ultrahigh pore volume drives up the amine stability and cyclic CO_2 capacity of a solid-amine@carbon sorbent. *Adv. Mater.* **2015,** *27* (33), 4903-4909.